Structural characterization of iron species in Fe-ZSM-5 catalysts and the elucidation of their role in the mechanism of NO_x reactions

Dissertation

zur

Erlangung des akademischen Grades

doctor rerum naturalium (Dr. rer. nat.)

der Mathematisch-Naturwissenschaftlichen Fakultät

der Universität Rostock

vorgelegt von:

M. Sc. Roxana Pérez Vélez

geb. am 12.03.85 in San Salvador el Seco, Puebla

aus Rostock

Rostock, Oktober 2014

urn:nbn:de:gbv:28-diss2015-0041-9

Gutachter:

1. Prof. Dr. Ralf Ludwig
   Institut für Chemie, Universität Rostock
   Dr.-Lorenz-Weg 1, 18059 Rostock
2. Prof. Dr. Angelika Brückner
   Leibniz-Institut für Katalyse e. V. an der Universität Rostock
   Albert-Einstein-Straße 29a, 18059 Rostock

Datum der Einreichung: 24. Oktober 2014

Datum der Verteidigung: 20. Januar 2015

Die vorliegende Arbeit entstand in der Zeit von März 2011 bis Oktober 2014 im Leibniz Institute für Katalyse an der Universität Rostock, LIKAT.

Nicht alles was zählt, kann gezählt werden,
und nicht alles was gezählt werden kann, zählt.

(Albert Einstein)

Acknowledgements

This work would not be possible without the supervision of Prof. Dr. Angelika Brückner at the Leibniz Institute for Catalysis (LIKAT) at the University of Rostock. I express my sincere gratitude to her for giving me the opportunity to work in this interesting research project, for the financial support, constant assistance, encouragement and interesting scientific feedbacks.

I would like to express my deepest acknowledgement to Dr. Ursula Bentrup for the guidance, continuous teaching, the experience shared and advice, which help me to learn a lot and to overcome many difficulties.

Special thanks to Prof. Dr. Wolfgang Grünert and Dr. Inga Ellmers for the enthusiastic discussions and fruitful collaboration in this research project.

My sincere appreciation is extended to Christine, Leif, Christiane, Max, Dirk, Suresh, Jana and Anja for the pleasant working atmosphere and for all their help especially at the beginning of my stay in LIKAT.

I would also like to thank Nils, Andrea, Denise, Esteban and all the members of the catalytic *in situ* studies and analytical group for their direct or indirect help, kindness and great parties at LIKAT.

I appreciate the facilities and assistance at LIKAT provided by the workshop, administration and purchasing departments.

Finally, my heartfelt thanks go to my family for their unconditional support and love, and to my friends in Rostock for making my Ph.D. life more enjoyable.

Roxana Pérez Vélez

Rostock, October 2014

Dedicated to my lovely family…

Abstract

The abatement of NO_x from waste gases of stationary sources is a relevant topic of environmental catalysis, in which the selective catalytic reduction of NO_x by ammonia (NH_3-SCR) has been widely applied. A potential catalyst for this reaction is Fe-ZSM-5, which shows high performance at temperatures above 400 °C when NO is the main component (standard SCR), and at lower temperatures (250 °C) when additional NO_2 ($NO/NO_2 = 1$) is present (fast SCR). Identification of the active species and understanding of the reaction mechanism are fundamental to improve the efficiency, stability and selectivity of the catalyst. This information is impossible to obtain with routine characterization techniques. However, analyzing the catalyst under real reaction conditions, by means of *in situ* and *operando* spectroscopy, offers a suitable methodology. In this work, Fe-ZSM-5 catalysts were prepared by different techniques, and investigated for the different NH_3-SCR reactions of NO_x reactions, using *in situ* and *operando* EPR, UV-Vis and FTIR spectroscopy. In the EPR and FTIR analysis, specially developed reaction cells were applied. The *operando* EPR and *in situ* UV-Vis spectroscopic studies of the fast SCR reaction demonstrate the crucial role of NO_2 for the effective reoxidation of single Fe^{2+} to (active) isolated Fe^{3+} sites at β and γ sites in the zeolite lattice, which are responsible for the higher activity in the fast SCR. Additionally, surface nitrates observed during *in situ* FTIR measurements are formed at Fe^{3+}. The formation of surface nitrates was found to be the main pathway in the reaction mechanism of fast SCR. The catalyst performance in the NO oxidation was shown to be enhanced by previous contact with the standard SCR reaction.

Die Reduktion von NO_x aus Abgasen stationärer Quellen ist ein wichtiges Thema der Umweltkatalyse, wobei die selektive katalytische Reduktion von NO_x mittels NH_3 (NH_3-SCR) einen etablierten und weit verbreiteten Prozess darstellt. Ein potentieller Katalysator für diesen Prozess ist Fe-ZSM-5, der eine hohe Katalysatorleistung bei Temperaturen oberhalb 400°C zeigt, wenn NO die Hauptkomponente des Abgases ist (Standard-SCR), und bei deutlich niederen Temperauren (250°C), wenn zusätzlich NO_2 ($NO/NO_2 = 1$) vorhanden ist (schnelle SCR). Die Identifizierung der aktiven Spezies und die Kenntnis des Reaktionsmechanismus sind unabdingbare Voraussetzungen für die Verbesserung von Effizienz, Stabilität und Selektivität der Katalysatoren. Diese Informationen sind jedoch nicht mittels Routinecharakterisierungstechniken zugänglich. *In situ*- und *operando*-Spektroskopie

stellen dagegen eine geeignete Methodik dar, die Katalysatorwirkungsweise unter realen Reaktionsbedingungen zu analysieren. In dieser Arbeit wurden Fe-ZSM-5-Katalysatoren, die mit verschiedener Präparationstechniken hergestellt wurden, in beiden NH_3-SCR-Reaktionen von NO_x mittels *in situ*- und *operando*-EPR-, -UV-Vis- sowie -FTIR-Spektroskopie untersucht. Für die EPR- und FTIR-Studien wurden spezielle Reaktionszellen eingesetzt.

Die *operando*-EPR- und *in situ*-UV-Vis-spektroskopischen Untersuchungen der schnellen SCR-Reaktion demonstrierten die bedeutsame Rolle von NO_2, nämlich die effektive Reoxidation von Fe^{2+} zu aktiven, isolierten Fe^{3+} Zentren an β und γ Positionen im Zeolith-Gitter, welche für die höhere Aktivität in der schnellen SCR verantwortlich sind. Darüber hinaus werden Oberflächen-Nitrat-Spezies an diesen Fe^{3+} Zentren gebildet, was *in situ*-FTIR-spektroskopisch nachgewiesen wurde. Die Bildung von Oberflächen-Nitrat-Spezies wurde als Hauptweg im Reaktionsmechanismus der schnellen SCR identifiziert. Darüber hinaus konnte gezeigt werden, dass die Katalysatorleistung in der NO-Oxidation durch eine vorher durchgeführte Standard-SCR-Reaktion deutlich gesteigert werden kann.

List of abbreviations

^{27}Al-NMR	Aluminum nuclear magnetic resonance
BET	Brunauer, Emmet and Teller (theory)
DRIFTS	Diffuse reflectance infrared Fourier transform spectroscopy
UV-Vis-DRS	Diffuse reflectance ultraviolet-visible spectroscopy
EPR	Electron paramagnetic resonance spectroscopy
EXAFS	Extended X-ray absorption fine structure spectroscopy
Fe-ZSM-5	ZSM-5 zeolite loaded with iron
FTIR	Fourier transform infrared spectroscopy
GHSV	Gas hourly space velocity
H-TPR	Hydrogen temperature-programmed reduction
ICP-AES	Inductively coupled plasma atomic emission spectroscopy
ICP-OES	Inductively coupled plasma optical emission spectrometry
MCD	Magnetic circular dichroism
MFI	Mordenite Framework Inverted
MS	Mass spectrometry
NH_3-TPD	Ammonia temperature-programmed desorption
^{29}Si-NMR	Silicon nuclear magnetic resonance
SSIE-I-Na/Ca	Solid state ion exchanged catalyst loaded with Na or Ca
TEM	Transmission electron microscopy
wt.%	Weight percent
XAS	X-ray absorption spectroscopy
XRD	X-ray diffraction
ZSM-5	Zeolite Socony Mobil-5

Table of contents

1. Introduction and objectives

Introduction

The worldwide production and emission of NO_x (NO and NO_2) into the atmosphere represents a serious environmental problem. Due to the effect of NO_x on human health and ecosystems, its abatement and control are strictly required to preserve human welfare and ecological balance.

According to the natural and anthropogenic origins of NO_x, road transport comprises half of its total anthropogenic production. Therefore, regulations concerning NO_x emission limits in vehicles have become more stringent over the last years.

An efficient technology for the abatement of NO_x is the Selective Catalytic Reduction by NH_3 (NH_3-SCR), where NO and NO_2 are reduced to the harmless N_2 gas. For mobile sources, the NH_3-SCR of NO_x is performed in catalytic converters, where the three-way catalyst (V_2O_5-WO_3/TiO_2) has traditionally been used. However, V_2O_5-WO_3/TiO_2 has some disadvantages such as a restricted operating temperature range (350 - 400 °C), high sensitivity against side reactions like SO_2 oxidation, and decomposition at higher temperatures.

After the engine starts, the temperature in the converter is not high enough for the oxidation of NO to take place; therefore, the development of new catalysts with wider operating temperature windows, as well as higher selectivity and stability, is still a challenge. In particular, metal-exchanged zeolite catalysts have proved to be highly active in the NH_3-SCR of NO_x, they are cheap and show good thermal stability. For instance, Fe-ZSM-5 is already available as a commercial zeolite catalyst showing a better performance than the V_2O_5-WO_3/TiO_2 catalyst for the NO_x reduction. The catalytic performance of Fe-ZSM-5 at different temperatures depends on the NO/NO_2 ratio. When NO is present as the main NO_x component (standard SCR), good performance is accomplished above 400 °C, while in the case of $NO/NO_2 = 1$ (fast SCR), high activity is achieved at lower temperatures.

Several mechanisms have been proposed for standard and fast SCR, reflecting no real agreement in the reaction mechanism. One suggested mechanism of the standard SCR describes first the oxidation of iron species by O_2 gas which reacts with NO forming Fe^{3+}-N_xO_y [1]. The latter intermediate is finally reduced with ammonia to N_2 and H_2O and then leaves the reduced Fe^{2+}. Another recent mechanism describes HONO as an intermediate which reacts with ammonia to form NH_4NO_2 and rapidly decomposes to N_2 and H_2O [2]. The formation of NO^+ and subsequent formation of HONO in the presence of water have also been reported as mechanistic steps for standard SCR [3]. Additionally, the oxidation of NO to

NO_2 has been widely proposed as rate-limiting step of the standard SCR, while the oxidation of Fe^{2+} to Fe^{3+} has scarcely reported. For the fast SCR, a theoretical mechanism remarks the re-oxidation of iron by NO_2 and NH_2NO as an intermediate pathway of the reaction [4]. An alternative mechanism proceeds via formation of N_2O_3 from NO and NO_2, which by reaction with ammonia forms NH_4NO_2 and subsequently decomposes to N_2 and H_2O [5]. Finally the most accepted mechanism consists in the formation of nitrates, especially NH_4NO_3, and by further reaction with NO the nitrates are reduced to NO_2 and HONO, which by reaction with ammonia forms the NH_4NO_2 [6].

The efficiency of Fe-ZSM-5 also varies with the iron content and type of preparation method, because during the metal loading a multitude of iron species can be produced inside of the zeolite lattice. For instance, isolated iron at extraframework cationic positions, small Fe_xO_y clusters and Fe_xO_y nanoparticles [7-9]. The isolated and highly aggregated Fe_xO_y species can be distinguished in Fe-ZSM-5, by EPR and UV-Vis spectroscopic characterization. Based on these and other techniques such as TPD, Mössbauer and FTIR spectroscopy, the catalytic activity of SCR reactions has been tried to be correlated with specific iron species.

It has been proposed that isolated and oligonuclear Fe_xO_y clusters work in the standard SCR, while only small amounts of isolated iron sites execute the fast SCR [7, 10]. In contrast, other authors correlated the activity of the standard SCR with oxo-Fe^{3+} species. The temperature has also been considered as factor, it has been proposed that isolated iron species contribute to activity below 300 °C and Fe_xO_y species at higher temperatures [11, 12]. Similar to the disagreement about the mechanisms of the reactions, there is still a controversy regarding the iron species active for fast and standard SCR.

Characterization of Fe-ZSM-5 by spectroscopic techniques such as UV-Vis and EPR offer also valuable information about the dispersion and oxidation state of iron. IR spectroscopy can evidence the state of the surface intermediates or acidity using probe molecules like pyridine. Additionally, techniques like XRD offer the possibility to observe modifications of crystal structures. In general, every technique provides specific information; thus, the application of several spectroscopic techniques aids to extend the comprehension of the catalytic system. The common spectroscopic characterization techniques bring only information about the catalyst before and after catalytic reaction, limiting the investigation to the initial and final state of the catalyst and not during the working conditions. Detailed information about the working principles of catalysts under real operating conditions can only be realized by *in situ* and *operando* spectroscopic techniques. The *in situ* spectroscopic

methods allow the investigation of the active sites, electronic and structural changes in the catalyst, as well as reaction intermediates under reaction conditions (temperature, pressure and reactants). Moreover, the *in situ* measurements are done in the range from picoseconds to minutes, considering that the formation of bonds and completeness of the catalytic cycle occurs within this time. Furthermore, o*perando* spectroscopic methods combine the *in situ* spectroscopic characterization with simultaneous measurements of catalytic activity and selectivity, so by *operando* methods the analysis of the active catalysts is directly confirmed.

Since normal spectroscopic techniques cannot completely explain the working state of Fe-ZSM-5 and the underlying fundamental mechanisms of the NH_3-SCR of NO_x, *in situ* and *operando* methods are required. In this work, *in situ* and *operando* EPR, FTIR and UV-Vis spectroscopic techniques were applied to get deeper comprehension of the active sites and reaction mechanism of the NH_3-SCR of NO_x over Fe-ZSM-5.

Objectives

All the different results, which are discussed in more detail in section 2, illustrate that, despite extensive previous research work, there are still different opinions on the nature of active sites that catalyze the different reactions: NO oxidation, standard SCR and fast SCR. Moreover, the different reaction steps and intermediates in the mechanism of these reactions are controversially discussed. Major reasons for this situation may be that 1) the Fe speciation in the Fe-ZSM-5 catalysts studied by different groups was very different due to different synthesis and pretreatment procedures, 2) the spectroscopic methods used for their characterization so far (e. g. UV-Vis-DRS, EPR, XAS and/or Mössbauer spectroscopy) show different sensitivity for the detection of different Fe species and 3) the conditions for spectroscopic *in situ* studies performed occasionally differed from those during real catalytic reaction conditions. These three aspects limit the comparability of different previous studies. Therefore, it is the aim of this work to elucidate structure-reactivity relationships in three relevant reactions, named standard and fast SCR as well as NO oxidation, using a series of Fe-ZSM-5 catalysts with low Fe content, in which the nature of the Fe species has been deliberately influenced by different synthesis methods.

After comprehensive *ex situ* characterization (mainly by EPR and UV-vis spectroscopy) for elucidating the distribution of single Fe sites as well as of Fe_xO_y clusters, the interaction of these species with different feed components (NO, NO_2, O_2, NH_3 and mixtures of them) and at different temperatures shall be investigated using *in situ*- and/or *operando*-EPR and -UV-vis-spectroscopy (for analyzing reaction-dependent changes of the nature of iron species), as well as *in situ* FTIR spectroscopy to identify surface intermediates.

Based on the integrated evaluation of the results, the specific iron species that participate in standard and fast SCR as well as in NO oxidation shall be identified and a unifying mechanism shall be proposed.

2. State of the art

2.1 NO_x abatement and control technologies

Nitrogen oxides (NO_x) comprise nitrogen oxide (NO), nitrogen dioxide (NO_2) and nitrous oxide (N_2O). NO is a colorless and tasteless gas that oxidizes rapidly to NO_2 in the atmosphere. NO_2 is a yellowish-orange to reddish-brown gas with a pungent odor, it is a precursor of ground-level ozone (smog), contributes to acid rain which damages ecosystems and accelerates corrosion in the form of nitric acid. Additionally, NO_x has a direct harmful effect on human health [13-15]. N_2O is a greenhouse gas; in 2011 it accounted for about 5% of all U.S. greenhouse emissions from human activities. The warming impact of 1 kg of N_2O on the atmosphere is over 300 times that of 1 kg of carbon dioxide [16]. Because of its environmental relevance, NO_x abatement is an important topic of further research.

NO_x is produced by both, natural and anthropogenic sources. Natural origins are for instance the electrical activity of thunderstorms, volcanic activity, biomass burning e.g. forest fires, and bacterial organisms [17, 18]. Anthropogenic sources are classified as stationary, mobile or biogenic processes; they are produced by atmospheric nitrogen oxidation at high temperatures > 1300 °C, by the combustion of fossil fuels and industrial wastes, or ammonia oxidation. Stationary sources include electric power plants boilers, industrial boilers, iron and steel mills, cement and glass manufacture, coal-burning incinerators, diesel engines in stationary processes, petroleum refineries and nitric acid plants [19]. Mobile sources consist of non-road and road transport (aircrafts, locomotives, marine vessels and vehicles, respectively); road transport contributes with approximately 50% of total NO_x emissions from anthropogenic origin. For example, the European environment agency (EEA) reported in 2010 that the road transport has produced 40% of all NO_x emissions in the European Union [20]. The NO_x emitted from Diesel or lean burn engines consist primarily of NO (over 90%) [21].

The European emission standard for light commercial vehicles (type and size: Euro 5) stipulates a maximum NO_x emission of 235 ppm for diesel and 82 ppm for gasoline vehicles [22]. The environmental protection agency in the USA (EPA) established the maximum concentration of NO_2 in the air to protect public health and welfare (primary and secondary standard) as 53 ppb [19]. According to the limits for air contaminants of the United States department of Labor, 25 ppm of NO are allowed by volume at 25 °C and 1 atm, the permissible exposure limits (PELs) are 8 hours TWAs (Time-Weighted Averages) [23].

Due to the new regulations about NO_x emissions and its damaging effects, several technologies are developed for the control and abatement of NO_x. To prevent NO_x generation in combustion and high temperature processes, contact time or temperature can be reduced by optimization of burner design (low-NO_x burner), by controlling fuel/air ratio (low excess air), over-fire air system, catalytic combustion, and by injection of water, steam or air in boilers. Additionally, an alternative to avoid NO_x formation is reducing nitrogen as a reactant by using ultra-low nitrogen fuel or oxygen instead of air. When NO_x is produced by ammonia oxidation in nitric acid plants, wet scrubbers are used as control technology. On the other hand, when the NO_x is already formed after combustion or at high temperatures, the applied technologies for regulating NO_x emissions are the so called post-treatment or aftertreatment methods. Post-treatment methods comprise chemical reduction of NO_x to N_2 by the selective catalytic reduction with ammonia, urea or cyanuric acid, the selective non-catalytic reduction, and fuel reburning. Other aftertreatment methods cover the oxidation of NO_x with subsequent absorption, taking advantage of the better solubility of NO_x at higher valence, and the use of sorbents to adsorb NO_x [14, 19]. Most of the mentioned methods are suited for stationary applications.

Considering that a significant amount of NO_x is emitted by mobile sources, in particular vehicles, new energy technologies such as hybrid vehicles and those motorized by fuel cells or hydrogen are in development in order to improve fuel efficiency and reduce emissions [24]. Despite the effort in new advances, the catalytic technologies like traditional catalytic converters applied since 1975 are still the functional technology to reduce emissions, due to their low cost and relative effectiveness. These methods are based on the catalytic NO_x decomposition, NO_x storage and reduction (NSR) and selective catalytic reduction (SCR) by NH_3 or hydrocarbons [5, 25, 26].

2.2 Selective catalytic reduction of NO_x with NH_3

The most efficient aftertreatment technology in NO_x abatement is the SCR of NO_x with NH_3 (NH_3-SCR), patented in the U.S. by Engelhard Corporation in 1957 [15]. Nowadays, it is a worldwide applied process on stationary sources and commercially attractive for mobile applications, i.e. it is already an applied technology in diesel vehicles [13, 15, 26-28]. NH_3-SCR broadly consists in reducing selectively NO_x with ammonia in the presence or absence of oxygen to harmless nitrogen and water by the aid of an appropriate catalyst. For safety and toxicity reasons in mobile applications, NH_3 is supplied from

nitrogen-containing chemicals such as urea which decompose in the presence of water into NH_3 and CO_2 [5, 29].

2.2.1 Type of NH_3-SCR reactions

Nitrogen oxide (NO), being the main NO_x component in exhaust gases, can react with a stoichiometric amount of NH_3 in the presence of oxygen according to the "standard SCR" reaction (Equation 2.1):

$$4NO + 4NH_3 + O_2 \rightarrow 4N_2 + 6H_2O \quad \Delta H = -4.07 \times 10^5 \text{ J/mol } NH_3 \qquad (2.1)$$

The standard SCR reaction works well at high temperatures (> 400 °C); however, it shows lack of efficiency at low temperatures which is considered disadvantageously for some specific applications such as diesel vehicles [27]. One alternative reaction that displays high activity in NO_x reduction at lower temperatures (180 - 300 °C) is the so-called "fast SCR" reaction, where an equimolar amount of NO and NO_2 reacts with NH_3 (Equation 2.2):

$$NO + NO_2 + 2NH_3 \rightarrow 2N_2 + 3H_2O \quad \Delta H = -3.78 \times 10^5 \text{ J/mol } NH_3 \qquad (2.2)$$

For the applicability of fast SCR on diesel vehicles, a part of the NO from engine exhaust is catalytically oxidized upstream of the SCR converter to NO_2 [6, 27, 30]. Nevertheless, it is not easy to establish the optimal NO/NO_2 ratio (Equation 2.2), because the activity of an oxidation catalyst, e.g. a diesel oxidation catalyst (DOC), varies with the temperature and flow rate of the exhaust gases.

In recent years a new reaction named "enhanced SCR" has shown higher performance than the standard SCR at low temperatures, but lower activity than the popular fast SCR; even though the pre-oxidation of NO is avoided which is beneficial for practical applications. In the enhanced SCR, NO is reduced by both NH_3 and ammonium nitrate [13, 31], according to the following reaction (Equation 2.3):

$$2NO + 2NH_3 + NH_4NO_3 \rightarrow 3N_2 + 5H_2O \qquad (2.3)$$

When NO_2 is added in excess, it reacts with NH_3 (2.4).This reaction proceeds with a lower activity than the aforementioned SCR reactions, therefore it is less relevant.

$$3NO_2 + 4NH_3 \rightarrow 3.5N_2 + 6H_2O \quad \Delta H = -3.41 \times 10^5 \text{ J/mol } NH_3 \qquad (2.4)$$

2.2.1 Catalysts used in NH_3-SCR

A suitable catalyst is essential for a proper performance of NH_3-SCR of NO_x. Therefore, different catalysts have been developed in order to achieve high activity, selectivity and stability within wide operating temperature windows. Suitable catalysts are both metal oxides and metal exchanged zeolites.

The catalyst used in European diesel vehicles since 2005 for standard SCR is a three-way catalyst, based on TiO_2-supported V_2O_5 promoted with WO_3. Some problems of the V_2O_5-WO_3/TiO_2 catalyst are its high activity for the oxidation of SO_2 to SO_3, a restricted optimal working temperature between 350 - 400 °C (at 550 °C it loses activity), and the volatilization of toxic vanadia species above 650 °C [5].

In the development of new catalysts, several metal oxides have been studied. Thus, it was found that manganese oxides with lower crystallinity display an excellent performance at low temperatures, but with relatively low N_2 selectivity. Other catalyst types are the bimetallic and composite oxides, where MnO_x-CeO_2 exhibits high activity and complete N_2 selectivity in the range of 100 - 150 °C, although it shows poor performance in the presence of H_2O and SO_2. The Pt/FC/C catalyst (platinum/fluorinated activated carbon/ceramic) is a catalyst with high water resistance along with over 90% NO conversion within 170 - 210 °C, although with a high cost since it contains a noble metal [28]. Besides metal oxides, the ion exchanged zeolite catalysts such as Fe-, Cu-, Mn- and Ce-zeolites have proved to be active in NH_3-SCR of NO_x. Furthermore, they have the advantage of lower cost and good thermal stability. Fe and Cu-based zeolites catalysts have been reported as the most effective, durable and suitable catalysts for the operating temperature range. Fe-zeolites show slightly lower reactivity at low temperatures, while Cu-zeolites are less reactive at high temperatures [26, 32, 33].

Suitable and amply studied zeolites for NH_3-SCR of NO_x comprise mordenite, ferrierite, Beta-zeolite, Y-zeolite and ZSM-5 [5, 6]. Fe-zeolites have been shown to be active in additional reactions, for instance N_2O decomposition, SCR with hydrocarbons, oxidation of benzene to phenol, epoxidation of propene and oxidative dehydrogenation of propane [34-36].

Particularly, iron-loaded ZSM-5 reveals higher activity than vanadia-based catalysts and also remarkable durability in the presence of H_2O and SO_2 for NO_x reduction in the NH_3-SCR [37, 38]. Additionally, it is already commercialized as automotive catalyst for SCR. The performance of Fe-ZSM-5 catalyst can be altered by diverse factors such as the Si/Al ratio of the zeolite, the ion-exchange degree or the preparation method. Thus, a correlation between the preparation method of Fe-ZSM-5 catalyst and their activity in the NH_3-SCR has been described [28]. Preparation procedures comprise aqueous or liquid ion-exchange (LIE), chemical vapor deposition (CVD) or solid state ion exchange (SSIE), improved aqueous or improved liquid ion-exchange (ILIE), and mechanochemical routes (MR) [39]. Differences in the preparation method influence the formation of diverse Fe species [28]. Based on UV-Vis-DRS and EPR investigations, it has been observed that Fe-ZSM-5 samples with low Fe content prepared by MR and ILIE methods produces highly dispersed Fe species as isolated

iron ions, while samples prepared by CVD and SSIE reflect considerable amount of isolated sites, but also Fe_xO_y clusters. Besides, LIE produces preferably large iron oxides clusters and small amount of isolated Fe sites [40].

According to Schwidder et al. [7], Fe-ZSM-5 catalysts prepared by SSIE with $FeCl_3$ achieved better activity in the fast SCR than those prepared by LIE with Fe content > 0.2 wt.%. Other authors mention that higher Fe loading in Fe-ZSM-5 and more isolated Fe^{3+} sites can be obtained using SSIE method, but increasing excessively the Fe content could lower the activity, similar to what happened by hydrothermal aging [8].

2.3 Structure-reactivity relationships of Fe-ZSM-5 in the NH_3-SCR

In order to correlate structure and composition of the catalyst with its activity, selectivity and stability not only the study of the active sites is important. Likewise, the synergetic interaction between active site and core structure, as well as the pure influence of the support are relevant. The latter can offer a high surface area along with a defined pore structure.

ZSM-5 has an aluminosilicate framework structure that consists of a three-dimensional channel system with an opened 10-ring of ca. 5.1 x 5.4 Å, and belongs to the MFI framework type [41]. Loading iron into the ZSM-5 zeolite leads to a complex material. Based on the characterization by spectroscopic and analytical techniques, different coexisting iron species could be distinguished, such as isolated Fe sites at extraframework cationic positions, binuclear oxo-ions, small oligonuclear Fe_xO_y clusters and Fe_xO_y nanoparticles [7-9]. UV-Vis and FTIR studies have shown specific cationic sites which can be occupied by transition metals in the MFI structure. The cationic iron sites named α, β and γ, along with their location are described as follow: α sites are located at the straight channels, β sites at the deformed six-membered rings at the intersection of straight and sinusoidal channels and γ sites at the sinusoidal channels (Figure 2.1) [42, 43].

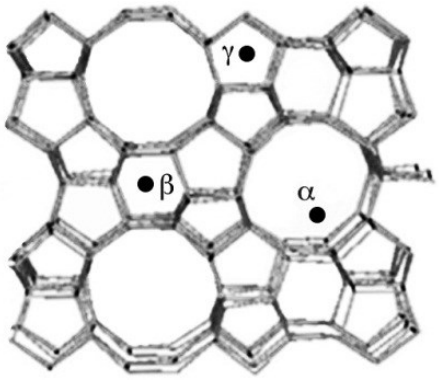

Figure 2.1 Pore positions of isolated Fe sites in Fe-ZSM-5.

In several studies, it was tried to attribute the activity in standard and fast SCR to specific sites of Fe-ZSM-5. Hence, based on spectroscopic studies (EPR, UV-Vis, FTIR), it was proposed that both isolated and oligonuclear Fe_xO_y clusters participated in standard SCR, whereas just a small amount of isolated Fe sites are working for the fast SCR [7, 10]. A correlation between exchanged oxo-Fe^{3+} sites and the catalytic performance in standard SCR was also found using temperature programmed desorption (TPD) of NH_3 and NO_2, as well as UV-Vis, Mössbauer and FTIR spectroscopies [44]. As another point of view, Brandenberger et al. [11, 12] referred activity in terms of turnover frequencies (TOF) of different Fe species to the temperature applied in the NH_3-SCR of NO_x. At temperatures < 300 °C isolated iron sites catalyze the reaction, while at higher temperatures Fe_xO_y species contribute mainly to the activity. The decomposition of NO_2 into NO and O_2 has also been studied and proposed to occur at the binuclear iron sites in Fe-ZSM-5 [45].

The role of Brønsted acid sites has also been discussed. A study over HY zeolite shows that Brønsted acid sites catalyze the decomposition of ammonium nitrite, an intermediate of the NH_3-SCR reaction [46]. Schwidder et al. [47] described that Brønsted acidity plays a vital role in the isobutane-SCR performance, while in NH_3-SCR large reaction rates were also achieved with non-acidic catalysts, even though acidity increases the activity, probably by the formation of more favorable iron sites. Using NH_3-TPD-FTIR and DRIFT spectroscopy in the NH_3-SCR of NO, it is described that Brønsted acidity of the catalyst is not a crucial factor for high activity because acidic sites are not required for activation of adsorbed NH_3, but might influence the iron dispersion [48]. Temperature programmed surface interaction (TPSI) and steady-state reaction analysis indicate that both Brønsted acid sites and added iron oxide are essential for NH_3-SCR of NO_x [49].

Despite these efforts, there is still significant controversy concerning the nature of active iron sites as well as the acidity effect over Fe-ZSM-5 for NH_3-SCR reactions. More agreement has been found in terms of the iron redox cycles which are needed for high catalytic performance. It has been reported that the permanent reduction of Fe^{3+} to Fe^{2+} under reaction condition is markedly lower in NH_3-SCR than during isobutane-SCR. Because the former reaction shows higher activity, it was concluded that reduced Fe^{2+} probably do not contribute to the catalytic activity. Additionally, a different reducibility was found for isolated tetrahedral and octahedral sites, the latter being more easily reduced [50]. Devadas et al. [51] proposed that faster reoxidation of Fe^{2+} to Fe^{3+} on Fe-ZSM-5 at temperatures above 300 °C, which explains the high activity in NH_3-SCR at high temperatures. A mechanistic study of the fast SCR on Fe-ZSM-5 catalysts has confirmed the significance of Fe^{3+} in the formation of the

intermediate surface nitrates and the interaction between acid sites and iron redox sites of the catalyst [33].

2.4 Mechanisms of NH_3-SCR over Fe-ZSM-5

Concerning the mechanism of the NH_3-SCR on Fe-ZSM-5, several proposals exist for the standard and fast SCR reactions as well as for the NO oxidation reaction which is considered as an important intermediate reaction of the standard SCR.

2.4.1 NO oxidation mechanism

NO oxidation (Equation 2.5) is one of the reactions that has been amply studied, and is considered by some authors as the rate-limiting step of standard SCR on metal-exchanged zeolite catalyst [4, 26, 32, 37, 51].

$$NO + 0.5O_2 \rightarrow NO_2 \quad \Delta H = -5.7 \times 10^4 \text{ J/mol NO} \qquad (2.5)$$

A theoretical investigation about the NO oxidation mechanism on Fe-ZSM-5 was done by density functional theory (DFT). This theoretical mechanism described as starting species an isolated iron $Z^-\{FeO\}^+$ where NO adsorbs forming $Z^-\{FeONO\}^+$, and from which NO_2 desorbs after co-adsorption of oxygen leaving behind $Z^-\{FeO_2\}^+$. Then, a second NO molecule reacts with $Z^-\{FeO_2\}^+$ to produce another NO_2 molecule and regenerates the initial $Z^-\{FeO\}^+$ site. It was also calculated that in the presence of water dihydroxylated and monohydroxylated iron sites are formed which exhibit lower or no activity for the oxidation [37]. Brandenberger et al. [5] mentioned a similar mechanism of NO oxidation over Fe-zeolites (Equation 2.6):

$$NO + Fe^{3+}\text{-}O \rightarrow Fe^{3+}\text{-}ONO \rightarrow Fe^{2+} + NO_{2(ads)} \qquad (2.6)$$

The formed Fe^{2+} is re-oxidized by gaseous O_2 from the reaction mixture.

Experimental and kinetic studies of NO oxidation in presence of feed NO_2 over Fe- and Cu-ZSM-5 have shown that NO oxidation is inhibited by increasing amounts of NO_2 in the NO_x feed, due to either obstruction of the active NO oxidation sites by competitive adsorption of NO_2, or oxidization of the transition metal which hinders oxygen adsorption and subsequent surface reaction. Moreover, pretreatment of the catalysts by different oxidizing/reducing agents (O_2, NO_2, H_2, and NH_3) did not disturb the steady state of only NO oxidation [32]. In contrast to that, our recent studies found that pretreatment in a feed containing a reducing agent, for instance NH_3, boost the activity for NO oxidation [52].

2.4.2 Mechanism of the standard SCR

A catalytic cycle of the standard SCR on Fe-ZSM-5 was first suggested by Delahay et al. [1]. The cycle starts with the Fe^{2+} oxidation with O_2 giving the Fe^{3+}-O, on which the extraframework oxygen reacts with NO to form a surface nitrogen oxide Fe^{3+}-N_xO_y (commonly adsorbed NO_2). Then, this Fe^{3+}-N_xO_y reacts with NH_3 forming N_2 and H_2O, while Fe^{3+} is reduced to Fe^{2+}, closing the cycle. Furthermore, they have proposed the reoxidation of Fe^{2+} as rate-limiting step of the reaction.

In addition to NO_2 as intermediate, adsorbed NO^+ has been introduced in the mechanism of standard SCR on BaNa-Y catalyst. The role of NO^+ is the formation of HONO in the presence of water [53]. Recent studies have identified nitrites/HONO as intermediates in the standard SCR reaction over Fe-ZSM-5 + BaO/Al_2O_3 mixture, in which BaO is used for trapping nitrites on Fe-sites [2]. Moreover, a mechanism for the standard SCR at low temperature was proposed (Equations 2.7, 2.8 and 2.9).

$$Fe^{3+}\text{-}OH + NO \rightarrow Fe^{2+} + HONO \quad (2.7)$$

$$HONO + Si\text{-}(ONH_4)\text{-}Al \rightarrow NH_4NO_2 + Si(OH)Al \quad (2.8)$$

$$NH_4NO_2 \rightarrow N_2 + 2H_2O \quad (2.9)$$

The nitrosonium ion has been detected on Fe-ZSM-5 by DRIFT spectroscopy, which is formed after adsorption of NO by participation of either Brønsted acid sites of the zeolite (Equation 2.10) or exchange Fe sites (Equation 2.11) [5].

$$2NO + 0.5O_2 + 2Si(OH)Al \rightarrow 2Si(O^-NO^+)Al + H_2O \quad (2.10)$$

$$NO + Fe^{3+} \rightarrow NO^+ + Fe^{2+} \quad (2.11)$$

Based on kinetic models the dual-site Langmuir-Hinshelwood mechanism was proposed for standard SCR on Fe-ZSM-5[26]. In this case NH_3 is adsorbed on acidic sites while NO oxidation occurred on Fe-sites. Then NH_3 reacts with surface NO_2 or HONO to form the NH_4NO_2 intermediate, which decomposes to N_2 and H_2O (Equation 2.9). It is not excluded that part of the NO_2 could also be formed by Eley-Rideal mechanism, where gaseous NO reacts with adsorbed O_2.

According to the temperature programmed surface interaction (TPSI) and steady-state dynamic reactions, a dual mechanism including Lewis (iron) and Brønsted acid sites is proposed, in which the presence of iron oxide deposited in H-ZSM-5 zeolite enhances NH_3 conversion over Lewis sites in standard SCR. Over H-SZM-5, the interaction of NO with NH_3(ads) on Brønsted sites results in N_2O formation [49].

2.4.3 Mechanism of the fast SCR

On V_2O_5-WO_3/TiO_2 catalyst the global fast SCR reaction is associated with a redox cycle involving the very effective re-oxidation of reduced V-sites by surface nitrates , which explains the higher rate of the fast SCR reaction compared to standard SCR chemistry, wherein the catalyst reoxidation is carried out by gaseous oxygen [54].

Theoretical investigations have tackled the mechanism of fast SCR over Fe-ZSM-5, in which NH_3 activation via amide species is proposed by Brüggemann and Keil [4]. It suggests the adsorption of NH_3 on isolated iron sites ($Z^-\{FeO\}^+$) as the first step of the reaction, followed by an internal rearrangement and NO adsorption forming the nitrosamine iron hydroxyl ($Z^-\{NH_2NOFeOH\}^+$). A further desorption of NH_2NO produces the monohydroxylated iron ($Z^-\{FeOH\}^+$), while NH_2NO decomposes easily into N_2 and H_2O. Finally, in order to recover the original active site a second NH_3 molecule is adsorbed forming water, and by reaction with NO_2, a second nitrosamine is obtained and the $Z^-\{FeO\}^+$ is recovered. On the other hand, Li and Li [9], propose a similar mechanism remarking the oxidation state of iron, Fe(III) as essential active site. In contrast to the above mentioned mechanism, NO is first adsorbed, the subsequent adsorption of NH_3 creates a reduced site ($Z^-\{Fe(II)OH\}^+$). The renewal of the oxidized active site occurs only with NO_2, but not with O_2 or NO + O_2, in coaction with NH_3.

An alternative mechanism of the fast SCR reaction proceeds by N_2O_3 formation from NO and NO_2 (Equation 2.12), which might easily adsorb on zeolites. This mechanism is based on the assumption that equimolar amount of NO and NO_2 produce a high yield of N_2O_3, where nitrogen has a suitable oxidation state (N^{3+}) to react with ammonia (N^{3-}) forming NH_4NO_2 (Equation 2.13) [5].

$$NO + NO_2 \rightarrow N_2O_3 \quad (2.12)$$

$$N_2O_3 + 2NH_3 + H_2O \rightarrow 2NH_4NO_2 \quad (2.13)$$

Another well accepted mechanism for the fast SCR at low temperatures on Fe-ZSM-5 was proposed by Grossale et al. [6], it involves NH_4NO_3 and related surface species as intermediates. NH_4NO_3 is formed by interaction between NO_2 and NH_3 (Equation 2.14), subsequent reaction with NO reduces the nitrate (Equation 2.15), and the sum of both reactions explain the fast SCR reaction. Additionally, it was observed that NH_4NO_3 formation on Fe-ZSM-5 is favored at low temperatures (150 °C), whereas reactivity between NH_4NO_3 and NO + NH_3 is detected only at 190 °C.

$$2NH_3 + 2NO_2 \rightarrow NH_4NO_3 + N_2 + H_2O \quad (2.14)$$

$$NO + NH_4NO_3 \rightarrow NO_2 + N_2 + 2H_2O \quad (2.15)$$

On Fe-Beta zeolites the reaction (Equation 2.15) does not occur at 50 °C which is named as the blocking effect of NH_3 on the fast SCR, the blockage does not refer to the NH_3 competitive chemisorption on catalytic sites. Instead, NH_3 captures the nitrates in an unreactive species at low temperatures. The reaction (Equation 2.15) on Fe-Beta catalyst starts at 140 °C, but at 200 °C part of the ammonium nitrate begins to decompose into the undesired N_2O (Equation 2.16) [55].

$$NH_4NO_3 \rightarrow N_2O + 2H_2O \quad (2.16)$$

In further *in situ* FTIR studies, it was proposed that surface nitrates/nitrites formation happens on ferric sites in Fe-ZSM-5 (Equation 2.17). This was concluded from the fact that the nitrate band on the free iron H-ZSM-5 is five-fold smaller than on Fe-ZSM-5. Nitrites could not be detected by FTIR which is caused by either their high reactivity or by the fact that their characteristic bands are in the region of others zeolite bands. The reduction of nitrates by NO is also related to the reduction of the iron sites (Equation 2.18). Finally, the surface nitrite or nitrous acid can interact with NH_3 or NH_4^+ (adsorbed on Brønsted sites) forming ammonium nitrite which decomposes immediately into N_2 and H_2O (Equation 2.19) [33].

$$NO_2 + Fe^{3+}\text{-}OH \rightarrow HONO + Fe^{3+}\text{-}NO_3 + H_2O \quad (2.17)$$

$$2NO + Fe^{3+}\text{-}NO_3 \rightarrow 2NO_2 + Fe^{2+}\text{-}NO \quad (2.18)$$

$$HONO + NH_3 \rightarrow NH_4NO_2 \rightarrow N_2 + H_2O \quad (2.19)$$

NO_2 can be similarly stored in the form of nitrates on Cu-ZSM-5 as well as Fe-ZSM-5 at 150 °C, those surface nitrates are reported to be unstable in the presence of NO creating NO_2 in the gas phase, which is in agreement with the abovementioned (Equation 2.15) [32].

As aforementioned the mechanism of the fast SCR has been proposed via NH_2NO formation and the reoxidation of Fe^{2+} by NO_2 been remarked. On the other hand, other authors have suggested a mechanism which proceeds via formation of N_2O_3. However, for these two proposed mechanisms neither NH_2NO nor N_2O_3 have been experimentally detected. Additionally, a mechanism that involves NH_4NO_3 and NH_4NO_2 as intermediates have been suggested, their formation is proposed to occur on ferric sites in Fe-ZSM-5, but no real nature of these ferric sites have been described. Based on this controversy about the mechanism of the fast SCR and nature of iron species involve on the intermediate reactions, in this work comprehensive *in situ* FTIR and EPR spectroscopic studies were done over Fe-ZSM-5.

2.5 Characterization of Fe-ZSM-5 catalysts

There are three levels of fundamental research on heterogeneous catalysis for the development of better and more efficient catalysts; the so defined macroscopic, mesoscopic and microscopic levels [56]. The macroscopic level is related with the engineering aspects of a reaction, the test reactors and the catalyst bed. The mesoscopic level comprises the structure-reactivity relationship, activity per unit surface area and/or kinetic studies. The third level corresponds to the comprehension of the mechanism, theoretical modeling and surface science. Spectroscopy, microscopy, diffraction as well as thermoanalytical techniques are amply used in the mesoscopic and microscopic studies.

Investigations at all levels have been performed in this work with the aim to derive a complex picture on the operation of Fe-ZSM-5 catalysts in SCR reaction.

2.5.1 Spectroscopic characterization

Spectroscopic characterization techniques are based on exposing the sample to a beam of e. g. photons, electrons, ions, neutral atoms and/or to magnetic, electrical or thermal fields which interact with it and emit a response that is analyzed in order to get information about the surface chemistry, intermediates, active and spectator species, and the bulk structure.

Methods such as UV-Vis, EPR, EXAFS and Mössbauer spectroscopy have been used to characterize Fe-ZSM-5 for the NH_3-SCR of NO_x. Likewise, other techniques have been employed such as TEM, XRD, MCD, TPD or TPR. FTIR spectroscopy has been also widely applied in order to study the surface species formed in the reaction over Fe-ZSM-5 [1, 7, 34, 44, 51].

This work focused on the *in situ* characterization of the Fe-ZSM-5 catalyst with the application of FTIR, EPR and UV-Vis spectroscopy. Therefore, a more detailed description of the principles and possibilities of these spectroscopic methods is given.

2.5.1.1 FTIR spectroscopy

Infrared radiation (IR) is usually divided into three spectral regions called near-, mid- and far-IR. Mid-IR is widely used for characterization in catalysis; it corresponds to the range of the electromagnetic spectrum from 400 to 4000 cm^{-1}, frequency (ν) denoted in terms of wavenumber ($\bar{\upsilon}$), by its dependence $\bar{\upsilon}=\nu/c$ (c being the speed of light). Thus, $\bar{\upsilon}$ is directly proportional to the energy of the quanta ($E=h\nu$) [57].

Absorption of radiation with a frequency in the mid-IR promotes the transition between molecular vibrational levels, but only vibrations leading to a variation in the dipole

moment in the molecule will lead to an absorption band in IR spectroscopy, due to the selection rules. This distinguishes IR from Raman spectroscopy, where the selection rules require that the molecular polarizability changes during the vibration [56]. The intensity of the IR band is proportional to the change in dipole moment; hence, species with polar bonds like OH exhibit a strong IR band, while that with covalent bonds such as N=N display a weak band. In general, the vibrational frequencies (ν) increase as the strength of the bonds rise, as well as the mass of the vibrating atoms decreases. Additionally, the interaction of different functional groups or chemical surroundings in the molecule changes the vibrational frequency giving a characteristic frequency of certain bonds in the molecule; this enables the identification of functional groups or species, for instance, on the surface of heterogeneous catalysts. Different vibrational OH modes can be distinguished in Fe-ZSM-5, such as isolated hydroxyls, hydroxyls attached to extraframework aluminum or acidic bridged hydroxyls [58]. Furthermore, intermediates of the NH_3-SCR of NO_x reaction such as NO^+, Fe^{n+}-NO and N_xO_y, can also be detected by their characteristic vibrations in IR [59].

2.5.1.2 EPR spectroscopy

Elementary particles for instance electrons are characterized by scalar quantities such as mass or charge, as well as by a vector quantity called angular moment or spin (S). The spin has an associated magnetic moment (μ) which is antiparallel to the spin itself (Equation 2.20),

$$\mu = - g_e (\mu_B/\hbar) S \qquad (2.20)$$

where g_e is the g value of a free electron, μ_B is the Bohr magneton, and $\hbar = h/2\pi$ (with h being Planck's constant).

In absence of a magnetic field, the magnetic moments and therefore the corresponding spin vectors of free electrons are randomly aligned; but in the presence of a magnetic field the magnetic moments tend to align in the orientation of the z axis of a Cartesian frame, producing a splitting of the energy level. The splitting of the electron spin energy level into two levels by an external magnetic field is called the Zeeman Effect (Figure 2.2, a). With two energy levels, the electrons assume one of the two spin states S_z, which have an opposite orientation along the z axe and take the values of $S_z = 1/2$ and $S_z = -1/2$. In the absence of an external magnetic field both states are degenerated [60].

The energy splitting between the two spin states is proportional to the applied magnetic field; applying the spin Hamiltonian to the wavefunction of the spin states, the energy difference between this two states is obtained (see equation in Figure 2.2, a). Through absorption of the specific energy difference, usually in the microwave region, the inversion of

the spin of an unpaired electron is undergone, giving a spectrum of the spin transition (Figure 2.2, b), which is the principle of electron paramagnetic resonance (EPR). Considering this concept, EPR is only applied for the characterization of materials with unpaired electrons.

In practical applications, EPR spectra are commonly recorded and introduced in the form of a first derivative (Figure 2.2, c).

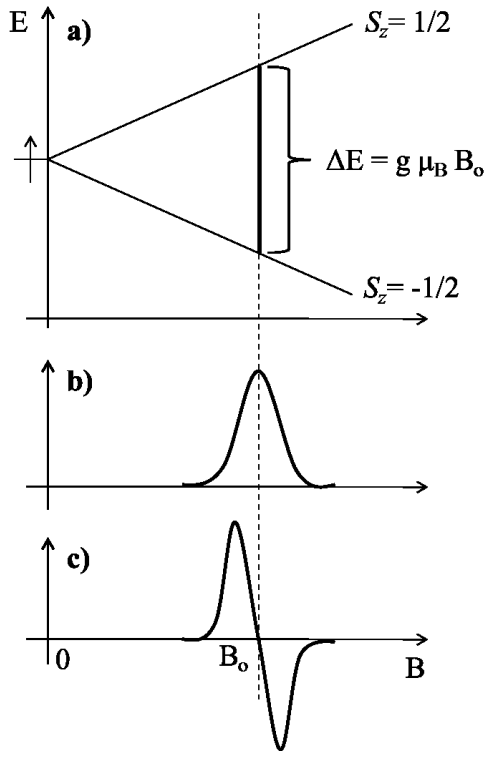

Figure 2.2 Zeeman Effect for an isolated electron in a magnetic field B (g correspond to the g value and B_o is the field of resonance) a); absorption spectrum b) and first derivative EPR spectrum c).

The relevant information obtained by EPR concerns the nature, symmetry and electronic structure of the paramagnetic center and of its surroundings. For example in Fe-ZSM-5, EPR spectroscopy offers knowledge concerning symmetry, electronic structure and the extent of aggregation of Fe^{3+}. Since Fe^{3+} contains five unpaired electrons in high spin configuration, their corresponding EPR spectrum is possible to obtain. Due to the iron located in specific sites in ZSM-5 which gives defined iron Fe^{3+} centers, there is a characteristic EPR spectrum for Fe-ZSM-5, where signals at $g \approx 6$, 4.3, 2.3 and 2 have been observed. The signals at $g \approx 6$ and 4.3 were assigned to an isolated Fe^{3+} in strongly distorted octahedral and tetrahedral coordination, respectably. Whereas, the signal of $g \approx 2$ was attributed to a highly symmetric isolated Fe^{3+} sites and $g \approx 2.3$ to Fe_xO_y clusters [50].

2.5.1.3 UV-Vis spectroscopy

UV-Vis spectroscopy covers the electromagnetic region from 50000 - 10000 cm^{-1} (200 - 1000 nm). By adsorption of energy in the UV-Vis range, pure electronic transitions can be obtained for isolated atoms, while rotational and vibrational motions are also simultaneously excited for molecules. As the energy or excitations roughly follow the order $\Delta E_{electronic} > \Delta E_{vibrational} >> \Delta E_{rotational} \approx 10^3$, the transitions are basically determined by the change in the electronic energy [61]. However, low energy transitions such as vibrations typically co-exist, and are responsible for the band shape; thus, the UV-Vis spectra are considered to be composed of bands (as opposed to lines). The position of the band corresponds to the energy difference between the two electronic levels involved in the transition [62]. For observing an electronic transition, the transition must satisfy several conditions formulated in the selection rules; otherwise they are forbidden and unseen, or weakly observed due to the small absorption coefficients.

Electronic transitions in complexes referred as ligand-to-metal charge transfer (LMCT) and intervalence charge transfer (IVCT); and transitions in extended solid structure like bandgap transitions [62].

The UV-Vis spectrum provides information on the electronic structure of molecules, the valence and coordination of metal cations, the particle size, the bandgap of solids and the presence and nature of defects in solids.

In UV-Vis spectra of Fe-ZSM-5, the d-d transitions of Fe^{3+} are very weak and almost undetectable, since they are spin and Laporte forbidden. The observed transitions in the ultraviolet region are the LMCT of $O^- \rightarrow Fe^{3+}$, which are spin and dipole allowed. These LMCT bands appear regularly at high energy values, yet they can also emerge at lower energies ($\lambda > 300$ nm) when there is a higher nuclearity of iron like e.g. in clusters. Different Fe^{3+} species have been characterized by the position of the bands [10, 34], such as isolated tetrahedral and octahedral Fe^{3+} sites found at $\lambda < 250$ nm and between 250 - 300 nm, respectably; small oligonuclear Fe_xO_y clusters located between 300 - 400 nm and Fe_xO_y nanoparticles at $\lambda > 400$ nm.

2.5.2 *In situ* and *operando* spectroscopic characterization

For rational development and improvement of catalysts, as well as reliable understanding of their performance under real reaction conditions, *in situ* and *operando* characterization methods are necessary. They have been established thanks to the technological developments in cell-design, data acquisition and analysis of obtained chemical

information. However, industrial catalysts and catalytic processes are often very complex and the development of suitable *in situ* characterization methods is still challenging [63].

In heterogeneous catalysis, the structural and electronic properties of the active sites in a catalyst are usually affected by the chemical environment in which the reaction operates. Therefore, *in situ* techniques are applied to investigate the active sites and characterize their electronic and structural properties during operative reaction conditions such as temperature, pressure and reactant concentrations. Additionally, time is an important parameter to be considered in the investigation of a catalytic process. The activation and breaking of chemical bonds occurs in the range of picoseconds and the full reaction cycle in the rate of milliseconds to minutes; hence, optimal characterization might be done in this time range. In order to obtain information about the catalytic processes, the *in situ* experiments can be performed under steady-state conditions, without variation of temperature, pressure or reaction rate. Furthermore, information regarding the reaction mechanism is achieved in a non-steady-state, in which structural properties of the catalyst and lifetime of surface intermediates are perturbed by changing temperature or pulsing the concentration of reactants [64].

Combining simultaneous measurements of catalytic activity/selectivity and *in situ* spectroscopy characterization of the catalysts is called *operando* spectroscopy. This methodology allows the characterization of the catalytic materials under realistic catalytic operative conditions [65, 66].

An example for *in situ* investigations of Fe-ZSM-5 is the *in situ* EPR study of the α-oxygen (O^- radical anion) that was confirmed upon contact with N_2O [67]. Also, *in situ* soft X-ray absorption spectroscopy found that Fe-ZSM-5 is an extremely flexible redox system, where the iron is dominantly in the oxidation state Fe^{3+} [68]. Similarly, *in situ* FTIR or DRIFTS was used to investigate the Brønsted acidity of Fe-ZSM-5 and intermediates of the mechanism for NH_3-SCR of NO_x [2, 8, 33].

By an extensive characterization of Fe-ZSM-5 in the standard SCR with *in situ* UV-Vis and EPR spectroscopy, the oxidation of NH_3 at high temperatures was reported to occur on Fe_xO_y clusters. Since in the catalyst with high iron content Fe-Z(1.2) (1.2 wt.% Fe) the NH_3 conversion increase at high temperatures (in comparison to the NO conversion), while in catalysts with low iron content Fe-Z(0.3) and Fe-Z(0.2) the NO and NH_3 conversions are equal over the whole temperature range [10].

Catalyst characterization by combining *in situ* spectroscopic methods has also been done on metallo-zeolites. For example Sobalik [69] proposed an approach to the quantitative *in situ* FTIR/UV-Vis study in the NH_3-SCR of NO, and N_2O decomposition.

2.5.3 Other characterization techniques

XRD is amply used in the catalyst characterization of zeolites, hence for Fe-ZSM-5 to analyze changes in the crystal structure during the thermal aging on the NH_3-SCR of NO_x, or identified crystalline Fe_2O_3 particles forming due to the preparation [1, 8].

The coexistence of small particles between 5 - 20 nm and larger particles around 20 - 50 nm in Fe-ZSM-5 was determined with TEM [10, 51].

Hydrothermal deactivation of Fe-ZSM-5 during the reduction of NO with NH_3 has been investigated and characterized by several techniques: H-TPR, DRIFTS, ^{27}Al-NMR, ^{29}Si-NMR and XAS [70]. Additional characterization of Fe-ZSM-5 was done measuring the BET surface area, determining iron content by ICP-AES, or by investigating Brønsted acidity with NH_3-TPD [44].

3. Methodology

3.1 Synthesis of the catalysts

Fe-ZSM-5 catalysts were synthesized by the project partners at the University of Bochum. The catalyst labeled CFeZ (Zeolyst product: CP7117) was purchased from Zeolyst International Company (USA), having a Si/Al ratio of 12.1 and iron content of 0.82 wt.%. It was calcined in order to remove the NH_4^+ ions still present in the sample. This was done under flow of synthetic air (20.5%), with a ramp of 2 K min^{-1} from room temperature to 150 °C. After 15 minutes of isothermal period, the temperature was ramped at 5 K min^{-1} and kept at 500 °C for 5 hours.

The catalysts were synthesized in Bochum by different preparation methods such as improved liquid ion exchange (ILIE), liquid ion exchange (LIE), solid state ion exchange (SSIE-I) and solid state ion exchange with pre-introduced co-cation (SSIE-I-Na/Ca) [71]. The labels of the catalysts correspond to the preparation method and iron content, for example the sample ILIE-0.46 was prepared by improved liquid ion exchange and contains 0.46 wt.% Fe. For the sample SSIE-I-Na, the suffixes rep, low and high mean reproduce sample (sample synthesized in a second batch), lower and higher amount of co-cation, respectively (Table 4.1).

The parent material NH_4-ZSM-5 with a Si/Al ratio of 13.89 was supplied by Tricat Zeolites GmbH Bitterfeld, now a branch of Clariant Company. The H form (H-ZSM-5) was obtained by calcination of NH_4-ZSM-5 in synthetic air (20.5%) at 500 °C for 5 hours. The SSIE-I samples were prepared by heating the H-ZSM-5 mixture with $FeCl_3 \cdot 6\ H_2O$ under N_2 flow, the heating ramps are described as follows: first, the mixture was heated to 150 °C with a temperature ramp of 2 K min^{-1} to protect the pore system of the zeolite from being destroyed by vaporized water. Then, the temperature was increased to 300 °C with a rate of 5 K min^{-1} and kept for 1 hour. After cooling, the sample was washed with deionized water and dried at room temperature. For the SSIE-I-Ca/Na series, the NH_4-ZSM-5 was initially exchanged in aqueous solution of $NaNO_3$ or $CaCl_2$ with different concentrations, and the product was transferred into the H form as mentioned above. Partial exchange of NH_4^+ by Na^+ or Ca^+ ions was done in order to modify the site distribution of the iron subsequently introduced.

The preparation of ILIE samples involved an exchange of NH_4-ZSM-5 with Fe^{2+} generated *in situ* from iron powder in 0.1M HCl. It was achieved by stirring the suspension at pH=1 for 5 days at room temperature and under inert gas. Afterwards, the sample was washed with water to remove all chloride and finally it was dried at room temperature.

In the LIE samples, the NH_4^+ in NH_4-ZSM-5 are exchanged by Fe^{3+} using a solution of $Fe_2(C_2O_4)_3 \cdot 6H_2O$ (0.01M) for 24 h under exclusion of light.

The final step after the different preparation methods was the calcination of all samples, which was done in synthetic air at 600 °C for 2 h.

3.2 Catalytic activity tests

The catalysts were tested in the NO oxidation, standard SCR and fast SCR reactions. All catalytic tests were done by the project partners at the University of Bochum, more details are described elsewhere [71].

Catalytic data were measured in a parallelized reactor setup containing six microflow quartz reactors (4.2 mm i.d.) in the temperature range of 150 - 600 °C. In standard SCR, the feed consists of 1000 ppm NO, 1000 ppm NH_3, and 2% O_2, balanced with He, while in fast SCR 500 ppm NO and 500 ppm NO_2 instead of 1000 ppm NO were dosed. In NO oxidation, 1000 ppm NO and 2% O_2, balanced with He were dosed. For all reactions, the same Gas Hourly Space Velocity (GHSV) of 750 000 h^{-1} was adjusted by the use of 10 mg catalyst (250 - 350 µm particle size) and a total flow of 183.3 ml min^{-1}. Conversions were measured at steady state at a given temperature for all six reactors, before the reactors were heated to the next reaction temperature (temperature step: standard – 50 K, fast – 25 K, heating rate 5 K min^{-1}). The product gas was analyzed for NO, NO_2, and NH_3 conversions by using non-dispersive IR photometry for NO and NH_3, and UV spectrometry for NO_2 (XStream X2, Rosemount Analytical; Emerson). To monitor the formation of side products, in particular N_2O and to check the NH_3 conversion, a quadrupole mass spectrometer (Omnistar, Pfeiffer) was employed. N_2O was not formed to any significant extent in the experiments. During standard SCR, NO_2 could not be detected either. For the analysis of fast SCR reaction mixtures, an NH_3-trap (inert towards NO_x; Bühler) was inserted prior to the XStream to prevent the formation of ammonium nitrate in the cuvettes. NH_3 and NO_2 conversions were then evaluated from the mass-spectrometric data. The quality of the analysis was checked in special experiments with N_2 analysis and the N balance was found to close within ± 5%. The catalytic behavior will be reported in terms of conversions changing with temperatures.

The reaction rates r_{Fe} are normalized to the amount of iron present, as follow:

$$r_{Fe} = \frac{1}{v_i n_{Fe}} \frac{dn_i}{dt}$$

where v_i is the stoichiometric coefficient and i stands for NO (NO oxidation and standard) or NO_x (fast).

3.3 Catalyst characterization

The iron, aluminum and silicon contents were determined by ICP-OES (inductively coupled plasma optical emission spectrometry) and AAS (atomic absorption spectroscopy), using a Varian 715 ES spectrometer and AA220 Varian, respectively. ICP-OES analyses were carried out after dissolution of the samples in HNO_3 +HCl/HF at 200 °C for 2 hours in a microwave oven. For AAS measurements, 30 mg (for the determination of Fe) or 100 mg (for the determination of Na or Ca) of the catalyst were melted with 400 mg Na_2O_3 /$LiBO_2$ in a muffle furnace and posteriorly dissolved in diluted HNO_3.

The pore volume and pore diameter of the catalyst were analyzed by physisorption of N_2; using a Belsorp-max instrument (BEL). Prior to the analysis, the samples were dehydrated at 300 °C for 2 hrs. The determination of the pore volume was done via the BJH method, while the pore diameter was established by the Saito-Foley method (considering a cylindrical pore geometry) [72].

3.3.1 *In situ* and *operando* spectroscopic characterization

3.3.1.1 FTIR spectroscopy

The *in situ* FTIR measurements were carried out on a Nicolet 6700 FTIR spectrometer (Thermo Scientific) equipped with a heatable and evacuable homemade reaction cell with CaF_2 windows. Different gas mixtures with a total flow of 50 ml min^{-1} were provided by mass flow controllers (Bronckhorst) and introduced through the gas inlet. With a heating coil and thermocouple the temperature was controllable in the range from room temperature to 450 °C, the desired temperature and respective ramps were differently established according to the specific experiment. The CaF_2 windows were constantly cooled down with water in order to avoid damage caused by the high temperature (Figure 3.1, left).

The powder samples were pressed at 8 tons into self-supporting discs with a diameter of 20 mm and a weight of 50 mg. The pressed sample was located in a quartz sample-holder and introduced in the reaction cell, as show in a partial constructed cell (Figure 3.1, right). Posteriorly, the cell was placed inside of the compartment, and then the orientation of the cell was fixed to the most suitable measuring point where the IR beam can properly transmit through the sample disc. Once the suitable position has been found, it was used to perform all the experiment.

For *in situ* FTIR measurements, temperatures and concentrations of the gases were varied during the experiments; detailed values of these parameters are given together with the results (next chapter). The spectra were collected in transmission mode using the program

OMNIC, in the range from 4000 to 1000 cm^{-1} and with a resolution of 2 cm^{-1}. The background spectrum was carried out without the cell and with only dried-air inside of the cell compartment at room temperature.

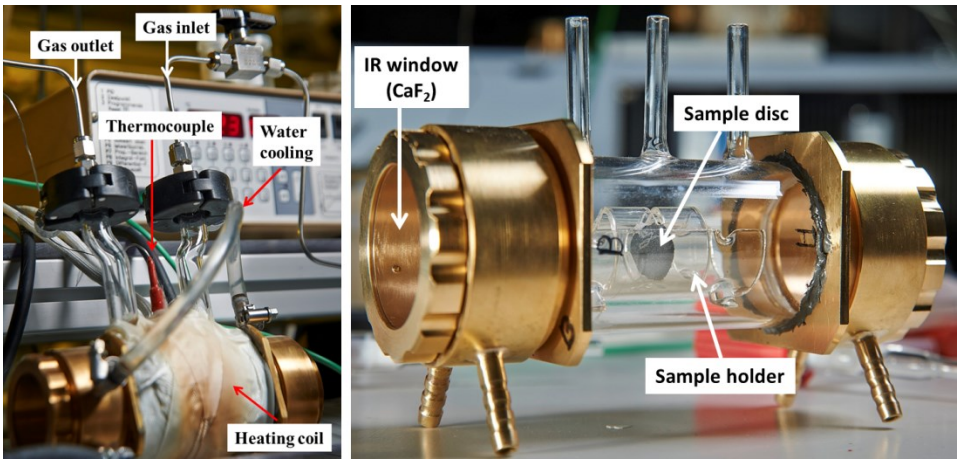

Figure 3.1 Cell used for the *in situ* FTIR measurements.

In order to determine the acidity of the catalyst, the adsorption of the probe molecule pyridine was used. Pyridine adsorption measurements were performed using Brucker Tensor 27 spectrometer. The preparation of the sample disc, usage of the same homemade cell and the establishment of the appropriated position of the cell were also done as described above.

The samples were pretreated by heating in He up to 400 °C, and keeping at this temperature for 10 minutes. Afterwards, the sample was cooled down to 150 °C, and by passing Ar (50 ml min^{-1}) through a saturator filled with pyridine, the pyridine was dragged into the cell. The pyridine adsorption was done at this temperature, while the pyridine desorption was carried out heating the cell in vacuum up to 400 °C in 50 °C steps, in which the spectra were taken. The spectrum of the pretreated catalyst was subtracted from the spectrum of pyridine adsorption. The Brønsted acidity value was calculated from the spectrum at 150 °C.

3.3.1.2 EPR spectroscopy

Operando EPR experiments were performed in X-band on a cw-spectrometer ELEXSYS 500-10/12 (Bruker), with a microwave power of 6.3 mW, a modulation frequency of 100 kHz, and modulation amplitude of 0.5 mT (6900G). The spectrometer was equipped with a heatable homemade quartz plug-flow reactor, the inlet was connected to gas-dosing mass flow controllers (Bronckhorst) and the outlet was connected to the quadrupole mass spectrometer (Omnistar, Pfeiffer Vacuum GmbH) for the online product analysis (Figure 3.2).

Around 30 mg of sample of particle size between 315 - 250 μm were used for all *operando* experiments. The concentration of the gases and temperature was adjusted for every experiment as will be described in the results chapter.

The *ex situ* EPR measurements were carried out with the same spectrometer and parameters, using standard EPR tubes where the as-received sample was introduced for the room and low temperature measurement.

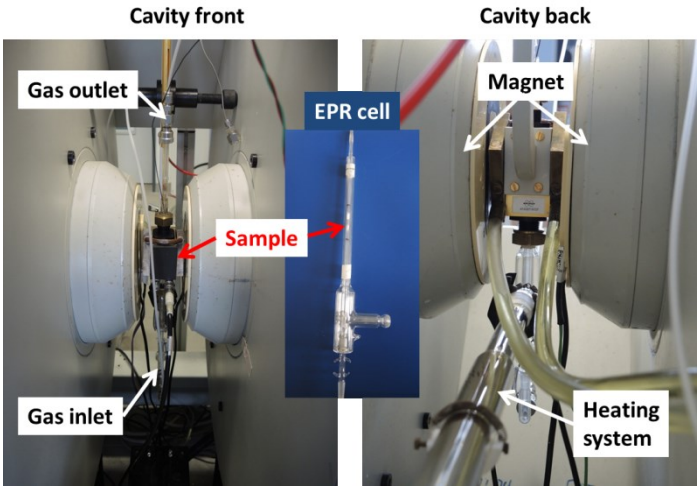

Figure 3.2 *In situ* cell in the cavity of the EPR spectrometer.

3.3.1.3 UV-Vis spectroscopy

UV-Vis-DR spectra of as-received samples were recorded at room temperature using a Cary 400 spectrophotometer (Varian) equipped with a diffuse reflection accessory (Praying mantis, Harrick). For measurements, 30 mg of catalyst powder were filled into the sample holder in the sample compartment of the Praying mantis. $BaSO_4$ was used as reference material to record the baseline. The spectra were collected in diffused reflection mode in a range from 200 to 800 nm. All spectra were converted into the Kubelka-Munk function F(R). For quantitative analysis the spectra were deconvoluted using the GRAMS/32 code (Galactic).

In situ UV-Vis experiments were measured by either the same Cary 400 or the AvaSpec-2048 fiber optic spectrometer (Avantes) with a high temperature reflection probe of 1.5 mm diameter (FCR-7UV200-2-1,5x100-HTX), and AvaLight-DH-S-BAL as a light source. For *in situ* UV-Vis measurements, a high-temperature reaction chamber (Harrick) was set up in the Praying mantis accessory. During the experiments the temperature was controlled with the Automatic temperature controller (Harrick), and the gases (reactants) supplied by mass flow controllers (Bronckhorst). For each experiment, 55 mg of the samples with particle size 250 - 315 μm were filled into the reaction chamber.

3.3.2 Combined spectroscopic techniques (DRIFT/UV-Vis-DRS)

Some analyses were done by the coupling system DRIFT/UV-Vis-DR. The IR measurements were done with a Nicolet 6700 FTIR spectrometer and a DRIFTS high-temperature reaction cell (Harrick). For UV-Vis measurement, a high temperature reflection probe of 1.5 mm diameter (FCR-7UV200-2-1,5x100-HTX) was implemented into the Harrick cell (Figure 3.3). The high temperature reflection probe was connected to the AvaSpec-2048 spectrometer and the light source AvaLight-DH-S-BAL.

The temperature ramps during the experiment were controlled by the Automatic temperature controller (Harrick) in connection with cooling by a water circulation system. With mass flow controllers (Bronckhorst) the reacting gases were supplied in a total flow of 30 ml min^{-1}. The gases were introduced through the gas inlet from the bottom to the top, passing through the 55 mg of the sample (250 - 315 μm) in every experiment.

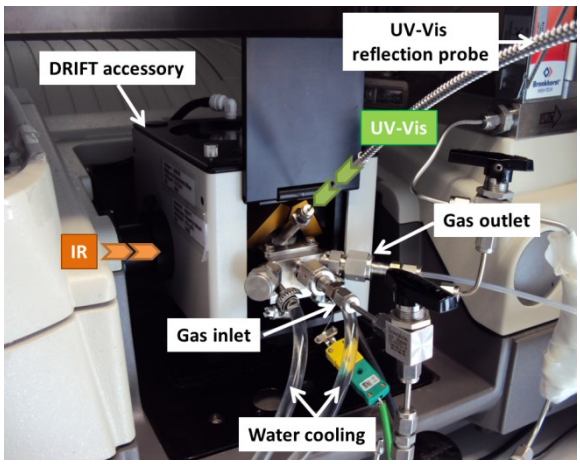

Figure 3.3 Coupling DRIFT/UV-Vis-DR systems.

4. Results and discussion

Fe-ZSM-5 catalysts were investigated for the different NH_3-SCR of NOx reactions (standard and fast SCR). For some samples, additional cations such as Ca or Na has been introduced to modify the iron speciation. In order to have a better understanding of the catalysts and their catalytic behavior, some physical and chemical properties were determined (Table 4.1).

The iron and secondary cation content, micropore volume (v_p), pore diameter (d_p), and Brønsted acidity are displayed for all investigated catalysts in Table 4.1. The iron content measured by ICP-OES fell in the range from 0.15 to 0.82 wt.%. The v_p decreased with the Fe and/or Na/Ca loading, which suggests an effective exchange in the cationic pore positions. The drop of v_p is markedly seen in the series of SSIE-I-Na/Ca catalysts, where the micropore volume decreased from 0.08 for SSIE-I to 0.05 for the sample with the highest amount of co-cations. The d_p of the Fe-loaded samples increased slightly in comparison to the H-ZSM-5 sample, which might be due to minor structural damage made during the preparation methods.

Table 4.1 Textural and chemical properties of Fe-ZSM-5 catalysts.

	Fe content (wt.%)	Exchange degree (Na/Al or Ca/Al)	v_p (cm^3g^{-1})	d_p (nm)	Brønsted acidity*
H-ZSM-5	0.03	-	0.12	0.51	11.87
LIE-0.15	0.15	-	-	-	9.59
ILIE-0.46	0.46	-	-	-	13.65
ILIE-0.68	0.68	-	0.09	0,56	11.25
SSIE-I-Na-0.27-rep	0.27		-	-	-
SSIE-I	0.24	-	0.08	0.52	-
SSIE-I-Ca	0.28	0.24	0.06	0.54	-
SSIE-I-Na(low)	0.27	0.52	0.07	0.54	-
SSIE-I-Na(high)	0.26	0.83	0.05	0.54	-
CFeZ	0.82	-	-	-	10.32

* Derived from the area of the IR band at 1544 cm^{-1} at 150 °C

The Brønsted acidity value was obtained by integration of the IR band intensity of pyridine fixed to Brønsted acid sites (band at 1544 cm^{-1} after adsorption of pyridine) and is also shown in Table 4.1. The acidity of Fe-loaded samples was mostly lower than the acidity of H-ZSM-5 due to cation exchange, in which protons in the extraframework positions are

replaced by iron ions. An exception occurred for the ILIE-0.46 sample, which showed more Brønsted acid sites than H-ZSM-5; this can be explained by defects or vacancies produced in the framework structure during the preparation treatment.

4.1 Determination of active sites in the fast SCR reaction

The identification of active sites for the fast SCR, and their preferred formation by specific preparation methods are a topic of interest, since fast SCR performed much better than standard SCR at low temperature with Fe-ZSM-5. Some studies have already been done in this respect, for instance Schwidder et al. [7] have claimed that standard SCR proceeds on isolated and oligomeric Fe sites, while fast SCR over small concentration of isolated iron sites. Yet, no detailed knowledge of the structure and position of such a sites is available so far. Therefore, it was the aim of this part of the thesis to identify the species responsible for catalyzing the fast SCR.

In order to determine catalytically active sites in fast SCR, various Fe-ZSM-5 samples were prepared in this work by different methods, tested in the NH_3-SCR reactions and characterized by *in situ* and *operando* spectroscopic techniques under standard and fast SCR conditions. The Fe-ZSM-5 catalysts applied in the study were ILIE-0.68, ILIE-0.46, SSIE-I-Na-0.27-rep, LIE-0.15; additionally, the Fe-free sample H-ZSM-5 was taken for comparison.

4.1.1 Catalytic activity

The catalytic and kinetic data of the investigated samples under standard SCR, obtained by the project partner at the University of Bochum, are reported in Figure 4.1. A similar conversion of NO and NH_3 was detected, even at high temperature, except for SSIE-I-Na-0.27-rep (compare A and B, Figure 4.1). It suggests that the samples predominantly contain isolated iron sites, inactive in the NH_3 oxidation, letting NH_3 act as a reducing agent and not being self-oxidized along the temperature range.

Higher NO conversion is obtained at temperatures above 400 °C for all Fe-ZSM-5 samples, while H-ZSM-5 showed almost no conversion in standard SCR along the entire temperature range. Around 80% of NO conversion is achieved at 550 °C with samples containing larger amount of iron (ILIE-0.68 and ILIE-0.46), while SSIE-I-Na-0.27-rep and LIE-0.15 show less than 50% of NO conversion at the same temperature (Figure 4.1, A). SSIE-I-Na-0.27-rep displays a slightly lower NO conversion than LIE-0.15, despite the fact that it contains a higher amount of iron. The reason might be that SSIE-I-Na-0.27-rep contains more Fe_xO_y clusters and nanoparticles which reduce the accessibility of all iron sites to the

reactants. The clusters and nanoparticles were observed in SSIE-I-Na-0.27-rep by UV-Vis and EPR spectroscopy, as described later (Figure 4.3 and Figure 4.4).

The activation energies of three samples obtained from the Arrhenius plot are indicated in Figure 4.1 C, the values are in agreement with those reported in the literature (44 - 61 KJ/mol [5]). There is a tendency of increasing activation energy in dependence on increasing iron content.

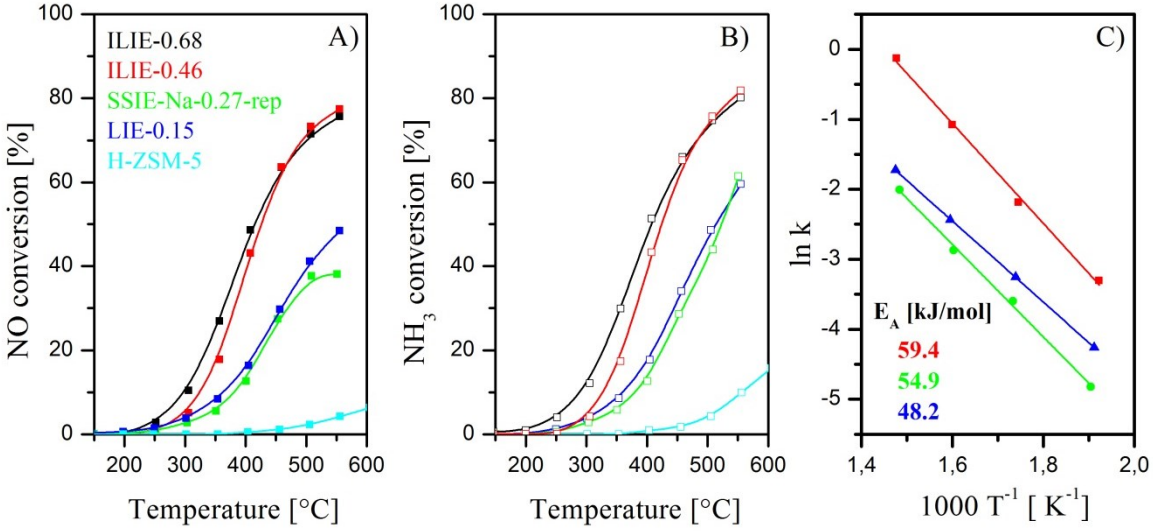

Figure 4.1 Standard SCR over Fe-ZSM-5 catalysts, dependence of NO (A) and NH_3 conversion (B) on temperature, and Arrhenius plot (C).

In Figure 4.2, the catalytic behavior in fast SCR is reported. Generally, all catalysts display higher activity at lower temperatures than in standard SCR. Almost 90% of the NO conversion is achieved at 300 °C for some catalysts (Figure 4.2, a).

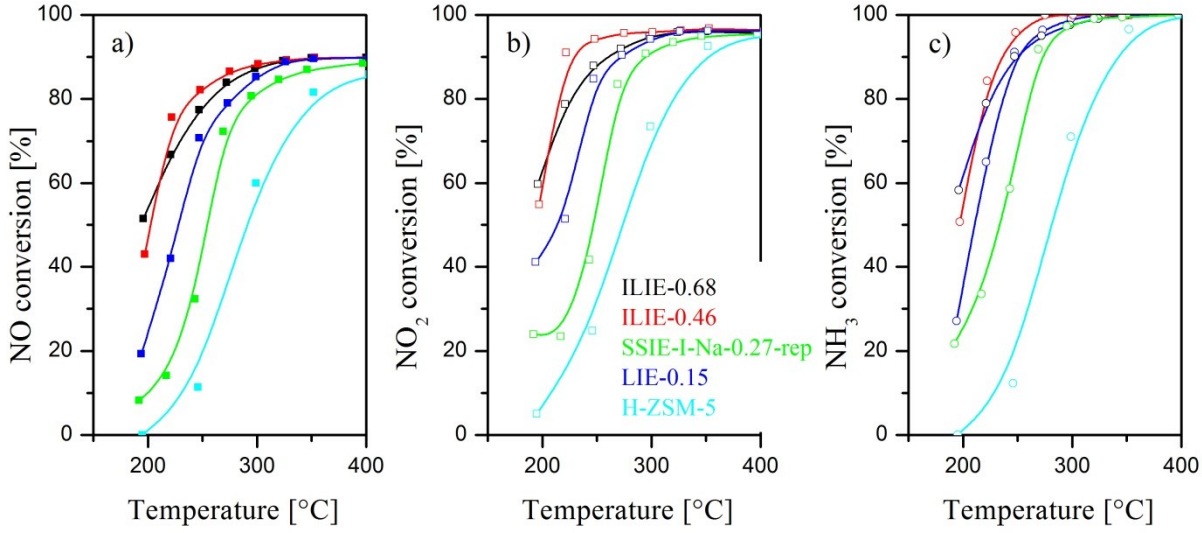

Figure 4.2 Fast SCR on Fe-ZSM-5 catalysts, dependence of a) NO, b) NO_2 and c) NH_3 conversion with temperature.

Contrary to the poor activity in the standard SCR, H-ZSM-5 shows some conversion in the fast SCR. However, its activity is still much lower compared to that of the Fe-loaded catalysts. The conversion in H-ZSM-5 might occur on the Brønsted acid sites at the zeolite structure or over the very small amount of iron contained as impurity (0.03 wt.%), which is seen by UV-Vis spectroscopy (Figure 4.3).

The most active catalyst in the fast SCR was ILIE-0.46, getting up to 82% NO conversion at 250 °C and > 90% NO_x conversion between 300 and 400 °C. Remarkably, despite its low iron content (0.15 wt.%) LIE-0.15 reached more than 70% of NO conversion at 250 °C, and got almost the same conversion as ILIE-0.46 above 350 °C. On the other hand, the catalyst with the highest iron content, ILIE-0.68, displayed similar NO conversion as ILIE-0.46, while SSIE-I-Na-0.27-rep showed much lower NO conversion that LIE-0.15 (Figure 4.2). This lack of correlation between iron content and catalytic performance in the fast SCR, as well as the high activity of catalysts with very low iron content supports the idea that special minority of iron species are responsible for the reaction, which prompted us to perform comprehensive spectroscopic studies to elucidate the particular nature of the active sites.

In all the cases the conversion of NO_2 is major compared to that of NO (compare Figure 4.2, a and b); at temperatures lower than 200 °C, the disparity could arise from side reaction where NH_4NO_3 is formed, as depicted by the Equation 2.14 (page 13).

4.1.2 UV-Vis and EPR spectroscopic characterization of as-prepared samples

As explained in section 2.5.1.3, UV-Vis spectra of Fe-ZSM-5 provide information about the $O \rightarrow Fe^{3+}$ LMCT transitions of isolated tetrahedral (< 250 nm) and octahedral (250 - 300 nm) Fe^{3+} sites, as well as the nature of small Fe_xO_y clusters (300 - 400 nm) and nanoparticles (< 400 nm) [10, 34].

The UV-Vis-DR (diffused reflectance) spectra were plotted as Kubelka-Munk functions, and the deconvoluted bands of as-received catalysts are displayed in Figure 4.3. The area of deconvoluted sub-bands was used to calculate the relative percentage (wt.%) for each iron species, assuming that the adsorption coefficients are similar for all species (Table 4.2).

It is clearly seen in Figure 4.3 that incorporation of Na induced the formation of Fe_xO_y clusters and particles (38%), owing to the blockage of cationic sites where isolated iron species tend to exchange. The LIE-0.15, ILIE-0.46 and ILIE-0.68 catalysts show similar UV-Vis spectra with 74% or more isolated iron species. Nonetheless, the bands of clusters

and nanoparticles of these catalysts increase considerably when the iron content arises, especially in ILIE-0.68. H-ZSM-5 contained traces of iron, therefore the bands of tetrahedral and octahedral species are also observed.

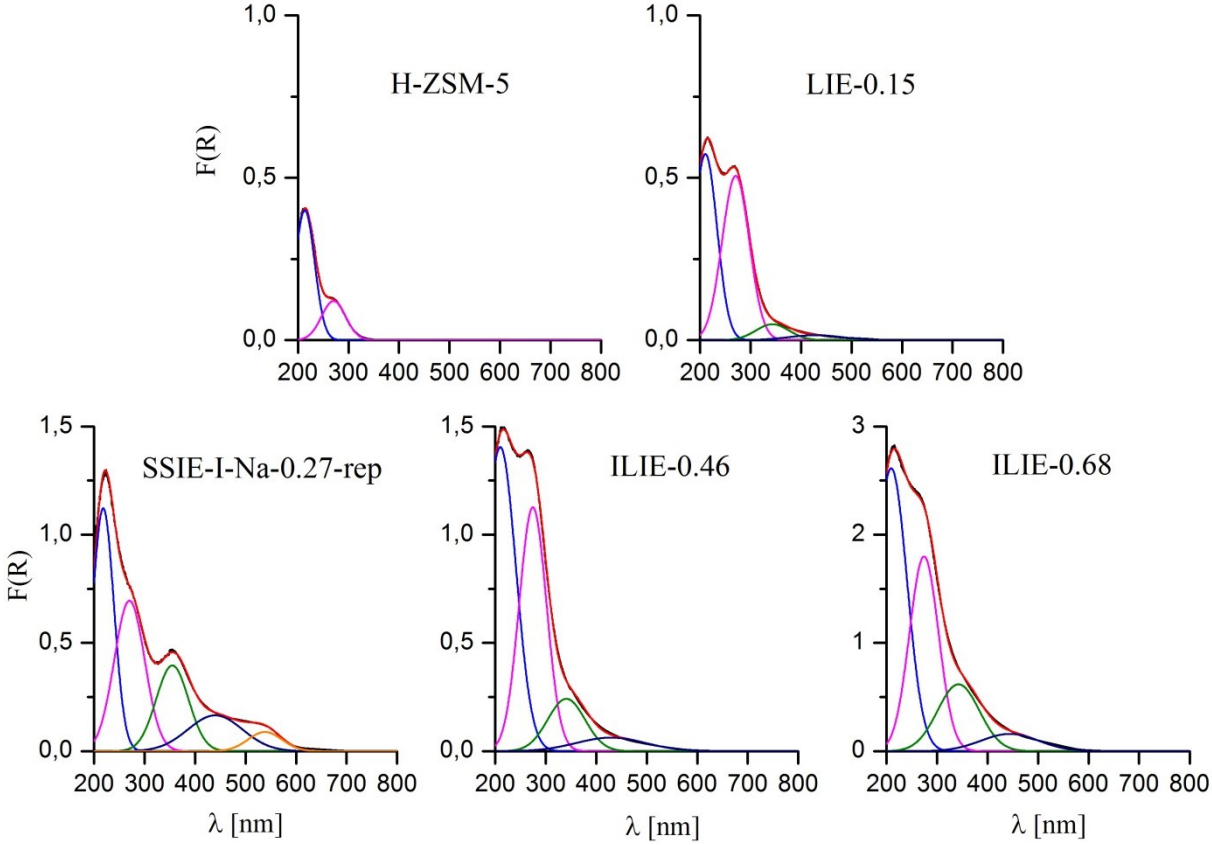

Figure 4.3 Deconvoluted UV-Vis-DR spectra of as-prepared samples measured at room temperature.

Table 4.2 Iron content of different iron species (wt.%) resulting from deconvoluted bands of the UV-Vis spectra, A [%].

	Single tetrahedral (<250nm)		**Single octahedral (250-300nm)**		**Small Fe_xO_y clusters (300-400nm)**		**Fe_2O_3 particles (>400nm)**	
	wt.%	**A[%][a]**	**wt. %**	**A[%][a]**	**wt. %**	**A[%][a]**	**wt. %**	**A[%][a]**
H-ZSM-5	-	67	-	33	-	-	-	-
LIE-0.15	0.053	36	0.081	54	0.009	7	0.004	3
SSIE-I-Na-0.27-rep	0.080	30	0.087	32	0.053	20	0.050	18
ILIE-0.46	0.177	38	0.197	43	0.058	13	0.028	6
ILIE-0.68	0.250	36	0.257	38	0.127	19	0.045	7

[a] Relative area of the UV-Vis subbands (Figure 4.3) derived from spectra deconvolution.

The catalysts were also characterized by EPR spectroscopy. The characteristic signals observed in the EPR spectra of Fe-ZSM-5 are that at g ≈ 6, 4.3, 2 and 2.3 (Figure 4.4). The

first three signals have been assigned to Fe^{3+} single sites in distorted octahedral, tetrahedral and highly symmetric coordination, respectively [50]; while the broad signals around g ≈ 2.3 - 2 are attributed to Fe_xO_y clusters of different size.

In order to distinguish between single Fe^{3+} sites with highly symmetric coordination and Fe_xO_y clusters (g ≈ 2.3 - 2), the EPR spectra of the catalysts were measured at room temperature and at 77 K (Figure 4.4). According to the Curie-Weiss law the line intensity of single Fe^{3+} sites increases with decreasing temperature. In LIE-0.15 the signal around g ≈ 2 (effectively increased at lower temperature (77 K), which indicates that the signal can be mainly assigned to isolated sites. Additionally, hyperfine lines are observed at g ≈ 2 for this sample, belonging to Mn^{2+} contained as a minor impurity. For ILIE-0.68, ILIE-0.46 and SSIE-Na-0.27-rep samples, the broad signals around g ≈ 2 did not increased at 77 K which indicates an antiferromagnetic effect from the Fe_xO_y clusters. This is in agreement with the observed bands of Fe_xO_y clusters and particles in the UV-Vis spectra of those samples.

The signals at low field were narrowed and increased in intensity at a low temperature, which is, as described above, a characteristic behavior of isolated sites.

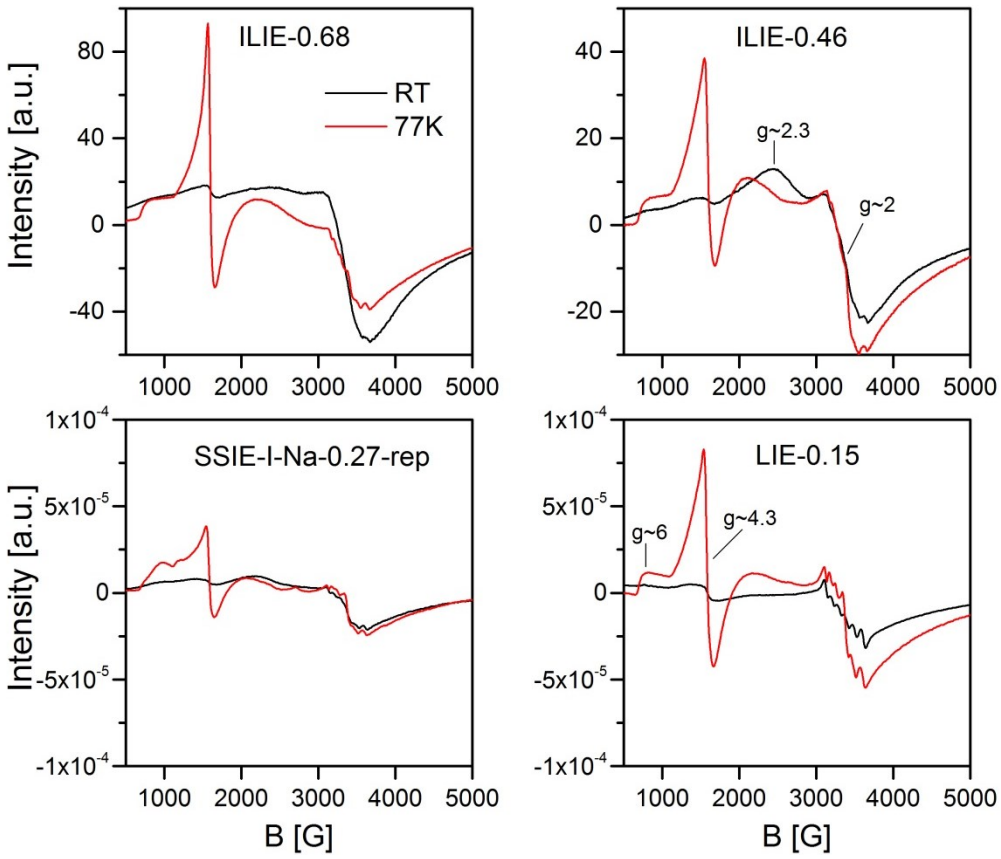

Figure 4.4 EPR spectra of Fe-ZSM-5 catalysts at room temperature (RT) and 77 Kelvin (77K).

Based on adsorption of NO, Lobree et al. [43] has reported three types of Fe^{2+} sites in Fe-ZSM-5. Additionally, three cationic positions have distinguished in the ZSM-5 lattice by

the visible d-d transition bands of Co^{2+} ions in dehydrated Co-ZSM-5, studied with Vis diffuse reflectance spectroscopy (Figure 2.1, page 9) [42]. The cationic positions are denoted as α, β and γ sites. This assignment can be extended to other ions like iron or copper. In agreement with this, our EPR spectra of Fe-ZSM-5 catalysts also show three types of isolated iron with different symmetry, and thus, degree of distortion. The distortion of the local iron site geometry should increase in the order α < β < γ. Based on this, the EPR signals are tentatively assigned as follows: signal at g ≈ 2 to α sites with highly symmetric Fe^{3+}; signal at g ≈ 6 to β sites where distorted octahedral Fe^{3+} are located, and signal at g ≈ 4.3 to γ sites which contain distorted tetrahedral Fe^{3+}.

4.1.3 *Operando* EPR/MS and *in situ* UV-Vis spectroscopic investigations

Operando EPR experiments for the standard and the fast SCR reactions were done at temperatures of 150, 250 and 400 °C. For the standard SCR experiment, an oxidative gas feed of 1000 ppm NO, 2% O_2 and Ar to balance the flow of 50 ml min^{-1} was introduced and kept until steady-state (20 - 30 minutes). Afterwards, in a complete mixture of standard SCR, 1000 ppm of NH_3 was added and kept until steady-state as well. The procedure was repeated for every temperature and the EPR spectra were taken in every steady-state (Figure 4.5 and Figure 4.6). For the fast SCR experiment, 500 ppm of NO and 500 ppm of NO_2 were introduced instead of 1000 ppm of NO (Figure 4.7 and Figure 4.8).

Figure 4.5 depicts the EPR spectra in the higher magnetic field region of Fe-ZSM-5 samples under oxidative (NO and O_2) and standard SCR (NO, O_2 and NH_3) conditions. For LIE-0.15 the signal at g ≈ 2 belongs to α iron sites, as previously described, while for the other catalysts this signal arises from α iron sites as well as from Fe_xO_y clusters. Both signals of α sites and Fe_xO_y clusters remain unchanged under oxidative and standard SCR compositions for all the catalysts, and at all different temperatures. It indicates that in the presence of a reducing agent, NH_3, the iron on α sites and clusters are neither permanently reduced nor modified.

A narrowing of the signal at g ≈ 2 was observed, when the temperature rose from 150 to 400 °C. The effect is reversible and independent of the gas composition. Therefore, it might be only induced by a thermal rearrangement of the magnetic domains.

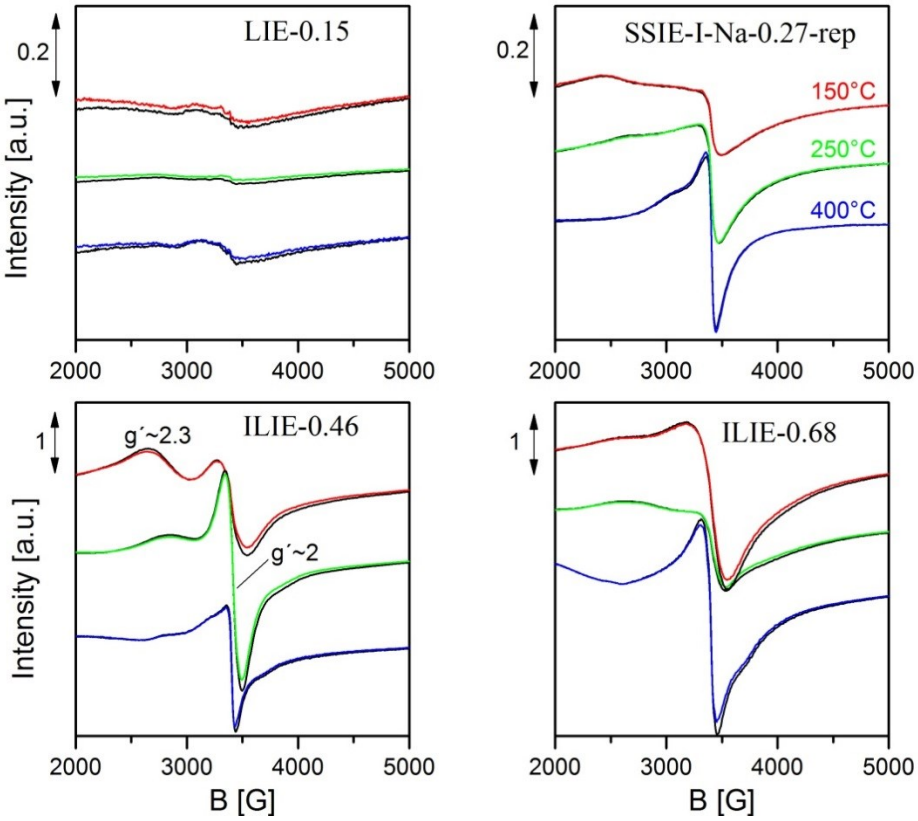

Figure 4.5 *Operando* EPR spectra in high field (above 2000 G), of Fe-ZSM-5 catalysts under standard SCR at 150, 200 and 400 °C. Gas mixtures: NO/O_2 (black lines) and $NH_3/NO/O_2$ (colored lines).

The *operando* EPR spectra in the low magnetic field region under oxidative and standard SCR conditions are displayed in Figure 4.6. The signals at g ≈ 6 and 4.3 (Fe^{3+} on β and γ sites) are well observed under oxidative conditions (Figure 4.6, black spectra). The splitting of the signal at g ≈ 6 is attributed to a weak rhombic distortion of the axial symmetry of the paramagnetic ion [73]. The spectra of SSIE-Na-I-0.27-rep displayed initially a lower amount of Fe^{3+} on γ sites than the other catalysts, a competition with the Na ions might be the reason. While raising the temperature, the signal of Fe^{3+} on γ sites decreased, this reflects a pure paramagnetic behavior according to the Curie law. On the other hand, the signal of Fe^{3+} on β sites increased which is in disagreement with the Curie law; this behavior can only be due to presence of Fe^{2+} which is converted to Fe^{3+} at higher temperature. Initial Fe^{2+} present in the catalysts, even in oxidative conditions (NO/O_2), was observed by FTIR spectroscopy, as will be explained later in this section (Figure 4.12).

When the complete mixture of the standard SCR feed was introduced, the signals of Fe^{3+} on β sites completely vanished and that of Fe^{3+} on γ sites were significantly diminished at all temperatures (Figure 4.6, colored spectra). This indicates that NH_3 reduce these Fe^{3+} species to Fe^{2+}, while O_2 from the feed was not able to reoxidize iron on β and γ sites under standard SCR conditions.

Several authors have proposed that iron contained in Fe-ZSM-5 takes part in a redox mechanism during the oxidation of NO to intermediates that are later reduced by NH_3 [1, 26, 74]. The intermediates to which NO is oxidized have not yet been clarified. Additionally, to undergo NO oxidation the initial iron must exists as Fe^{3+}, which self-reduces to Fe^{2+}. The reduced iron cannot initiate the oxidation of a new NO molecule, and thus, becomes an inactive catalytic center. It has been proposed that during the standard SCR an oxygen molecule from the gas phase reoxidizes this Fe^{2+} to the initial Fe^{3+} [1]. However, as suggested by the operando EPR results in Figure 4.6, this does not occur for all reduced Fe^{2+} species.

In the presence of NH_3 at low temperatures, the reduction of Fe^{3+} on β and γ sites is much faster than the reoxidation by O_2; therefore, it is suggested that they do not take part in the standard SCR at these temperatures. Indeed, the permanent reduction of iron on β and γ sites can be considered as one of the reasons for the poor activity in the standard SCR reaction at temperatures lower than 300 °C.

Certainly, the observed NO conversion at temperatures < 400 °C might occur on Fe^{3+} on α sites and Fe_xO_y clusters, which remain oxidized (Figure 4.5). Hence, they are capable of reducing and reoxidizing quickly enough to perform intermediate oxidation reactions involved in the global standard SCR.

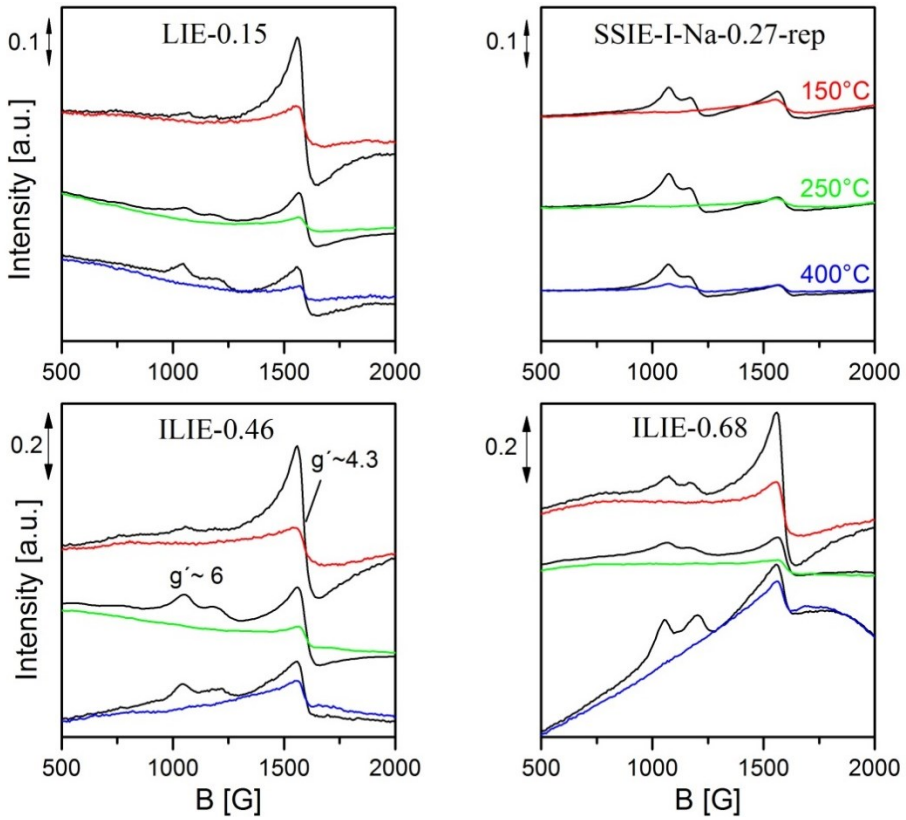

Figure 4.6 *Operando* EPR spectra in low field (below 2000 G), of Fe-ZSM-5 catalysts under standard SCR at 150, 250 and 400 °C. Gas mixtures: NO/O_2 (black lines) and $NH_3/NO/O_2$ (colored lines).

Operando EPR spectra in the higher magnetic field region under oxidative (NO, NO_2 and O_2) and fast SCR (NO, NO_2, O_2 and NH_3) conditions are displayed in Figure 4.7. Similar to standard SCR, the Fe^{3+} on α sites and Fe_xO_y clusters persist oxidized in the fast SCR reaction, even after contact with NH_3 from the complete mixture of fast SCR. Since the shape of the spectra does not change under gas mixtures, the formation or dissolution of Fe_xO_y clusters during the fast SCR reaction can be excluded.

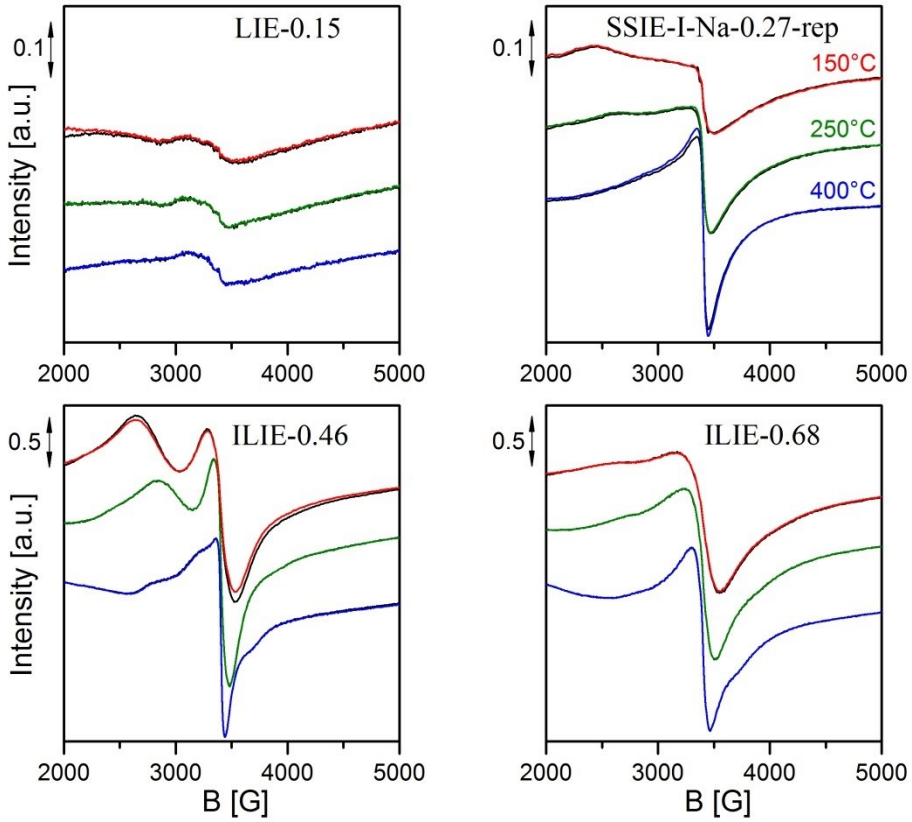

Figure 4.7 Operando EPR spectra in high field (above 2000 G) under fast SCR, at three temperatures. Gas feed: $NO/NO_2/O_2$ (black lines) and $NH_3/NO/NO_2/O_2$ (colored lines).

Operando EPR spectra in the low magnetic field region during oxidative and fast SCR conditions at three temperatures are depicted in Figure 4.8. At 150 °C, when the catalysts show less than 50% NO conversion, the Fe^{3+} signals at $g \approx 6$ (β site) and $g \approx 4.3$ (γ site) are reduced under the complete mixture of the fast SCR (Figure 4.8, red lines); similarly as observed in the standard SCR reaction. Interestingly, at 250 °C when the catalysts display more than 70% NO conversion, even in the catalyst with low iron content, the iron species on β and γ sites remain oxidized as Fe^{3+}, therefore these signals persist unchanged under the fast SCR feed (Figure 4.8, green lines). An analogous behavior was observed at high temperature (Figure 4.8, blue lines). Evidently, NO_2 present in the reactant mixture reoxidized the iron on

β and γ sites faster than their reduction by NH_3 or other intermediate reactions. Thus, NO_2 keeps iron at these sites as Fe^{3+} active state for the fast SCR.

An exception occurs in the case of SSIE-I-Na-0.27-rep which displays lower activity in fast SCR (Figure 4.2), where the Fe^{3+} on β and γ sites were reduced in the whole temperature range and NO_2 is not able to reoxidize them.

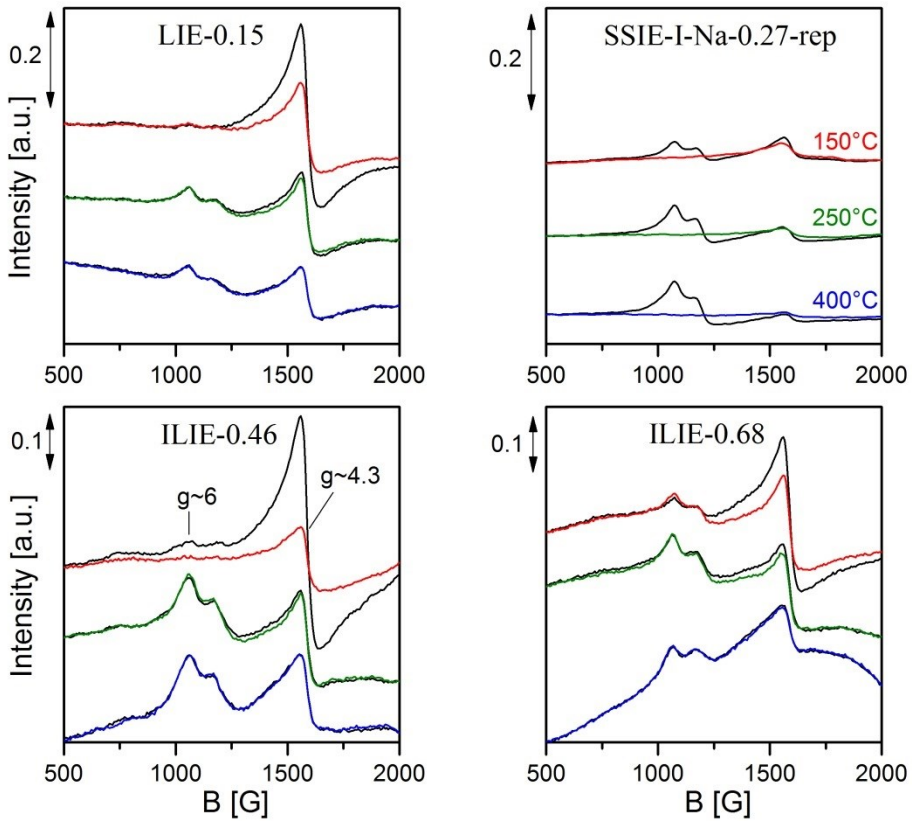

Figure 4.8 *Operando* EPR spectra in low field (above 2000 G) under fast SCR at 150, 250 and 400 °C. Gas feed: $NO/NO_2/O_2$ (black lines) and $NH_3/NO/NO_2/O_2$ (colored lines).

Operando EPR spectra in the low magnetic field of all catalysts at 250 °C under fast SCR reaction are compared in Figure 4.9. The signal intensity of Fe^{3+} at β sites ($g \approx 6$) follows the order ILIE-0.46 > ILIE-0.68 > LIE-0.15 > SSIE-I-Na-0.27; which is the same as the activity observed in the fast SCR at this temperature (Figure 4.2). The activity trend in the fast SCR does not correlate either with the total iron content or with the amount of different iron species calculated from the deconvoluted UV-Vis spectra (Table 4.2).

Considering the literature, it has been speculated that isolated sites are responsible for the activity in the fast SCR, but a more detailed specification of the nature of these sites was not possible at that time [7]. Furthermore, Fe^{3+} was described as a promoter for the formation of surface nitrates, a step of the fast SCR mechanism at low temperatures [33]. It implies that specifically isolated Fe^{3+} sites are required for the fast SCR reaction.

The fact that Fe^{3+} at isolated β and γ sites persist oxidized when the catalyst is highly active as well as that the signal intensity of Fe^{3+} on β sites follows the activity trend at 250 °C, lead to the conclusion that Fe^{3+} on β and γ sites are responsible for the higher activity of the fast SCR at low temperature.

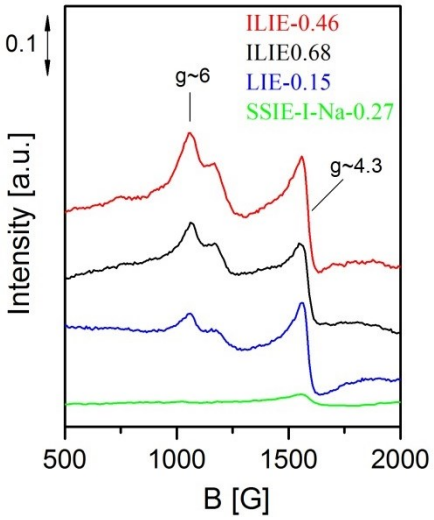

Figure 4.9 *Operando* EPR spectra of Fe-ZSM-5 catalyst under fast SCR at 250 °C.

Mass spectra of nitrogen production, measured simultaneously with the EPR spectra are displayed in Figure 4.10, the dashed squares represent the time when the fast SCR feed was flushed and the color indicates the temperature of record. The qualitative MS analysis shows that nitrogen is formed at 250 and 400 °C over all catalysts; while at 150 °C it was only seen on ILIE-0.46 and LIE-0.15.

The MS measurements were not calibrated; therefore a quantitative analysis was not possible. However, by the qualitative analysis the MS data confirms that the EPR spectra depicted above correspond to the catalysts in their active state.

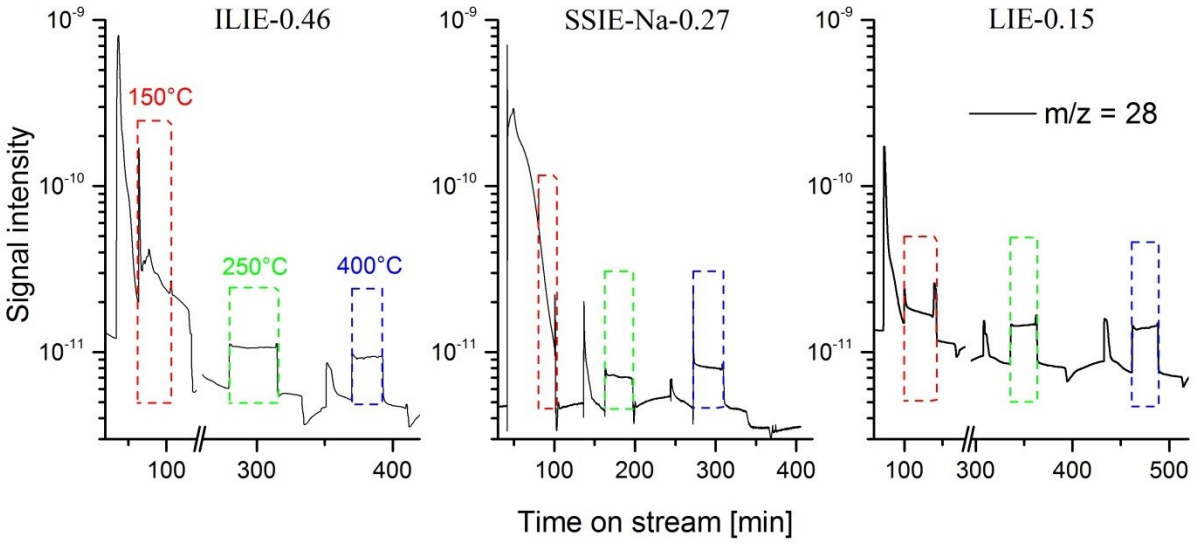

Figure 4.10 Mass spectra of the nitrogen production during fast SCR over different catalysts at 150, 250 and 400 °C, carried out parallel to the EPR measurements.

The *in situ* UV-Vis-DR spectra were measured in a setup which was previously described (section 3.3.1.3). For the experiments, 55 mg of the catalysts with particle size of 250 - 315 µm were filled into a Harrick reaction chamber. In the standard SCR experiment, the sample was heated up 250 °C in He flow; then 1000 ppm NO, 2% O_2 and 1000 ppm NH_3 were introduced. The total flow was of 50 ml min^{-1} balanced with the inert gas He. In the fast SCR experiment, 500 ppm NO and 500 ppm NO_2 were introduced instead of 1000 ppm NO. All the spectra were recorded at steady-state (20 - 30 min reaction) and converted into the Kubelka-Munk function.

The *in situ* UV-Vis spectra of Fe-ZSM-5 catalysts measured at 250 °C under standard and fast SCR environments are displayed in Figure 4.11. Due to the high temperature (250 °C), all the bands in the UV-Vis spectrum are broader and became more asymmetric, according to the Franck-Condon principle.

In Figure 4.11, different band intensities for both reactions were observed in ILIE-0.68 and ILIE-0.46 catalysts. The band intensity of isolated tetrahedral (λ < 250 nm) and octahedral (250 - 300 nm) sites as well as of the Fe_xO_y clusters (300 - 400 nm) was higher in the fast SCR. This is in agreement with the EPR measurements, which revealed that more Fe^{3+} was present during the fast SCR than during standard SCR. Especially, the catalyst ILIE-0.46 which showed the highest activity at this temperature (compare Figure 4.2). Small or almost no variations were observed in the catalysts with low iron content. This must be due to the fact that UV-Vis spectroscopy is not as sensitive as EPR spectroscopy; the minority of oxidized sites might be below the detection limits of UV-Vis spectroscopy.

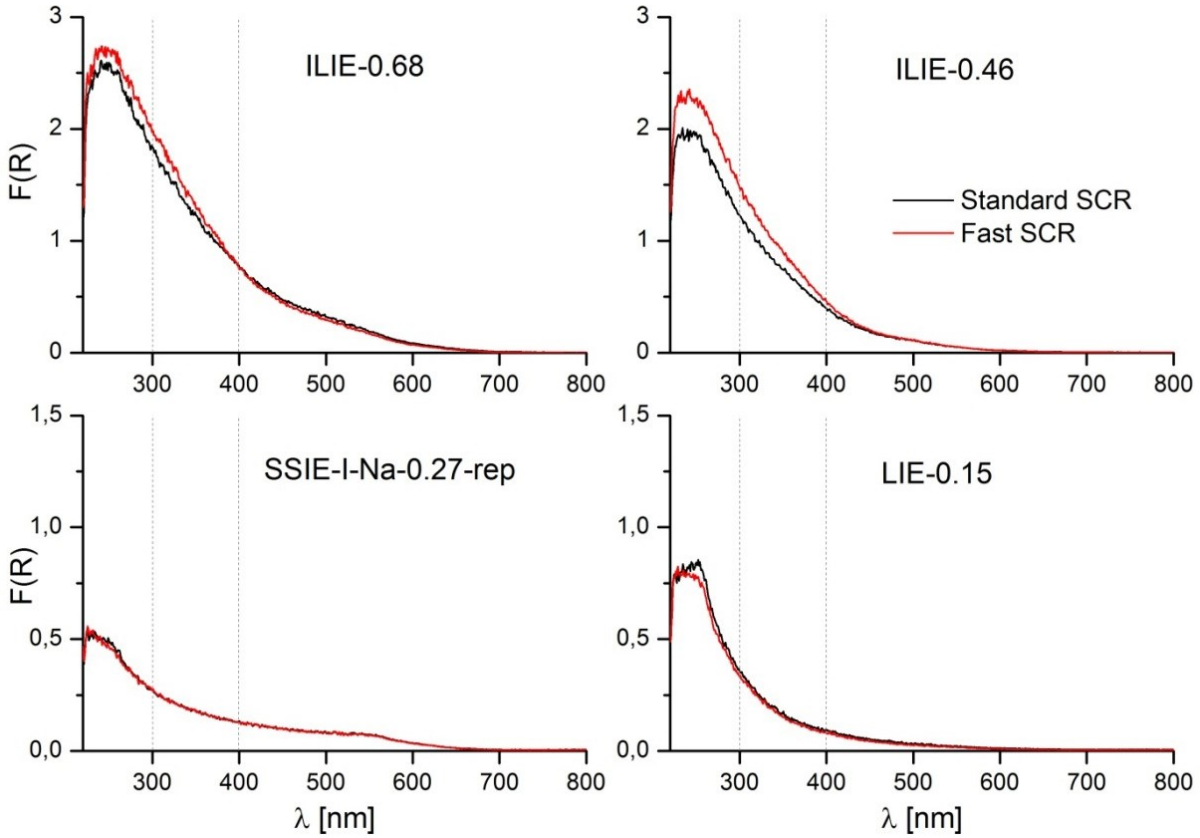

Figure 4.11 In situ UV-Vis-DR spectra during the standard and fast SCR at 250 °C. Gas feeds: $NO/O_2/NH_3$ (standard) and $NO/NO_2/O_2/NH_3$ (fast).

4.1.4 *In situ* FTIR experiments

In situ infrared investigations in transmission mode were done to get information about surface species related with the redox ability of iron under oxidative conditions and complete feed of standard and fast SCR. The experiments were carried out at 250 °C, a temperature at which the catalysts were considerably active in the fast SCR, but almost inactive in the standard SCR. The measurements were done in a homemade reaction cell as previously described (section 3.3.3.1). For all the experiments, the catalysts were pretreated by heating in He until 250 °C. In the first experiment, a mixture of 1000 ppm of NO and 2% O_2 was flushed for 25 minutes. In a second experiment, 1000 ppm of NO_2 balanced with He was introduced. Finally, the sample was exposed to a mixture of 500 ppm NO and 500 ppm NO_2. FTIR spectra were recorded after pretreatment and during the experiments. For better observation of the adsorbed surface species, the spectrum of the pretreated catalyst was subtracted from all subsequent spectra.

Figure 4.12 shows the *in situ* FTIR spectra of ILIE-0.46 under different gas compositions at 250 °C. By flushing NO and O_2 (Figure 4.12, A), the band at ~ 1884 cm^{-1} assigned to the nitrosyl complex Fe^{2+}-NO [33, 51] appears during the first minute which

discloses the presence of Fe^{2+} in the catalyst. With time the intensity of Fe^{2+}-NO band increases indicating formation of more reduced Fe^{2+}; meanwhile, a band related to adsorbed NO_2 [45, 74, 75] at ~ 1630 cm^{-1} also emerged. Indeed, oxidized Fe^{3+} is reduced by the formation of NO_2 as described in the mechanism of NO oxidation (Equation 2.6, page 11). Here it is remarkably seen that oxygen from the mixture is not capable to reoxidize the iron sites of the catalyst. In the first minute of reaction with NO_2, NO might be originated by the reduction of NO_2 (Equation 4.1) [33]. This NO reacts with the present Fe^{2+} forming the complex Fe^{2+}-NO, which is seen by the band at 1884 cm^{-1} (Figure 4.12, B).

$$NO_2 + Fe^{2+} \rightarrow NO + Fe^{3+}\text{-}O^- \qquad 4.1$$

Afterwards, the initial Fe^{2+} is oxidized by NO_2, indicated by the decreasing of the Fe^{2+}-NO band. The bands associated to surface NO_2 (1630 cm^{-1}) and surface nitrates at 1604 and 1575 cm^{-1} [33, 45, 74] increased with time.

On the other hand, similar behavior like with only NO_2 is observed when a mixture of NO/NO_2 was dosed (Figure 4.12, C); just the band intensity of the surface species Fe^{2+}-NO, NO_2 and nitrates changed. The lower intensity of the band of adsorbed NO_2 and surface nitrates suggests a reaction of the latter with the NO present in the gas mixture, as depicted by Equation 4.2. Besides, NO_2 oxidizes the reduced Fe^{2+} (Equation 4.1); thus, the band intensity of Fe^{2+}-NO decreased.

$$NO_3^- + NO \rightarrow NO_2^- + NO_2 \qquad 4.2$$

These FTIR experiments confirm the importance of NO_2, what is present in the fast SCR feed, to reoxidize iron sites.

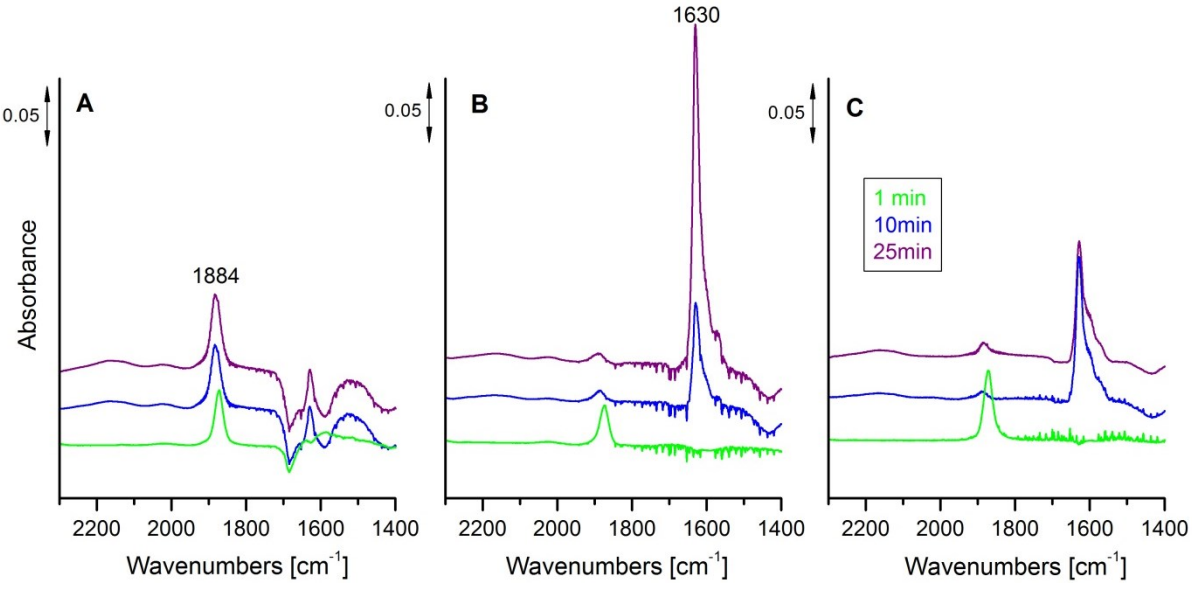

Figure 4.12 *In situ* FTIR spectra of ILIE-0.46 at 250 °C under: A) NO/O_2, B) NO_2 and C) NO/NO_2.

Another experiment over ILIE-0.46 was carried out at 250 °C, in which the complete mixture of the standard and fast SCR, respectively, was introduced. The reaction cell was closed (to observe adsorbates and gas phase products), and kept for 5 minutes (Figure 4.13). The band intensity of the Fe^{2+}-NO complex in the fast SCR is lower than in the standard SCR, meaning that there are more oxidized Fe^{3+} species present under fast than under standard SCR conditions, which is in agreement with the UV-Vis and EPR spectroscopic investigations, previously described.

As can be seen in Figure 4.13 an undesirable by-product of the reaction (N_2O) is formed in both reactions, with a slightly lower concentration in the fast SCR than in the standard SCR. This N_2O is mainly formed in the presence of NH_3 by the decomposition of ammonium nitrate (Equation 2.16, page 14).

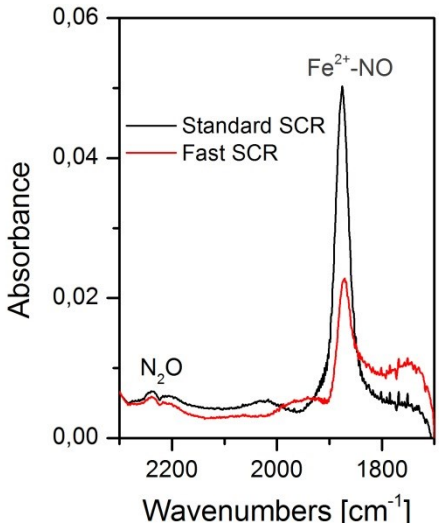

Figure 4.13 In situ FTIR spectra of ILIE-0.46 at 250 °C under standard and fast SCR reactions. Gas feeds: $NO/O_2/NH_3$ (standard SCR) and $NO/NO_2/O_2/NH_3$ (fast SCR).

4.2 Activation effect in the NO oxidation

The oxidation of NO to NO_2 over Fe-ZSM-5 has been frequently proposed as rate-limiting step of the standard SCR reaction [26, 32, 37, 51]. However, other studies have found that NO oxidation is slower than the standard SCR, which excludes its participation, since one reaction step could not be slower than the overall reaction [71].

In order to get a better insight into the relationship between NO oxidation and standard SCR reaction, a series of SSIE-I-Ca/Na samples with comparable iron content (0.26 ± 0.02 wt.%) was investigated. The SSIE-I-Ca/Na samples were previously exchanged with a catalytically inactive co-cation to promote the formation of specific iron species. As depicted by UV-Vis characterization (Figure 4.14), the amount of clusters increased with increasing the co-cation loading. For comparison and further characterization a commercial CFeZ sample was also investigated.

In preliminary catalytic test (at the University of Bochum) a surprising effect has been observed: It was founded that the activity of the samples for NO oxidation increases significantly after pretreatment in reducing conditions. Therefore, the study comprised three steps. At first all as-prepared samples were analyzed in NO oxidation (initial). After this, the samples were exposed to standard SCR environment at the same temperature and then the NO oxidation was measured again (activated). In fact, this procedure was done for analyzing the impact of the standard SCR (with reducing conditions) on the NO oxidation reaction.

In addition to the catalytic test, comprehensive *in situ* spectroscopic study were performed to find the reason for this activation effect that could be related to changes in the iron speciation.

4.2.1 Preliminary characterization

Initial characterization of the catalysts was made by UV-Vis and EPR spectroscopy. UV-Vis spectra of the samples after calcination and storage at room temperature are displayed in Figure 4.14. The SSIE-I-Ca/Na samples showed bands of Fe_xO_y clusters (300 - 400 nm [10]) and nanoparticles (above 400 nm [10]) despite their low iron content (Figure 4.14, A). Introducing a higher amount of co-cation promotes the formation of nanoparticles, as depicted by the absorption above 400 nm which is more pronounced for SSIE-I-Na(high). In contrast, the band of Fe_xO_y clusters at 350 nm diminished with increasing degree of exchange with an inert cation (Na/Ca).

On the other hand, CFeZ catalyst comprises 66% isolated sites (bands between 200 - 300 nm) and 34% Fe_xO_y clusters and nanoparticles (300 - 400 and $\lambda > 400$ nm, respectively).

Moreover, the shape of the spectrum of the commercial sample differs from the SSIE-I-Na/Ca series, it looks similar to the samples prepared by improved liquid ion exchanged method ILIE (Figure 4.3), which leads preferentially to samples with isolated iron sites.

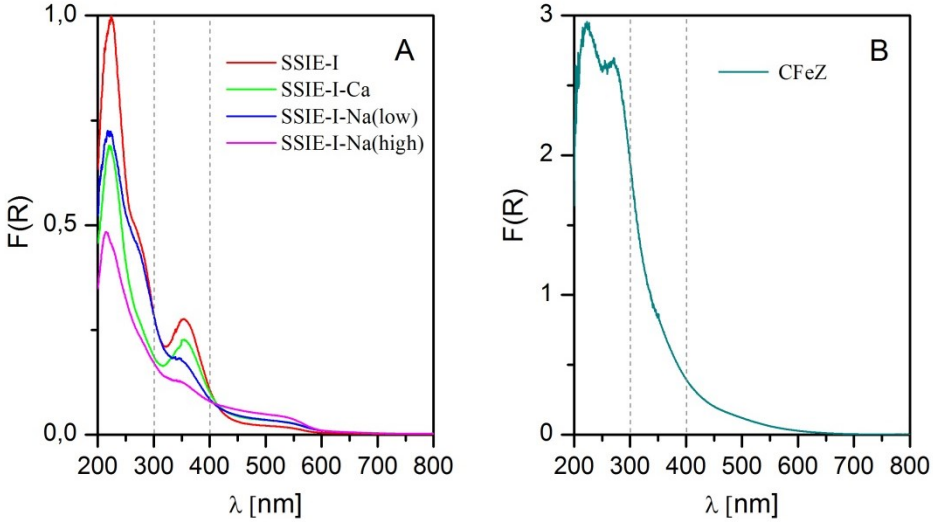

Figure 4.14 UV-Vis spectra at room temperature of received SSIE-I-Ca/Na samples and the calcined CFeZ.

Figure 4.15 shows EPR spectra at room temperature and the temperature of liquid nitrogen (77 K) of the SSIE-I catalysts with different loadings of Na or Ca, after pre-oxidation with NO/O_2 at 350 °C. The oxidation of the catalysts was done in order to create a maximum number of oxidized Fe^{3+} in the sample.

The intensity of isolated tetrahedral and octahedral sites ($g \approx 4.3$ and $g \approx 6$, respectively) increases at lower temperatures (Figure 4.15), according to the Curie Law; since the magnetization is inversely proportional to the temperature.

The range around $g \approx 2$ comprises broad signals at room temperature (RT) which disappear at 77 K, indicating the antiferromagnetic nature of the respective Fe^{3+} species. They arise from larger clusters and Fe_xO_y nanoparticles of different size and shape (Figure 4.15). In the corresponding UV-Vis spectra such species are reflected by bands above 400 nm (Figure 4.14). For example, in the sample SSIE-I these species are least pronounced in the UV-Vis and its EPR signal around $g \approx 2 - 2.3$ is lower compared to the other samples.

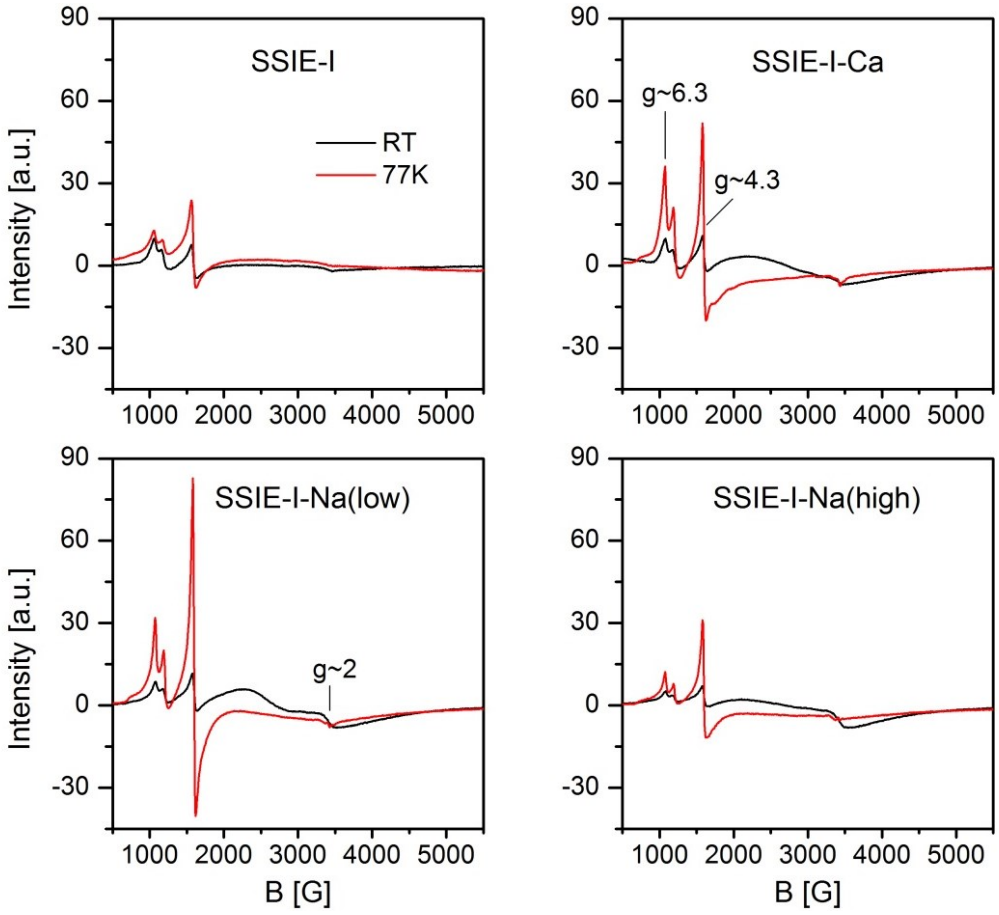

Figure 4.15 EPR spectra of SSIE-I-Na/Ca catalysts measured at room temperature (RT) and temperature of liquid nitrogen (77K), after oxidative pretreatment at 350 °C.

4.2.2 Catalytic activity

Figure 4.16 displays NO conversion of Fe-ZSM-5 catalysts during initial and activated NO oxidation. During initial NO oxidation, SSIE-I-Ca/Na catalysts show NO conversion below 5%, while the commercial CFeZ catalyst achieved ~11% (Figure 4.16, A), which is expected because the catalyst CFeZ contains three-fold more iron (0.82 wt.% Fe) than the SSIE-I-Ca/Na samples. The maximum of initial NO conversion is found between 350 - 400 °C for all the catalysts, at higher temperatures reversible NO_2 decomposition occurred.

Surprisingly, after the catalysts were exposed to standard SCR feed, the NO conversion increased remarkably (compare A and B, Figure 4.16). An up to 12 fold boost occurred for the series of SSIE-I-Ca/Na samples, compared to their initial state. For CFeZ, the conversion increased only weakly from 11 to 16% at 400 °C (initial and activated NO oxidation, respectively).

In Figure 4.16 B the maximum in the activated NO conversion curves of SSIE-I-Ca/Na samples are shifted to higher temperatures as follow: SSIE-I < SSIE-I-Ca < SSIE-I-Na(low) < SSIE-I-Na(high). The sample without co-cation (SSIE-I) displays the

maximum of NO conversion at a lower temperature, whereas the sample with a higher amount of co-cation (SSIE-I-Na(high)) shows the maximum at a higher temperature. Thus, major co-cation occupancy reduces the efficiency in the activated NO oxidation. All catalysts showed an NO conversion lower than the equilibrium of the reverse reaction (above NO/NO_2 equilibrium temperature), even after activation in standard SCR environment (Equation 2.5, page 11).

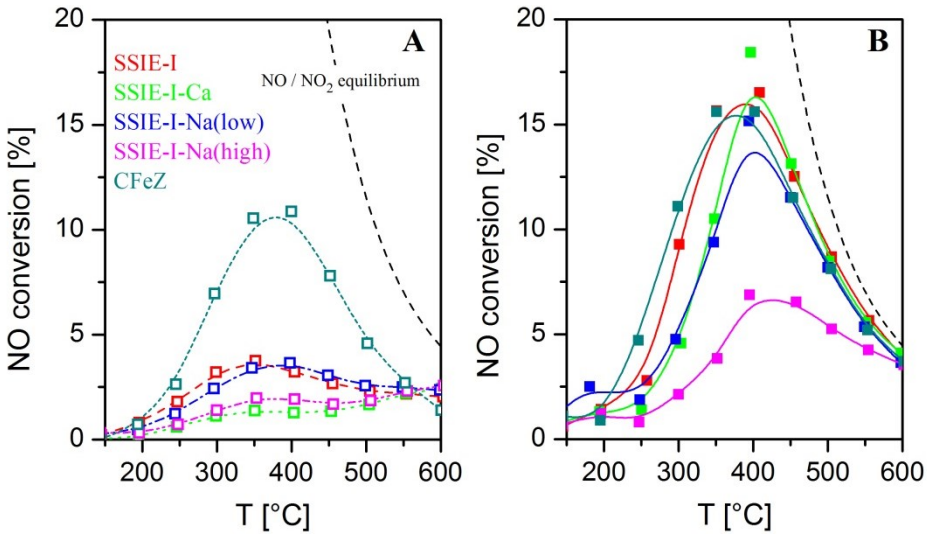

Figure 4.16 NO oxidation on different Fe-ZSM-5 catalysts of as-prepared samples "initial" NO oxidation (A) and after reaction with standard SCR mixture "activated" NO oxidation (B). Equilibrium of a reverse reaction is represented with black dashed lines.

The performance of standard SCR over these Fe-ZSM-5 catalysts is shown in Figure 4.17. CFeZ shows the highest NO conversion, which was expected due to its higher iron content. In the SSIE-I-Ca/Na catalysts, the NO conversion did not correlate with the co-cation/Al ratio(Table 4.1), and the shape of the curves differs from one another.

The NO and NH_3 conversions were similar up to ~ 400 °C, for the SSIE-I-Ca/Na catalysts. Above this temperature, NH_3 conversion is higher since NH_3 is consumed in the standard SCR reaction and also oxidized at high temperatures in the NH_3 oxidation reaction. In contrast, CFeZ shows nearly the same NO and NH_3 conversion along the whole temperature range (compare a and b, Figure 4.17). This might be due to the fact that the relative percentage of FexOy clusters with respect to the total iron content is higher in the SSIE-I-Ca/Na samples than in the CFeZ sample.

For an entire study, the fast SCR reaction was also measured over the SSIE-I-Ca/Na and CFeZ samples (Figure 4.18). CFeZ shows less conversion even at the higher iron-loading at temperatures below 300 °C, as described previously (section 4.1.1). On the SSIE-I-Ca/Na

series, the catalytic activity increases while decreasing the co-cation occupancy especially at temperatures lower than 250 °C (Figure 4.18, a) and b)).

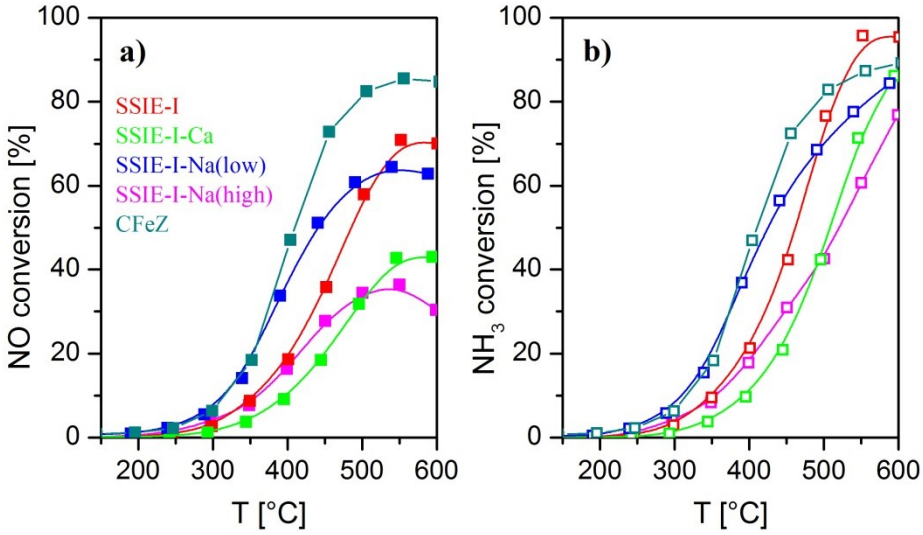

Figure 4.17 Standard SCR on Fe-ZSM-5 catalysts, dependence of a) NO and b) NH_3 conversion on temperature.

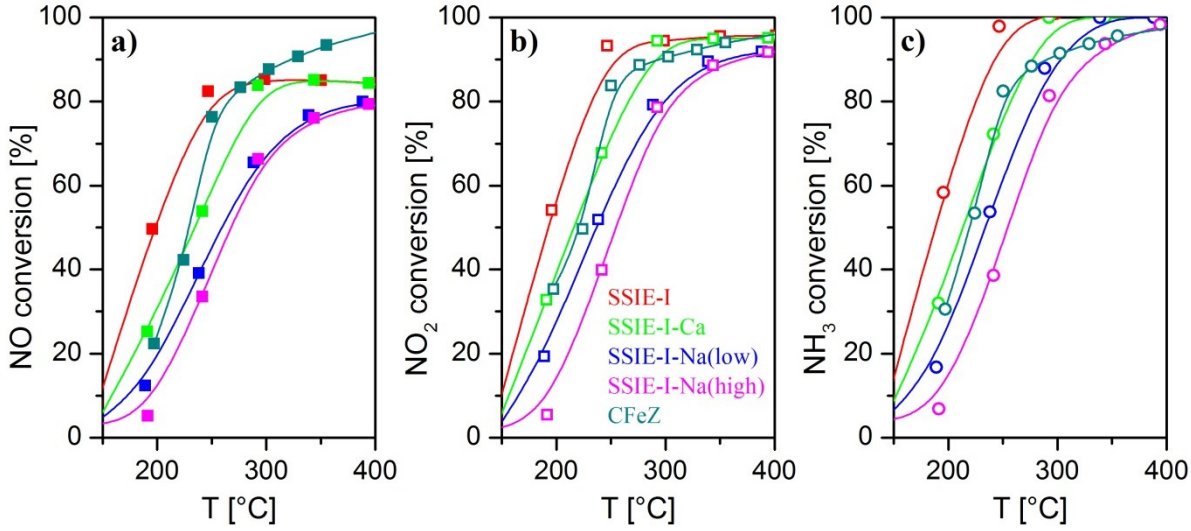

Figure 4.18 Fast SCR over Fe-ZSM-5 catalysts, dependence of a) NO, b) NO_2 and c) NH_3 conversion on temperature.

For the sake of correlation between the different reactions, the NO conversions of initial and activated NO oxidation, as well as standard SCR are plotted together in Figure 4.19. In SSIE-I, SSIE-I-Ca and CFeZ, the initial NO conversions were equal to standard SCR at low temperature, pointing it out as step of the later reaction (Figure 4.19, black and blue lines). However, in SSIE-I-Na(low) and SSIE-I-Na(high) the initial NO conversion in the NO oxidation reaction was lower than in standard SCR, excluding the NO oxidation reaction as intermediate step of the standard SCR reaction for these catalysts. The reason might be that

standard SCR proceeds by a different mechanism than NO oxidation to NO_2 and its successive reduction.

The comparison of the NO conversions of activated NO oxidation and standard SCR is shown in Figure 4.19, red and blue lines. On SSIE-I-Na samples, the activated NO conversion was still below than the NO conversion of the standard SCR, whereas the activated NO conversion for the rest of the catalyst was faster than standard SCR. Consequently, this investigation of our catalysts supports the idea that NO oxidation definitely cannot be considered as the rate-limiting step of the standard SCR reaction. Furthermore, the NO oxidation might not be proposed as the only or main pathway of the reaction mechanism of standard SCR.

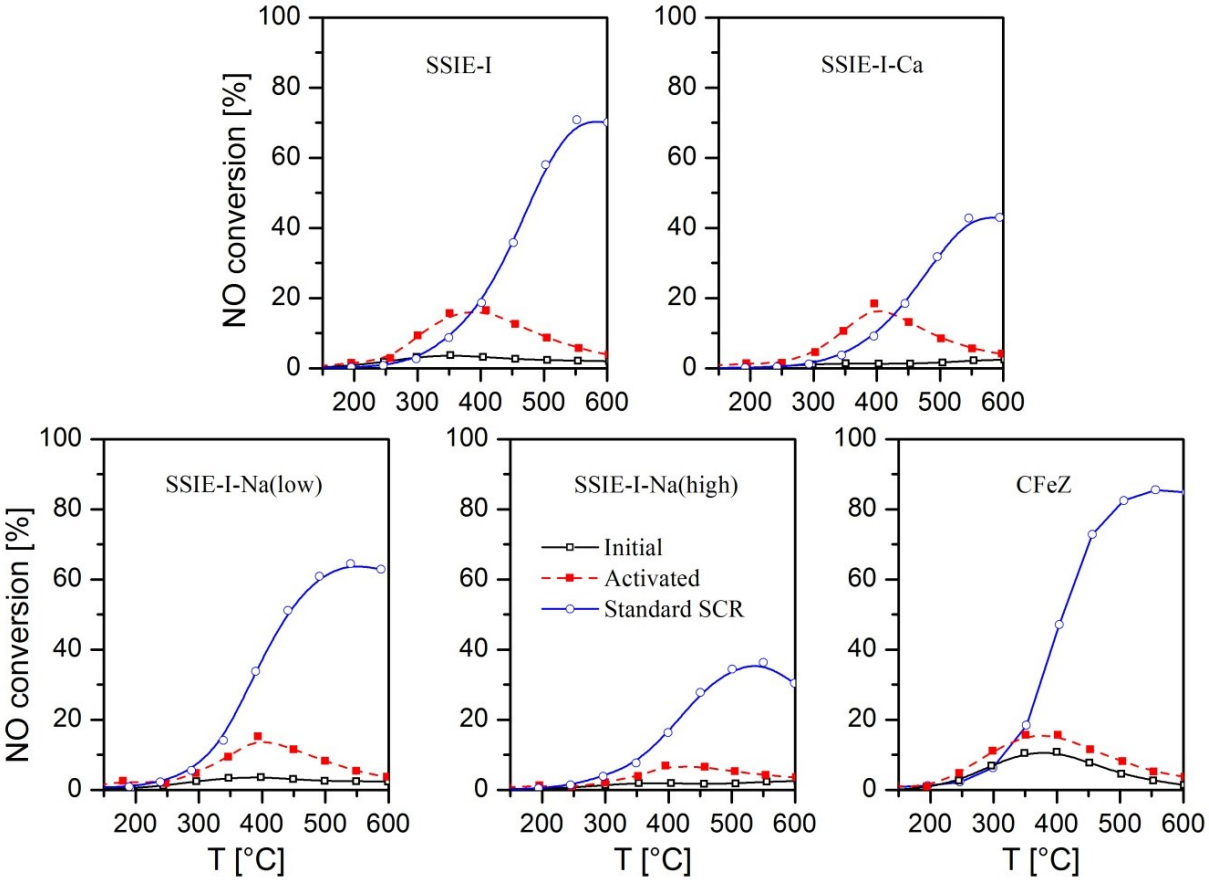

Figure 4.19 Comparison of NO conversion on Fe-ZSM-5 catalysts under NO oxidation (initial and activated) and standard SCR on temperature range.

4.2.3 Spectroscopic studies of the activation effect

4.2.3.1 *Operando* EPR/MS characterization

Operando EPR experiments were carried out in a system described previously (section 3.3.1.2). 50 mg of catalyst with a particle size of 250 - 315µm were introduced in the EPR cell. The cell was located in the cavity and heated up to 350 °C in a gas flow of 1000 ppm NO, 2% O_2 and Ar in balance. Then, the temperature of 350 °C was kept for 30 minutes in the oxidation mixture ($NO/O_2/Ar$), in order to reach the steady-state of "initial" NO oxidation. Afterwards, the activation was done by heating the catalyst up to 450 °C in flow of standard SCR feed ($NO/O_2/NH_3/Ar$), held at this temperature for 30 minutes and cooled down to 350 °C. Finally, the NO oxidation feed was again introduced for 30 minutes at 350 °C in order to observe the "activated" NO oxidation. The total gas flow was always 36 ml min^{-1}, corresponding to a GHSV of ~ 30 000 h^{-1} for the EPR experiments. All the EPR spectra were recorded in steady-state; while the mass spectrometer, connected to the outlet, was continuously measuring along the experiment.

Operando EPR spectra of the SSIE-I samples with different amount of Na or Ca were recorded at 350 °C under steady-state conditions of initial and activated NO oxidation (Figure 4.20). In all EPR spectra the signals of isolated octahedral ($g \approx 6$) and tetrahedral ($g \approx 4.3$) sites are displayed, as well as the highly symmetric sites ($g \approx 2$). Additionally, clusters signals were seen with distinct shape for each sample (around $g \approx 2$), as will be discussed later.

In Figure 4.20 is clearly seen that the *operando* EPR spectra in steady-state of initial and activated NO oxidation are almost equal (comparing colored and black lines), which means that with standard SCR treatment there was no significant modification neither in the redox behavior nor in the structure and dispersion of iron sites.

Indeed, the reason of this activation effect during the NO oxidation could not be clarified by EPR measurements. EPR might not be sensitive enough to distinguish small structural changes or the oxidation of NO into NO_2 occurs in a small amount of iron sites, where the changes are hidden by spectators in the spectra.

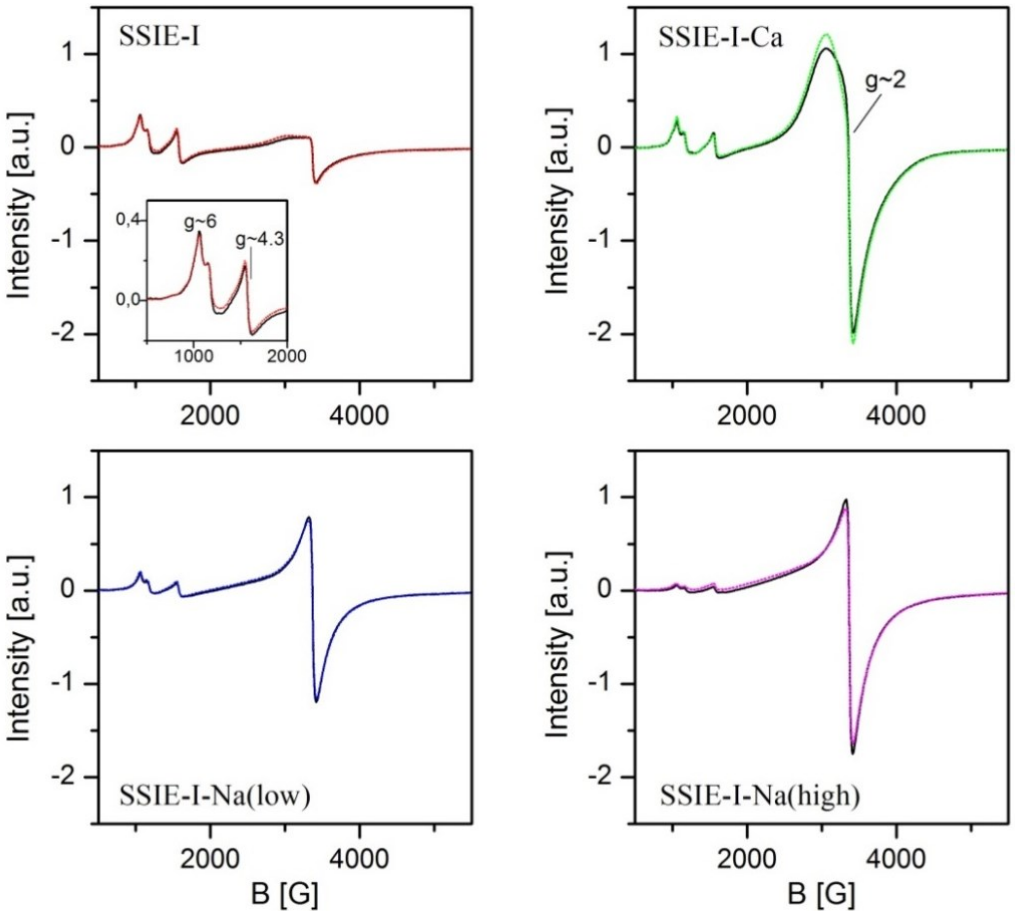

Figure 4.20 *Operando* EPR spectra of SSIE-I-Na/Ca catalysts at 350 °C under initial NO oxidation (black continues lines), and after contact with standard SCR conditions, meaning activated NO oxidation (colored dotted lines). Gas feed: $NO/O_2/Ar$.

The MS signal of NO_2 was recorded parallel to the above mentioned EPR experiments; it is shown in Figure 4.21. During the initial NO oxidation, NO_2 was produced slowly and reached a maximum that is still lower than that obtained during the activated NO oxidation. Additionally, in the activated NO oxidation the maximum conversion is achieved faster. A quantitative analysis is not possible with these data. However, the MS monitoring across the *operando* EPR/MS measurements and its qualitative analysis confirms the activation effect.

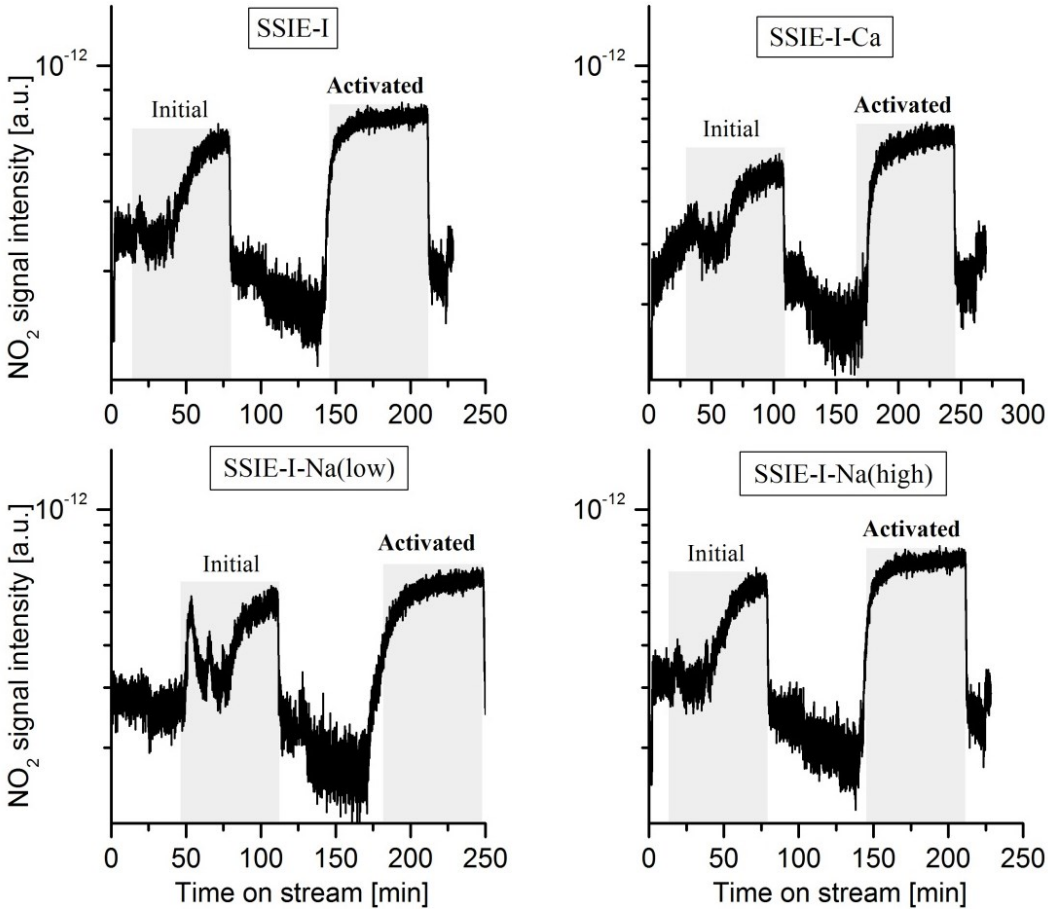

Figure 4.21 MS signal of NO_2 *for* SSIE-I-Na/Ca catalysts during initial NO oxidation and activated NO oxidation at 350 °C. Gas feed: $NO/O_2/Ar$.

Figure 4.22 gives a comparison of the SSIE-I-Na/Ca catalysts under steady-state of the activated NO oxidation measured at 350 °C. Here, clearly narrowing of the signal around $g \approx 2$ for SSIE-I-Na samples can be observed. It points to large clusters with high order where an effective spin exchange interaction can occur. SSIE-I-Ca showed a broad lobe which suggests the presence of smaller clusters or of clusters with higher disorder in their structure.

For a better analysis of the signals at low field, an insert of them was introduced in Figure 4.22. The signal of $g \approx 6$ and $g \approx 4.3$ are almost equal for SSIE-I and SSIE-I-Ca samples that show also similar activity in the NO oxidation. These signals are remarkably smaller for the SSIE-I-Na, especially in the sample with higher amounts of Na, in which the activity of fast SCR and NO oxidation was also the lowest, in relation with the other catalysts. Based on these results, it may be suggested that isolated sites also play a major role in the oxidation of NO to NO_2.

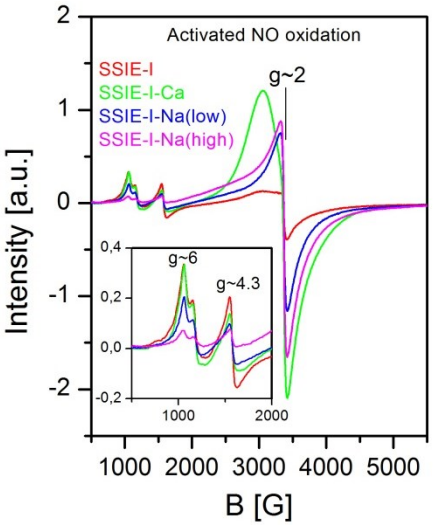

Figure 4.22 *Operando* EPR spectra of SSIE-I-Na/Ca catalysts at 350 °C under activated NO oxidation. Gas feed: $NO/O_2/Ar$. Signals in the low field are better displayed in the insert.

4.2.3.2 *In situ* UV-Vis spectroscopy

In situ UV-Vis spectra of the initial and activated NO oxidation were performed in the Harrick cell with a fiber optic spectrometer, except for SSIE-I-Ca which was measured with a Cary spectrometer; a previously described system (section 3.3.1.3). The experimental procedure is described as follows: the samples (particle size between 250 – 315 μm) were pretreated by heating in a flow of He up to 350 °C and keeping them under those conditions for 10 minutes. This temperature was measured at the bottom of the Harrick cell. However, we have found that the temperature at the surface of the sample is lower than the value measured at the bottom of the cell, by approximately more than 1/3.

The initial NO oxidation was conducted in a flow of 1000 ppm NO, 2% O_2 and He in balance, for 25 minutes to achieve the steady state. Afterwards, at isothermal temperature the standard SCR was conducted in a flow of 1000 ppm NO, 2% O_2, 1000 ppm NH_3 and He in balance. After standard SCR, the activated NO oxidation was done with the same gas flow as in the initial NO oxidation until getting the steady-state. The total gas flow was always 50 ml min^{-1}. The UV-Vis spectra were taken throughout the experiment.

In situ UV-Vis spectra under steady-state of initial and activated NO oxidation, as well as during standard SCR are displayed in Figure 4.23. Comparing the spectra of initial NO oxidation and standard SCR (Figure 4.23, black solid and dashed lines), a strong reduction of the isolated sites and significant reduction of small clusters are displayed during standard SCR for all catalysts. This is due to a reduction of Fe^{3+} with NH_3 present in the mixture. Interestingly, after standard SCR when the activated NO oxidation was performed, all the

previously reduced iron centers were completely reoxidized, which reflects a highly reversible redox system for these Fe-ZSM-5 catalysts.

Negligible changes were displayed between the spectra of initial and activated NO oxidation at steady state (Figure 4.23, black solid and colored dotted lines). Only a small reduction of the cluster band (300 - 400 nm) is detected. Similar to EPR characterization, the species promoting the activation effect turn out to be undetectable through UV-Vis experiments at steady-state.

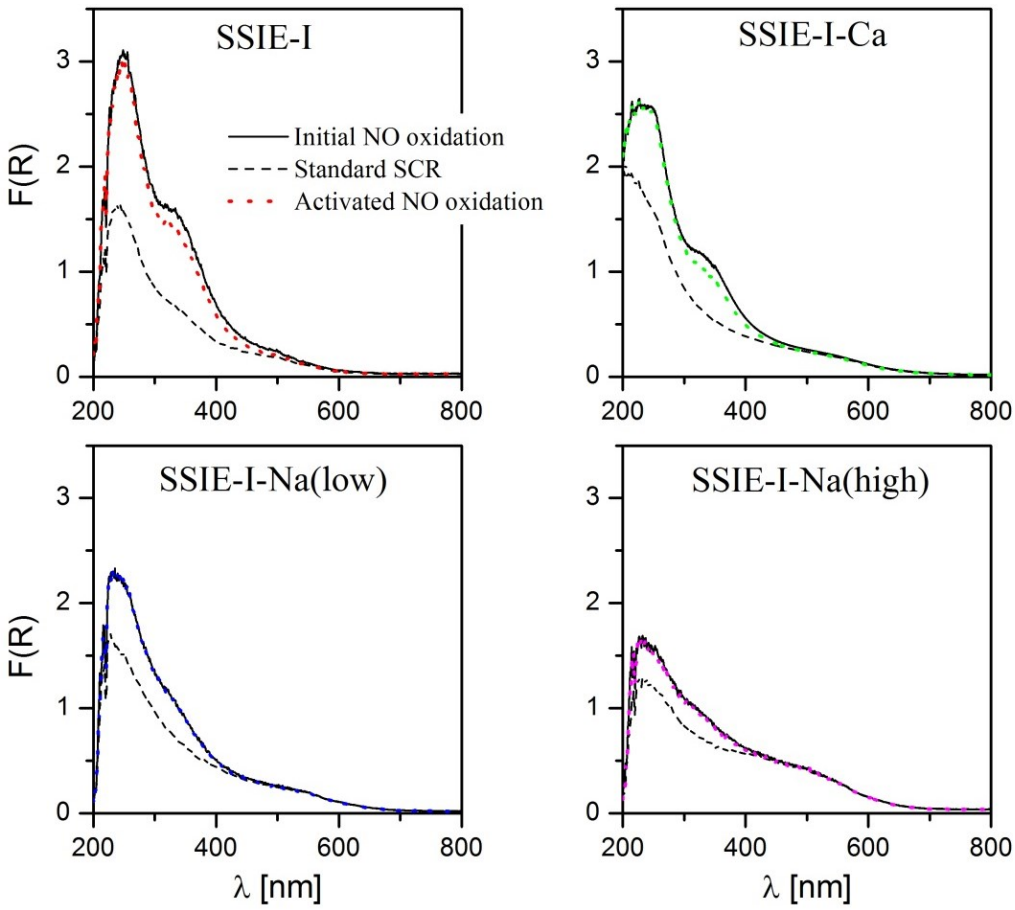

Figure 4.23 In situ UV-Vis diffuse reflectance spectra of SSIE-I-Na/Ca samples under steady-state initial NO oxidation, standard SCR and activated NO oxidation at 350 °C.

The absorbance of the *in situ* UV-Vis spectra during the initial and activated NO oxidation (described above) was also studied in dependence on time at particular wavelength for some of the SSIE-I-Na/Ca catalysts (Figure 4.24). The band of isolated Fe^{3+} sites (246 nm), which showed a strong reduction under standard SCR conditions, was used for these plots. The purpose was to monitor the redox behavior of isolated iron species during both initial and activated NO oxidation.

The plots show a difference between the oxidation of isolated iron species during the initial and activated NO oxidation. In the activated NO oxidation, it took a longer time to reach the steady-state compared to the initial NO oxidation (compare black and colored lines, Figure 4.24). Less than 5 minutes were required to reoxidize the isolated iron sites during the activated NO oxidation for both the most and less active samples (SSIE-I-0.24 and SSIE-I-Na(high), respectively). Therefore, a direct correlation between this delay and the activation phenomenon cannot be possible.

One of the reasons for the delay might be that some iron sites are blocked by adsorbates, produced during the standard SCR. Desorption of this adsorbates and accessibility of iron might occur slowly, similar to the oxidation of iron sites. Another reason could be that two oxidation reactions are occurring simultaneously, the oxidation of a bare Fe^{2+} by O_2 and the oxidation of Fe^{2+}-OH by the release of water. The Fe^{2+}-OH could be a product of the reaction under the standard SCR feed. Similar delay was observed for the band of clusters (plots not shown).

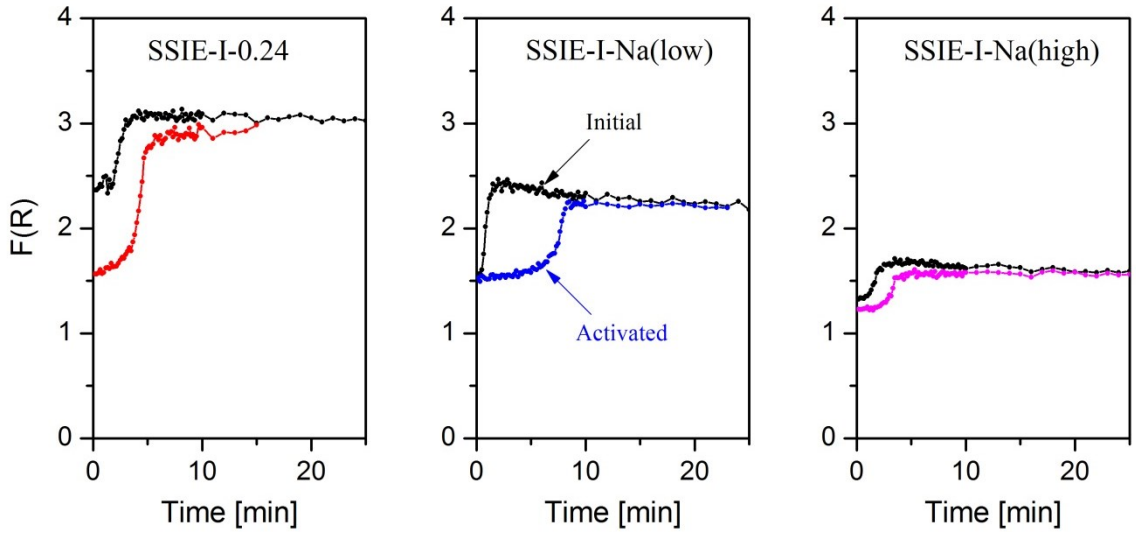

Figure 4.24 Dependence of the intensity of isolated sites band with time during the initial and activated NO oxidation at 350 °C of the band at 246 nm.

4.2.3.3 *In situ* FTIR spectroscopy

The initial and activated NO oxidation was also investigated by *in situ* FTIR spectroscopy. The *in situ* FTIR experiments were performed in a previously described setup (section 3.3.3.1). Each sample was pretreated by heating in a stream of He up to 250 °C and keeping it at this temperature for 10 minutes. After pretreatment, the initial NO oxidation was done switching to a gas mixture of 1000 ppm of NO, 2% O_2 and He to balance for a total flow of 50 ml min^{-1}. After 25 minutes of continuous flow, the cell was closed and held for 10

minutes in order to monitor not only the surface species but also the gas phase. Afterwards, the standard SCR gas mixture was fed and kept for 25 minutes at 250 °C in order to activate the sample. Then, the NO oxidation mixture was flushed again during 25 minutes to monitor the activated NO oxidation. Finally, the cell was closed and maintained for 10 minutes. The FTIR spectra were recorded at steady-state (25 minutes) and during the reactions when the cell was closed. The background spectra of He at 250 °C, which was taken immediately after pretreatment was subtracted from all the IR spectra.

The FTIR spectra of SSIE-I-Ca/Na catalysts under steady-state of initial and activated NO oxidation at 250 °C are shown on Figure 4.25. Mainly three surface species are seen at steady-state, which are the nitrosonium ion (NO^+) at 2130 cm^{-1} [59] , the nitrosyl iron complex (Fe^{2+}-NO) at 1885 cm^{-1} and the adsorbed NO_2 at 1630 cm^{-1}. The adsorbed NO_2 is only observed in SSIE-I, while NO^+ is displayed on both SSIE-I and SSIE-I-Ca, but not for the SSIE-I-Na samples. In the catalysts with co-cation, strong negative bands resulted by the subtraction with the pretreat spectrum, at 1640 cm^{-1} and in the range of hydroxyl groups at 3600 cm^{-1} (spectra not shown), which are assigned to adsorbed water. The assignment was confirmed by the disappearance of these bands at higher temperature (Figure 4.27), in which all the water is released. The strong negative band at 1640 cm^{-1} might hinder the observation of adsorbed NO_2 at 1630 cm^{-1}. Therefore, the band of adsorbed NO_2 is not seen in the samples loaded with Ca/Na.

The presence of reduced Fe^{2+} in all catalyst is confirmed by the band of the complex Fe^{2+}-NO, which is most pronounced in SSIE-I and least in SSIE-I-Na(high). Comparing the spectra after initial and activated NO oxidation, similar bands can be observed for each sample giving no evidence for a potential reason behind the activation effect. Certainly, the iron was reduced under standard SCR conditions (NH_3 containing mixture) and reoxidized by the activated NO oxidation mixture, as the intensity of Fe^{2+}-NO band was similar in the initial and activated spectra.

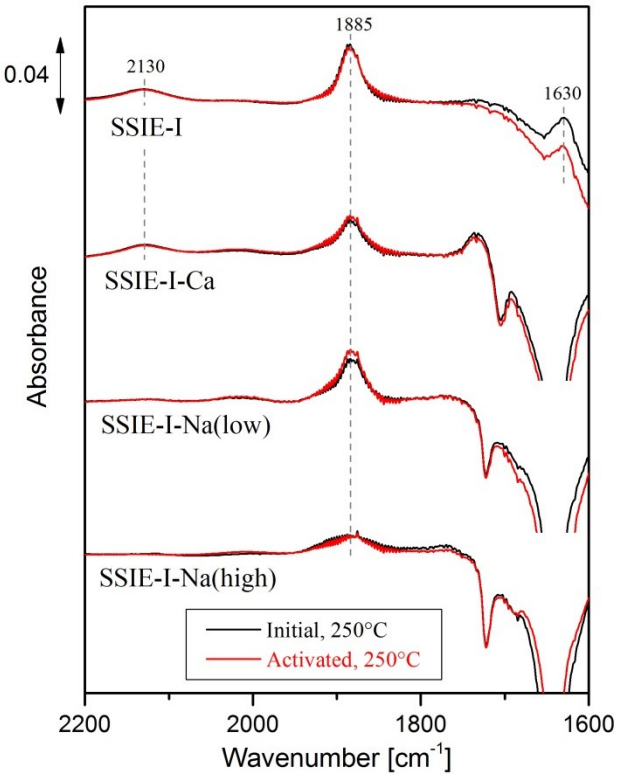

Figure 4.25 *In situ* FTIR spectra of SSIE-Na/Ca catalysts during initial and activated NO oxidation (after contact with standard SCR conditions), at 250 °C. Feed: 1000 ppm of NO, 2% O_2.

In order to analyze possible products removed by the flushing and the behavior of the surface species, the IR cell was closed and the reaction was monitored for 10 minutes. *In situ* IR spectra of 1 and 10 minutes for the initial and activated NO oxidation are both displayed in Figure 4.26. On SSIE-I catalysts, the intensity of the Fe^{2+}-NO band (1885 cm^{-1}) decreased after 10 minutes, while the band of adsorbed NO_2 (1630 cm^{-1}) increased (above blue spectra, Figure 4.26 A and B). The disappearance of the Fe^{2+}-NO band can be explained by the reoxidation of Fe^{2+} with NO_2, since NO_2 is formed and detected inside the cell. Fe^{3+} is not detected by IR because the complex Fe^{3+}-NO is unstable at this temperature. With no continuous flow a signal of weak physisorbed NO_2 could be observed with increasing intensity over time.

By comparing the initial and activated NO oxidation reactions after 10 minutes in a closed cell, a decreasing intensity of the Fe^{2+}-NO band at 1885 cm^{-1} can be seen for all the catalysts under activated NO oxidation (Figure 4.26, B), which is not the case in all the catalyst during initial NO oxidation (Figure 4.26, A). As previously described, the activation leads to higher production of NO_2 and therefore a higher possibility to reoxidize Fe^{2+}.

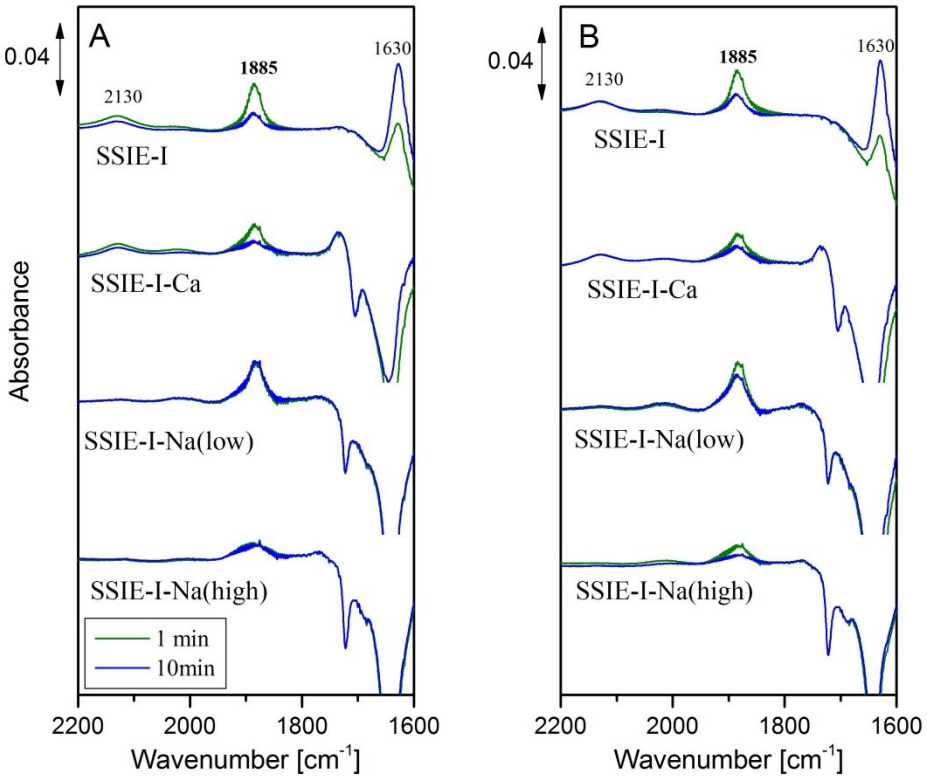

Figure 4.26 *In situ* FTIR spectra of SSIE-Na/Ca catalysts during initial (A) and activated (B) NO oxidation in a closed cell, at 250 °C. Feed: 1000 ppm of NO, 2% O_2.

A similar experiment was performed for the most and least activated samples (SSIE-I and SSIE-I-Na(high)), but instead of using 250 °C, higher temperature (350 °C) close to the maximum in the conversion curves was chosen (Figure 4.16). The *in situ* FTIR spectra of SSIE-I and SSIE-I-Na(high) on initial and activated NO oxidation at 350 °C are shown in Figure 4.27. At this temperature, the catalysts are more reactive for the NO oxidation and the adsorbed NO_2 is displayed for both SSIE-I and SSIE-I-Na catalysts.

A new band at 1598 cm^{-1} emerged, this band together with the band at 1630 cm^{-1} (overlap with the adsorbed NO_2 band) are assigned to different forms of surface nitrates [33]. The band of the iron nitrosyl complex is not observed in SSIE-I-Na(high) at 350 °C, only the characteristic rotation bands of the NO gas are observable. This suggest that SSIE-I-Na(high) does not contain iron sites capable to fixate NO, and explains its low activity in the NO oxidation, compared to the other catalysts.

At steady-state in SSIE-I (Figure 4.27, left plot a), the bands of all adsorbates are higher in the activated NO oxidation, which confirms that the catalyst became more active. After 10 minutes of the reaction in the closed cell (Figure 4.27, b), the intensity of the bands of adsorbed NO_2 and surface nitrates increased considerably, while the intensities of the NO^+ and Fe^{2+}-NO bands decreased.

A reason for the activation effect observed in Figure 4.16 can also not be concluded from the IR data.

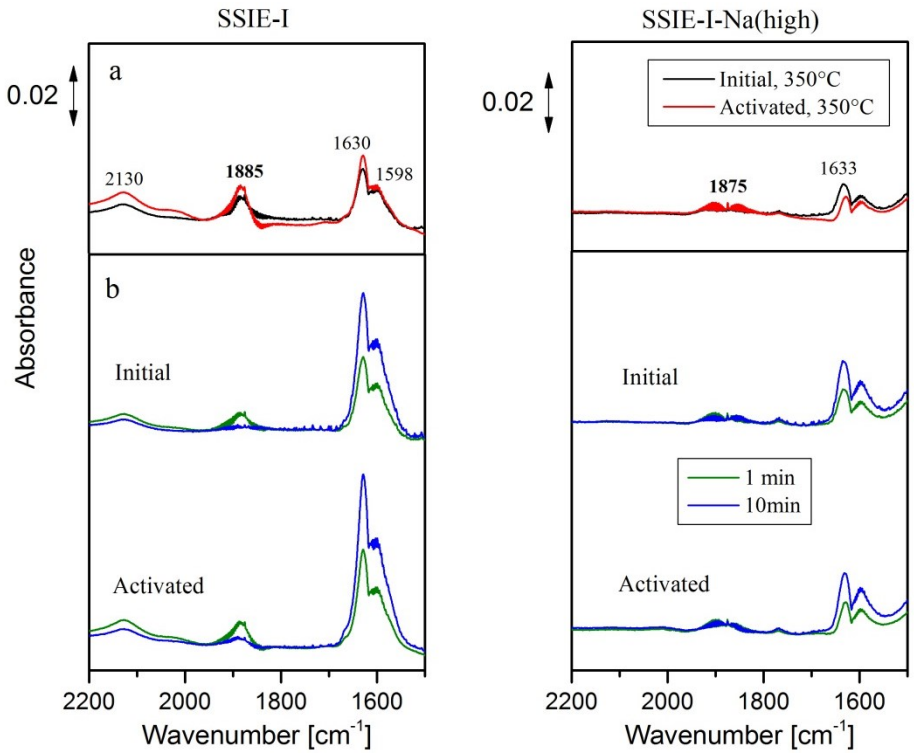

Figure 4.27 *In situ* FTIR spectra of SSIE-I and SSIE-I-Na(high) catalysts during initial and activated NO oxidation at steady-state (a) and with a closed cell (b), at 350 °C. Feed: 1000 ppm of NO, 2% O_2.

4.2.3.4 Coupling *in situ* UV-Vis-DR/DRIFTS analysis

The CFeZ catalyst was tested under initial and activated NO oxidation by coupled UV-Vis-DR/DRIFT spectroscopy in order to have a parallel information about the surface species (by DRIFTS) and aggregation or electronic changes (by UV-Vis-DRS). The coupling setup system is described in section 3.3.2. Approximately 50 mg of CFeZ with a particle size of 250 - 315 μm were used for the experiment. The catalyst was pretreated by heating it in a flow of He up to 250 °C and keeping for 10 minutes. At this temperature the NO oxidation gas mixture (1000 ppm NO, 2% O_2 and He) with a flow of 50 ml min^{-1} was dosed and the reaction was monitored by both DRIFTS and UV-Vis-DRS until steady-state. Afterwards, the standard SCR mixture (1000 ppm NO, 2% O_2, 1000 ppm NH_3 and He) was introduced and kept for 20 minutes. Switching to the NO oxidation mixture the activated NO oxidation was carried out; which was also monitored by both DRIFT and UV-Vis-DR spectroscopy until steady-state. Later, the temperature was increased in a flow of He up to 350 °C and similar to the reaction at 250 °C, the initial and activated NO oxidation were carried out and monitoring

by spectroscopy. The spectrum in He at 250 or 350 °C was subtracted to the IR spectra at steady-state, for the respective temperatures.

In Figure 4.28 A and B, the *in situ* DRIFT and UV-Vis spectra of CFeZ at 250 and 350 °C under steady-state of initial and activated NO oxidation are displayed. In the DRIFT spectra at 250 °C, the band of Fe^{2+}-NO complex was observed at 1887 cm^{-1}, which increased during the activated NO oxidation. At 350 °C during the activated NO oxidation a larger amount of NO^+ is produced (band at 2160 cm^{-1}). NO^+ might be formed either on the Brønsted acid sites or by the iron exchanged in cationic positions (Equation 2.10 and 2.11, respectively; page 12). The band of the Fe^{2+}-NO complex (1887 cm^{-1}) and NO_2 (1630 cm^{-1}) are observed at high temperature in both initial and activated NO oxidation (Figure 4.28, A).

The UV-Vis-DR spectra taken simultaneously to the DRIFT spectra displayed different behavior depending on the temperature. At 250 °C, the whole intensity of the UV-Vis spectra decreased upon activation, which agrees with the increasing intensity band of Fe^{2+}-NO. In contrast at 350 °C, the intensity of the UV-Vis spectra increased after activation.

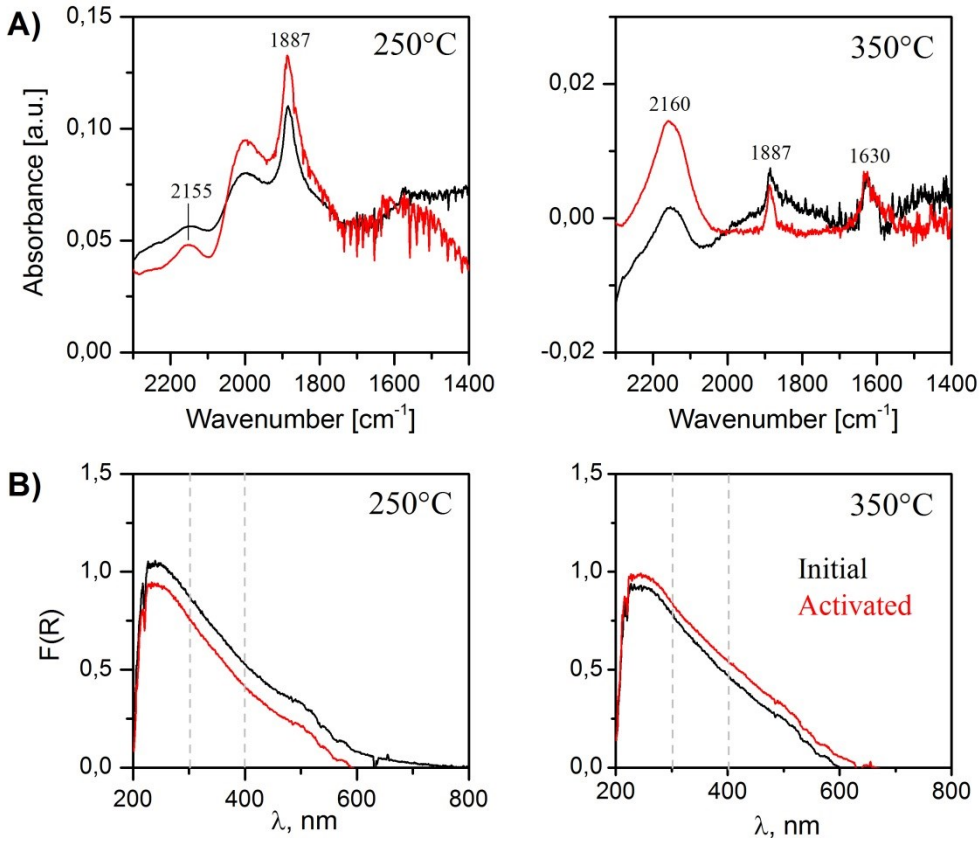

Figure 4.28 A) DRIFT and B) UV-Vis-DR spectra of CFeZ after 20 minutes of initial and activated NO oxidation (activated means after standard SCR) at 250 °C and 350 °C, left and right respectively.

4.3 Investigating the mechanism of NH_3-SCR of NO_x

Different mechanisms for standard and fast SCR have been proposed, as earlier discussed in section 2.4. In order to have a better understanding of the different steps of these reactions and the possible participation of specific iron species in the intermediate reactions, *in situ* FTIR and EPR spectroscopic studies have been done in this work. The investigation of the mechanism of the NH_3-SCR of NO_x reactions was realized using the commercial Fe-ZSM-5 catalyst, CFeZ.

4.3.1 Catalytic activity

The performance of CFeZ under standard and fast SCR reactions in dependence on temperature is shown in Figure 4.29. Similar to the reports in literature for other Fe-ZSM-5 catalysts [7, 76], higher activity was achieved at low temperatures during the fast SCR over the CFeZ catalyst (0.82 wt.% Fe content). At 250 °C, 76% NO conversion was reached during fast SCR, while only 3% NO conversion was detected during standard SCR. The latter reaction accomplished more than 70% NO conversion at 450 °C.

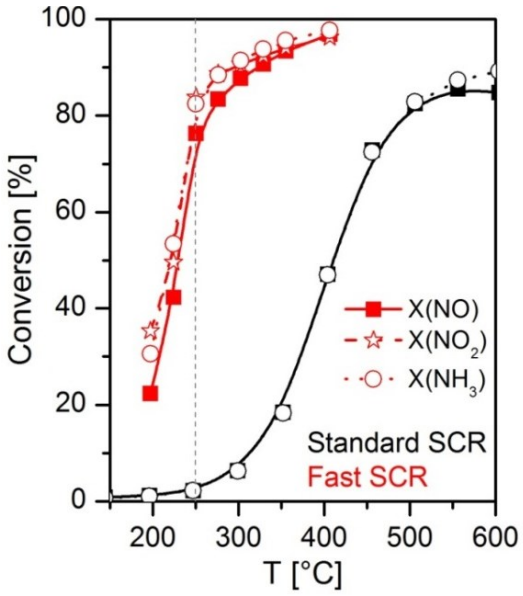

Figure 4.29 Dependence of standard (black line) and fast (red line) SCR over CFeZ on temperature. Standard SCR feed: 1000 ppm NO, 1000 ppm NH_3, 2% O_2 and He. Fast SCR mixture: 500 ppm NO, 500 ppm NO_2, 1000 ppm NH_3, 2% O_2 and He.

One of the reasons that the fast SCR showed higher NO conversion than standard SCR at low temperatures was attributed in this work (section 4.1) to the fast reoxidation of isolated iron sites by NO_2, keeping them active as Fe^{3+}. The main impact of NO_2 was observed on

isolated iron on β sites (iron in a distorted octahedral coordination), and a partial influence of NO_2 on isolated iron on γ sites (iron in a distorted tetrahedral coordination).

In addition to the specific active sites, the understanding of their redox capability in intermediate reactions and the reaction mechanism of the fast and standard SCR are relevant for a better control of the chemical reaction and performance of the catalyst. Therefore, several *in situ* EPR and FTIR experiments were carried out using different gas mixtures related to the composition of the NH_3-SCR of NO_x reactions.

4.3.2 *In situ* FTIR and EPR spectroscopic studies

In situ FTIR and EPR experiments with CFeZ were performed using the setup previously described (sections 3.3.1.1 and 3.3.1.2, respectively). 50 mg of the catalysts pressed in a self-supporting disc were used for the *in situ* FTIR experiments, while approximately 30 mg of the catalyst with particle size of 250 - 315 μm were applied in the *in situ* EPR experiments. The total gas flow was 50 ml min^{-1} for the *in situ* FTIR experiments and 30 ml min^{-1} for the *in situ* EPR experiments. To accomplish these total flows, an inert gas (He/Ar) was used for balance.

In the experiments different feed components (NH_3, NO_2, NO) and a mixture of gases (NO/O_2) were dosed into the FTIR and EPR cells, which contained either the pre-reduced catalysts, the pre-oxidized catalysts or the catalysts after reaction with NO_2 and NO. These experiments were done at 150 and 250 °C. The concentration of the feed components was 500 ppm at 150 °C and 1000 ppm at 250 °C. The mixture of NO/O_2 was achieved by adding 2% of O_2 to the feed of NO.

The pre-oxidized catalyst was obtained by heating the CFeZ in a flow of synthetic air to 400 °C, then cooling down in flow of inert gas to 150 or 250 °C and keeping at this temperature for 20 minutes. The pre-reduced catalyst corresponds to CFeZ after interaction with NH_3 for 20 minutes at the related temperature (150 and 250 °C). Additionally, CFeZ after reaction with NO_2 and NO was used as initial state of the catalyst.

All spectra were taken at steady-state (20 min). For the FTIR spectra, the spectrum of the pretreated catalyst was subtracted from all spectra recorded at steady-state. The EPR spectra were normalized by dividing every spectrum by the amplitude of the signal at $g \approx 4.3$ from the spectrum in inert gas after pretreatment; this normalization was done for all spectra in each experiment.

Furthermore, to study the reactivity of iron species under dosage of the complete mixture of the NH_3-SCR reactions, *in situ* FTIR and EPR experiments with the whole mixture of the standard and fast SCR were performed over CFeZ.

The experimental procedure of the *in situ* EPR experiments was similar to that described in section 4.1.3, but in these experiments the outlet of the gases was not connected to the MS spectrometer. In the *in situ* FTIR experiments, the sample was pretreated by heating in a flow of He to 150 or 250 °C. For the standard SCR reaction, first an oxidative mixture was streamed for 20 minutes, consisting of 1000 ppm NO, 2% O_2, balanced with He to the total flow of 50 ml min^{-1}. Afterwards, 1000 ppm NH_3 were added to achieve the complete mixture of standard SCR, and the reaction was monitored for 20 minutes. Finally, NH_3 was again removed, monitoring the catalyst in oxidative conditions for 20 minutes. For fast SCR reaction, a similar procedure as in the standard SCR was performed. In this case 500 ppm of NO and 500 ppm NO_2 were dosed instead of 1000 ppm NO. The *in situ* FTIR experiments were performed at 150 and 250 °C.

4.3.2.1 Reaction of feed components with a catalyst pre-oxidized at 400 °C in air

In situ EPR spectra of CFeZ under inert gas, after oxidative pretreatment, and under feed components at 150 °C and 250 °C are displayed in Figure 4.30. By reaction with the reducing agent NH_3 at 150 °C, the signal of distorted octahedral Fe^{3+} (β sites) was completely reduced and that of distorted tetrahedral Fe^{3+} (γ sites) partially diminished (Figure 4.30 A). Besides, NO promotes a decrease mainly in the signal of Fe^{3+} on β sites; this can be explained by the reduction of Fe^{3+} to Fe^{2+} during the oxidation of NO to NO^+ or NO_2 (Equations 2.6 and 2.11, pages 11 and 12, respectively). On the other hand, NO_2 strongly oxidized iron on γ sites and partially reduced Fe^{3+} on β sites. The oxidation of Fe^{2+} to Fe^{3+} on γ sites can be associated to the reduction of NO_2 to NO (Equation 4.1), while the reduction of Fe^{3+} to Fe^{2+} on β sites might be related to the formation of nitrates (Equation 4.3) and/or probable formation of NO^+ (Equation 2.11) from NO, being a product of the reduction of NO_2.

$$NO_2 + Fe^{3+}\text{-}O \leftrightarrow NO_3^- + Fe^{2+} \qquad 4.3$$

At 250 °C, NH_3 reduced completely the Fe^{3+} on β sites, and partially the Fe^{3+} on γ sites and Fe_xO_y clusters (Figure 4.30 B). In contrast to the observed effect at lower temperature, at 250 °C NO and NO_2 reacted similarly over isolated iron sites. At this temperature a part of the Fe^{2+} on γ sites was oxidized and a part of Fe^{3+} on β sites were reduced (Figure 4.30 B).

The partial reduction of Fe^{3+} on β sites is certainly attributed to the formation of NO^+ and NO_2^- in the case of reaction with NO, and NO^+ and NO_3^- in the reaction with NO_2. This result shows the capability of Fe^{3+} on β sites to oxidize NO_x to NO_{x+1} (being x = 1 or 2) in absence of added oxygen, this suggests that oxygen from the zeolite is able to react on this type of iron species. The surface species NO^+, NO_2 and NO_3^- were observed by FTIR and are discussed in detail below (Figure 4.34 and Figure 4.35 A).

The slight oxidation of Fe^{2+} on γ sites is explained by the reduction of NO_2 to NO over Fe^{2+} species oxidizing them to Fe^{3+}-O (Equation 4.1), and probably by the reduction of NO. A reaction which depicts the reduction of NO and oxidation of Fe^{2+} is proposed as follow (Equation 4.4):

$$NO + Fe^{2+}\text{-}OH \leftrightarrow HNO + Fe^{3+}\text{-}O \qquad 4.4$$

The nitroxyl HNO has often been postulated as intermediate in reactions which give N_2O [77].

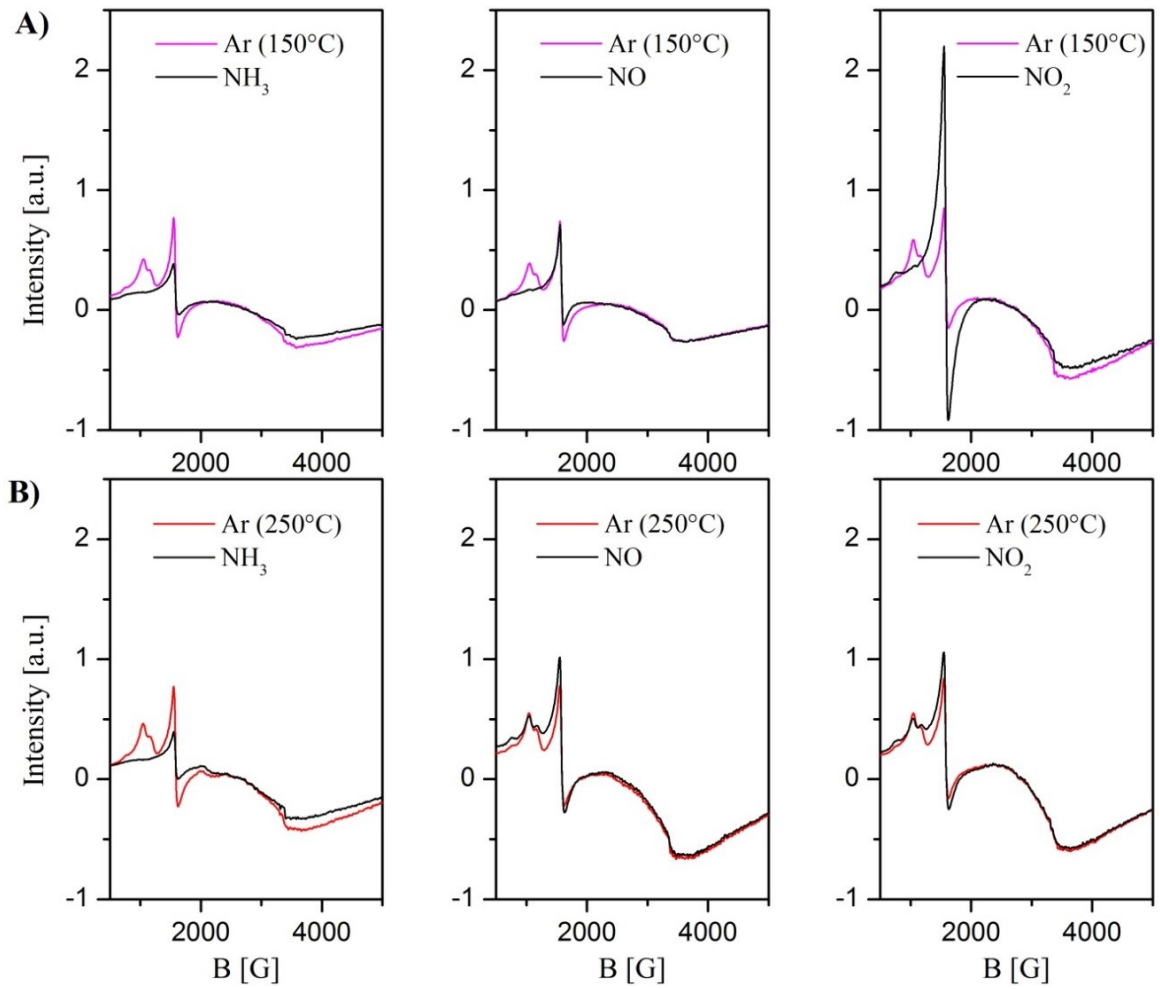

Figure 4.30 In situ EPR spectra of CFeZ at steady-state of reaction in inert gas and NH3, NO or NO_2; at 150 °C (A) and 250 °C (B).

4.3.2.2 Reaction of feed components with a catalyst pre-reduced in NH_3/He

In situ FTIR and EPR spectra of CFeZ obtained at 150 and 250 °C upon contact with NO, after reduction with NH_3, are displayed in Figure 4.31. During interaction of the catalyst with NH_3 the NH_4^+ bands at 1446 cm^{-1} (150 °C) and 1454 cm^{-1} (250 °C) are observed in the *in situ* FTIR spectra (Figure 4.31 A, green spectra). Additionally, the negative band of hydroxyl groups at 3600 cm^{-1} (Si(OH)Al) was also seen at both temperatures, while the negative band at 3664 cm^{-1} was only seen at 150 °C (Figure 4.31 A, green spectrum left). The band at 3664 cm^{-1} has been assigned to OH groups linked with extraframework iron (Fe-OH) [45]. This result confirms that NH_3 can be stored on the catalyst in form of NH_4^+, exchanging the proton from the Si(OH)Al groups at 250 °C and both Si(OH)Al and Fe-OH groups at 150 °C.

When NO reacted after reduction with NH_3 at 150 °C, the intensity of the NH_4^+ band in the FTIR spectra was partially diminished (Figure 4.31 A, blue spectrum left). In the EPR spectra, the signals of Fe^{3+} on γ sites became less intensive, and a new signal at $g \approx 2.07$ appeared (Figure 4.31 B, blue spectrum left). This latter signal could stem from paramagnetic NO adsorbed on iron sites or other Lewis sites of the zeolite, although the assignment of this signal has only been reported at low temperatures [73, 78]. The reduction of the signal of Fe^{3+} on γ sites can be due to a dipolar coupling between the paramagnetic NO and some Fe^{3+} sites, making them silent in EPR.

Upon reaction with NO after reduction with NH_3 at 250 °C, the band of Fe^{2+}-NO at 1875 cm^{-1} emerged and the NH_4^+ band was completely removed, while the band related to Si(OH)Al groups at 3600 cm^{-1} was recovered (Figure 4.31 A, blue spectrum right). A proposed reaction that explains the reduction of the NH_4^+ band at higher temperature (250 °C) by interaction with NO is the direct reaction between NO and NH_4^+ over the reduced Fe^{2+} species (Equation 4.5). The Fe^{2+} species are evidenced by the band of Fe^{2+}-NO surface species in the FTIR spectra (Figure 4.31 A, blue spectrum right).

$$NO + NH_4^+ + Fe^{2+} \rightarrow HNO + NH_3 + Fe^{3+} \qquad 4.5$$

The HNO species were not detected by FTIR spectroscopy. However, the reoxidation of all iron species during reaction with NO at 250 ° C was observed in the *in situ* EPR spectrum (Figure 4.31 B, blue spectrum right). This supports the above proposed reaction, in which part of the Fe^{2+} is oxidized to Fe^{3+} by NO.

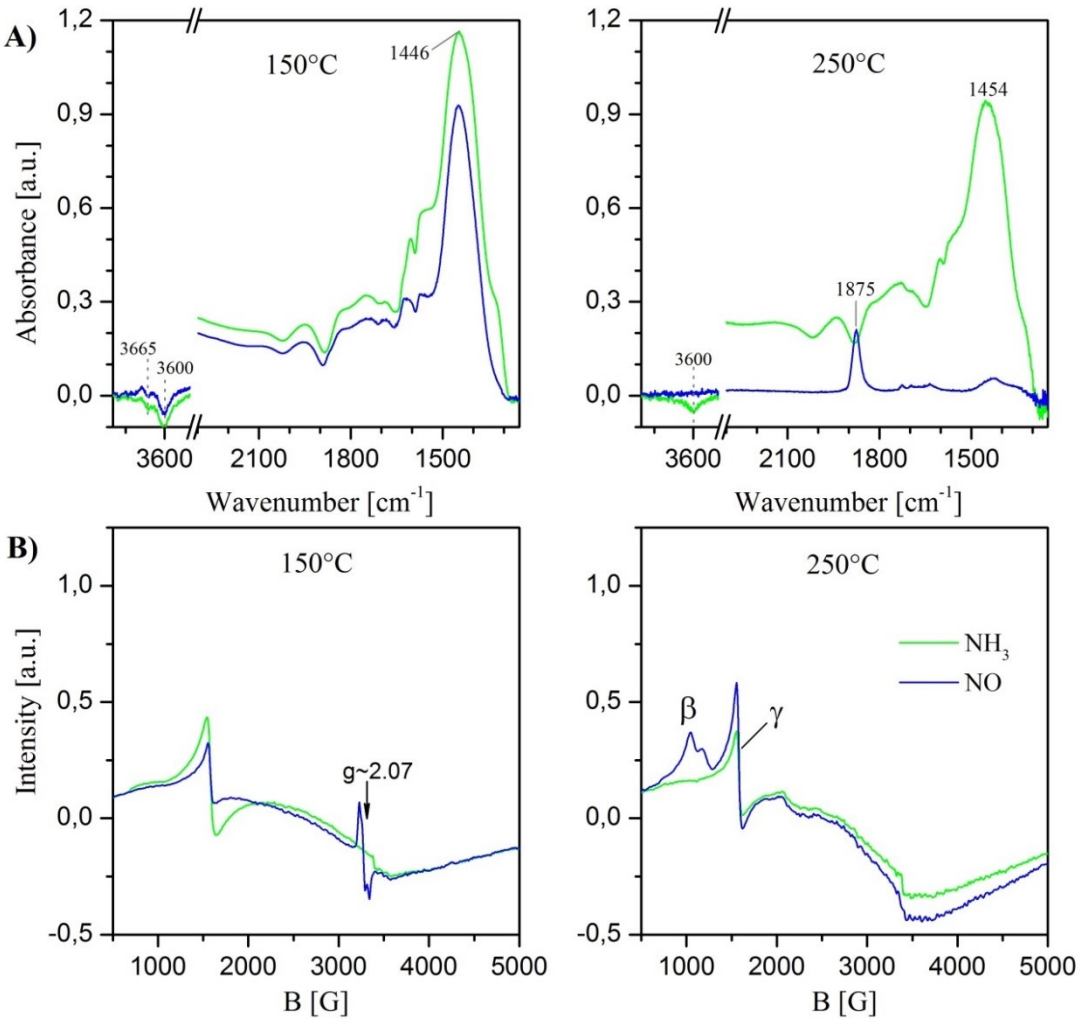

Figure 4.31 *In situ* FTIR (A) and EPR (B) spectra of CFeZ at 150 and 250 °C under NO, after pre-reduction with NH_3.

In situ FTIR and EPR spectra of CFeZ obtained at 150 and 250 °C during reaction with NO_2, after contact with NH_3, are shown in Figure 4.32. The *in situ* FTIR spectra of NO_2 after pre-treatment in NH_3 (Figure 4.32 A, red spectra) show the bands of adsorbed NO_2 (1632 cm^{-1}), surface nitrates (1575 cm^{-1}) and additional bands at 1616 and 1317 cm^{-1} at both temperatures. These latter bands can be attributed to nitrates located next to ammonium ions. The band of NH_4^+ remained almost unaffected at 150 °C, while it decreased significantly at 250 °C and shifted from 1456 to 1444 cm^{-1} (Figure 4.32 A, red spectra), which indicates higher reactivity at rising temperatures and a change in the chemical environment of the NH_4^+ species, since NH_4NO_3 might be formed. The diminishing of the NH_4^+ band can be associated with the decomposition of NH_4NO_3 into N_2O and H_2O (Equation 2.16, page 14). Moreover, due to the fact that a part of NO_2 is reduced to NO, the latter becomes available for reaction with NH_4NO_3 to produce NO_2, N_2 and H_2O, as described in the mechanism of the fast SCR (Equation 2.15, page 13). The stability of the NH_4^+ band at different temperatures agrees with

the reactivity of NH_4NO_3, described by Grossale et al. [6], who observed preferential formation of NH_4NO_3 at low temperature, while its reaction with NO was only detected at 190 °C.

The respective EPR spectra show that at 150 °C the intensity of the signal of Fe^{3+} on γ sites was strongly increased, the signal of Fe_xO_y clusters was partially enlarged and the signal of Fe^{3+} on β sites was not seen (Figure 4.32 B, red spectrum left). Similar behavior of the iron species was observed when NO_2 reacted after pretreatment in synthetic air at the same temperature (Figure 4.30 A, black spectra right). This indicates that in both cases NO_2 is able to reoxidize residual Fe^{2+} in γ positions.

At 250 °C all the signals of isolated iron on γ and β sites as well as Fe_xO_y clusters became more intense (Figure 4.32 B, red spectra right), pointing to effective reoxidation of residual Fe^{2+} in different geometry. Certainly, all kind of iron species were reoxidized at this temperature by the reduction of NO_2 (Equation 4.1), in which NO and Fe^{3+}-O are produced.

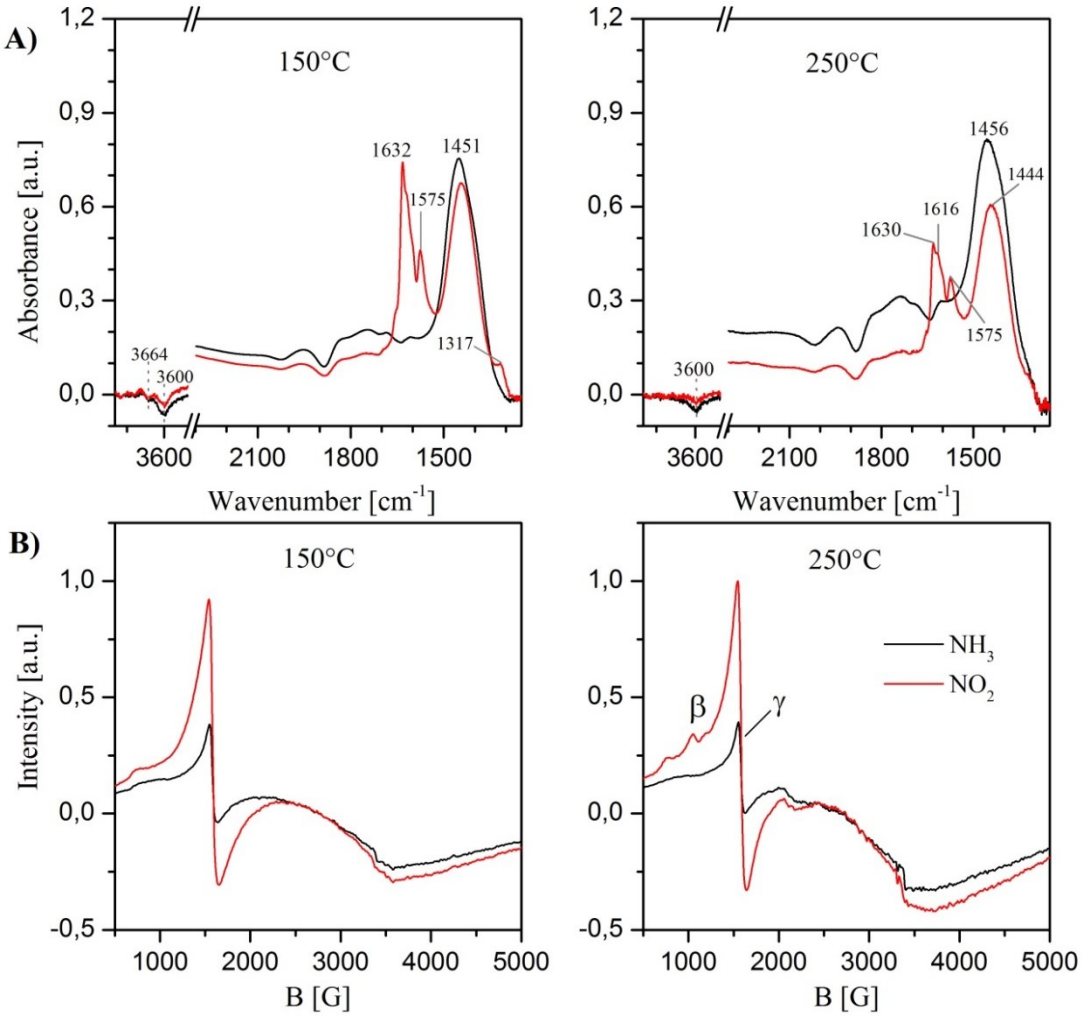

Figure 4.32 *In situ* FTIR (A) and EPR (B) spectra of CFeZ at 150 and 250 °C under NO_2, after pre-reduction with NH_3.

In situ FTIR and EPR spectra of CFeZ measured during reaction with NO/O_2, after reduction with NH_3, at 150 and 250 °C are shown in Figure 4.33. After reaction with NH_3, the mixture of NO/O_2 removes all the NH_4^+ stored on the catalysts at 250 °C, as observed by the vanishing of the NH_4^+ band at 1447 cm^{-1} and recovery of the hydroxyl bands at 3664 and 3600 cm^{-1}. In contrast, at 150 °C, the band of NH_4^+ remains (Figure 4.33 A). The high reactivity of the NH_4^+ species against NO at 250 °C was also observed in the absence of O_2 in the mixture (compare Figure 4.31 and Figure 4.33 A right), which suggests that the reaction between the NH_4^+ species and NO is independent of the O_2 gas, or NO_2 formed from the mixture of NO/O_2. Moreover, a competitive adsorption between the NH_4^+ species and NO^+ on the same surface sites might be considered. NO^+ results as product of the oxidation of NO.

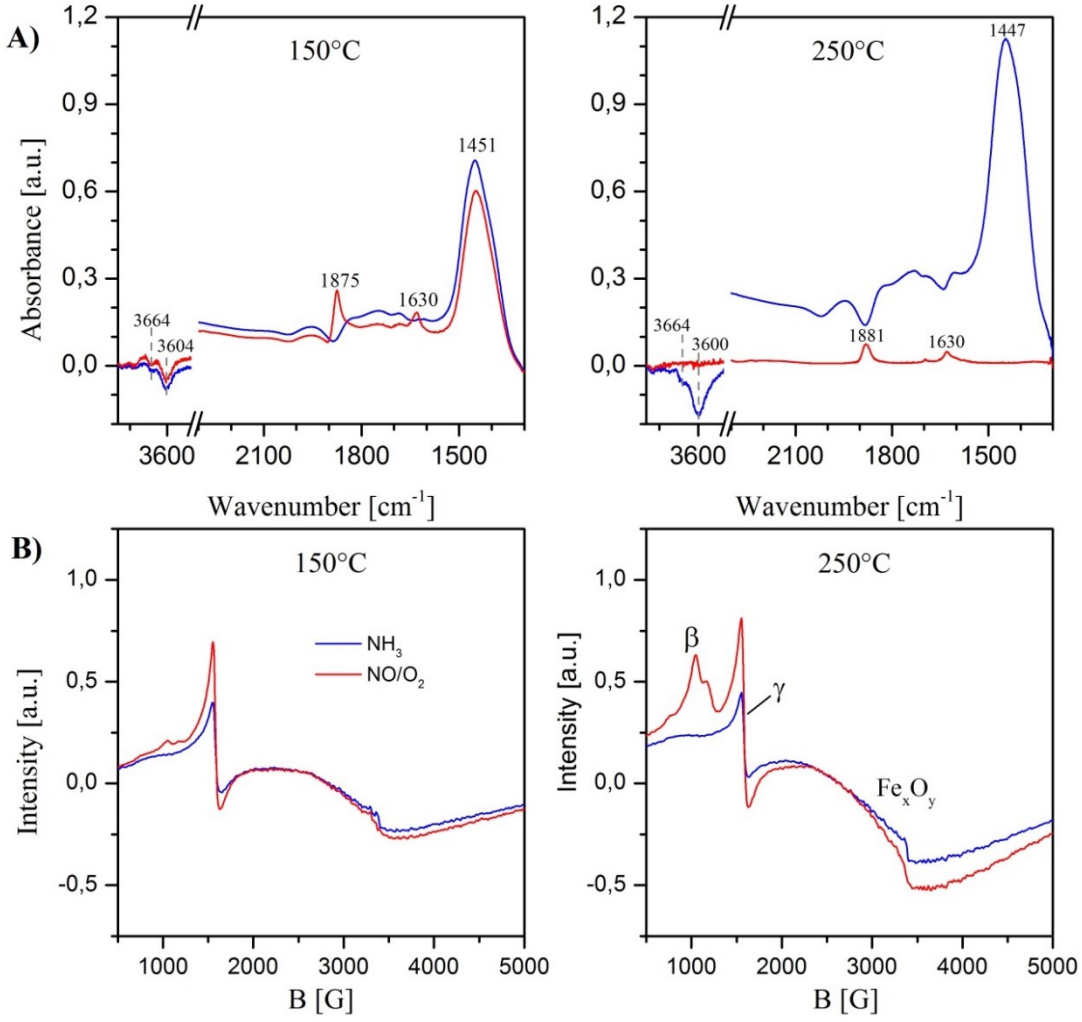

Figure 4.33 *In situ* FTIR (A) and EPR (B) spectra of CFeZ at 150 and 250 °C upon contact with NO/O_2, after pre-reduction with NH_3.

At both temperatures, the band of Fe^{2+}-NO (1875 cm^{-1}) and the band of adsorbed NO_2 (1630 cm^{-1}) were observed. Interestingly, the band of adsorbed NO_2 was notably seen when

O_2 was present in the mixture with NO at both temperatures, but when NO reacts alone it was just slightly seen (compare Figure 4.31 A). The band intensity of Fe^{2+}-NO was also smaller when oxygen was present in the mixture (compare Figure 4.31 and Figure 4.33 A). This suggests that gaseous O_2 from the mixture NO/O_2 promotes the formation of NO_2 and the oxidation of Fe^{2+} to Fe^{3+}.

The *in situ* EPR spectra confirm the oxidation of iron by the strong intensity of the signal of all Fe^{3+} species (β and γ sites, as well as Fe_xO_y clusters) at 250 °C (Figure 4.33 B). At 150 °C the signal of Fe^{3+} on β sites was slightly visible, with NO/O_2 more than with only NO, which means that adding oxygen, specifically favors the oxidation of β sites (compare with Figure 4.31).

4.3.2.3 Interaction of CFeZ with NH_3 after pretreatment with NO and NO_2

The *in situ* FTIR and EPR spectra of CFeZ obtained under reaction with first NO and then NH_3 at 150 and 250 °C are displayed in Figure 4.34. During interaction with NO, the bands of adsorbed NO_2 at 1628 cm^{-1}, Fe^{2+}-NO at 1877 cm^{-1} and a weak band at 2154 cm^{-1} were observed (Figure 4.34 A, blue spectra). This band at ≈ 2154 cm^{-1} might correspond to NO^+ species, as reported for H-ZSM-5 at 2133 cm^{-1} [59]; the shift to higher wavenumber can be due to the interaction of NO^+ with the iron present in CFeZ (0.82 wt.% Fe). The bands of adsorbed NO_2 and NO^+ species were more evident at 250 °C than at 150 °C, which indicates higher reactivity of the catalyst against NO at increasing temperature. In contrast, the intensity of the Fe^{2+}-NO band was remarkably stronger at 150 °C (Figure 4.34 A, blue spectra left), displaying a higher reduction degree of iron at this temperature. The same behavior was observed in the *in situ* EPR spectra, showing almost no the signal of Fe^{3+} on β sites at 150 °C (Figure 4.34 B, blue spectrum left and Figure 4.30).

Subsequent reaction with NH_3 causes a decrease of the band of Fe^{2+}-NO at 150 °C; probably by the reaction of NO and NH_3. At 250 °C this band was not observed which is due to either reaction or to overlapping with the strong overtone bands of NH_4^+ (Figure 4.34 A, green spectra). In the *in situ* EPR spectra, the signal of iron on β sites remained invisible and signals of iron on γ sites and clusters were partially reduced at both temperatures (Figure 4.34 B, green spectra).

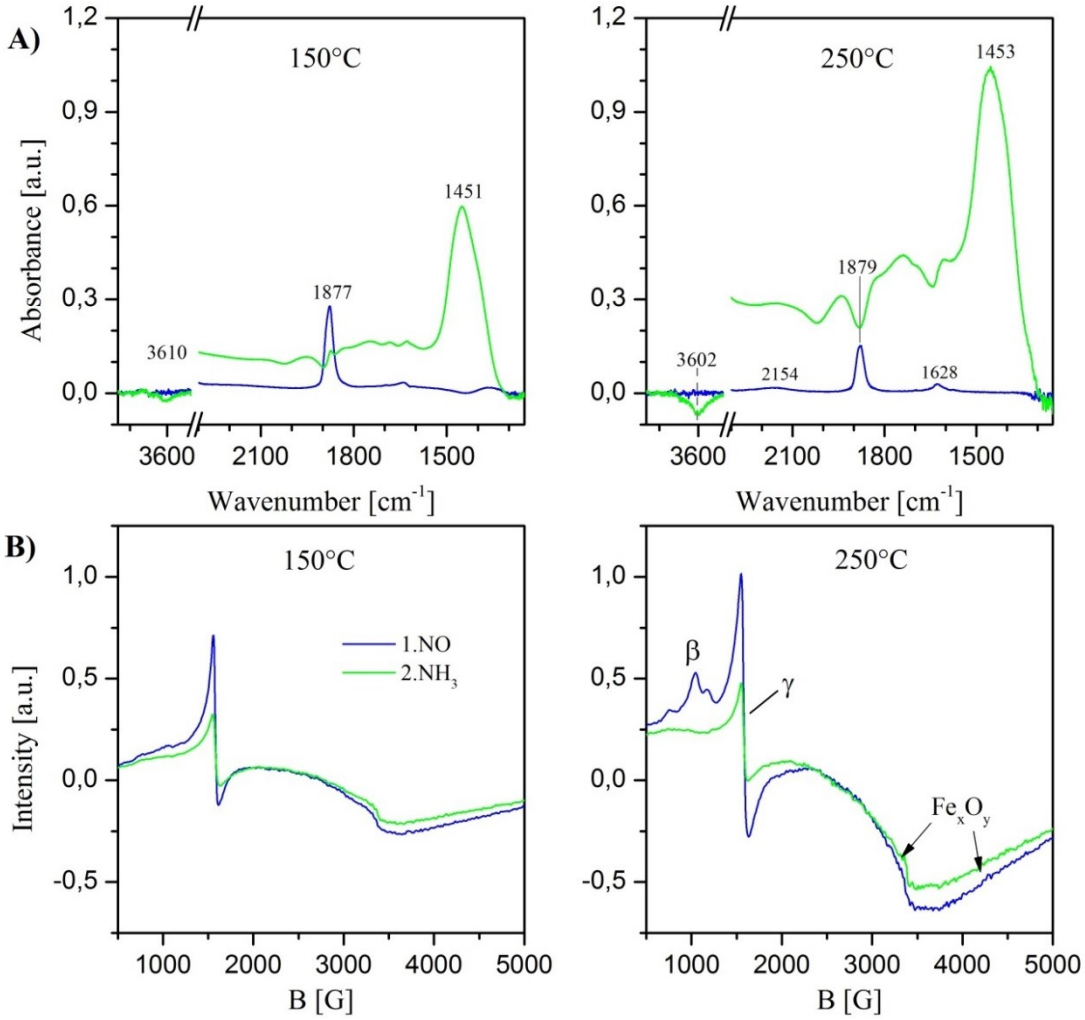

Figure 4.34 *In situ* FTIR (A) and EPR (B) spectra of CFeZ at 150 and 250 °C upon contact with NH_3, after reaction with NO.

In situ FTIR and EPR spectra of CFeZ under reaction with first NO_2 and then NH_3 at 150 and 250 °C are shown in Figure 4.35. When CFeZ first reacted with NO_2, the bands of adsorbed NO_2 (1632 cm^{-1}) and surface nitrates (1575 cm^{-1}) were observed at both temperatures. Additionally, the band of NO^+ at 2154 cm^{-1} was seen (Figure 4.35 A, black spectra). The existence of NO^+ is explained by the oxidation of NO which is a product of the reduction of NO_2. The oxidation and reduction reactions occur at distinct iron sites.

The sites that experience this redox behavior were observed by the *in situ* EPR spectroscopy (Figure 4.30). In particular, the reduction of NO_2 to NO is preferentially catalyzed by Fe^{2+} on γ sites and the oxidation of NO to NO^+ proceeds over Fe^{3+} on β sites. Additionally, the oxidation of NO_2 to NO_3^- can occur over Fe^{3+} on β sites.

On the other hand, Yeom et al. [3] have proposed the formation of NO^+ and NO_3^- by dimerization of NO_2 and further dissociation of the N_2O_4 (Equation 4.6). The facile equilibrium between N_2O_4 and NO_2 ($N_2O_4 \leftrightarrow 2NO_2$) is known in a restricted temperature

range from -10 °C to 140 °C, for instance at 135 °C NO_2 exist in 99% [77]. Since our investigations were done at temperatures (150 and 250 °C), in which formation of N_2O_4 is not favored and the characteristic vibration bands of N_2O_4 were not seen by FTIR spectroscopy, the formation of NO^+ and NO_3^- on CFeZ is not attributed to the dissociation reaction of N_2O_4.

$$2NO_2 \rightarrow N_2O_4 \rightarrow NO^+ + NO_3^- \qquad 4.6$$

Upon reaction with NH_3, after pretreatment with NO_2, the intensity of the band related to adsorbed NO_2 (1632 cm^{-1}) diminished and the band of surface nitrates (1575 cm^{-1}) remained. This suggests that surface nitrates are stable under NH_3 feed, while adsorbed NO_2 tends to react faster with NH_3, especially at 250 °C. Additionally, the NH_4^+ bands at 1445 cm^{-1} (150°C) and 1456 cm^{-1} (250 °C) emerged and the negative band of hydroxyls can be observed (Figure 4.35 A, blue spectra). In the respective *in situ* EPR spectra, it is seen that NH_3 reduces isolated iron on β and γ sites at both temperatures. The broad signal related to Fe_xO_y clusters was mainly diminished at 250 °C (Figure 4.35 B, blue spectra).

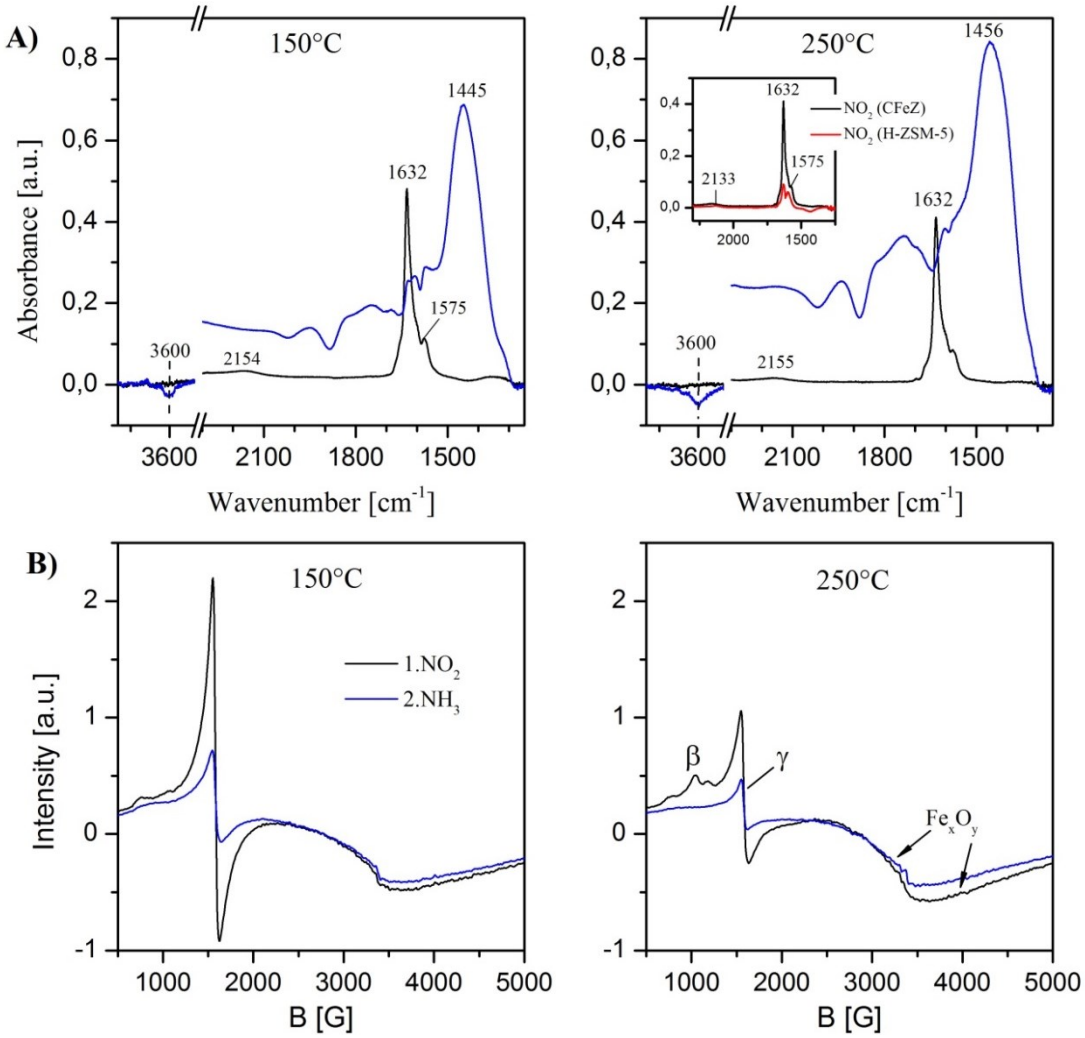

Figure 4.35 *In situ* FTIR (A) and EPR (B) spectra of CFeZ at 150 and 250 °C upon stream of NH_3, after reaction with NO_2. Furthermore, *in situ* FTIR spectra of CFeZ and H-ZSM-5 (insert) under reaction with NO_2 at 250 °C.

On the other hand, *in situ* FTIR spectra of both CFeZ and H-ZSM-5 upon NO_2 stream at 250 °C are displayed in the insert of Figure 4.35. The bands of adsorbed NO_2 and surface nitrates (1632 and 1575 cm^{-1}) were observed on CFeZ, as well as on H-ZSM-5 (1632 and 1598 cm^{-1}). The band of NO^+ appeared at 2133 cm^{-1} on H-ZSM-5,this band is often attributed to a NO^+ which replaces a H^+ site in the zeolite [59]. The band intensity of surface nitrates was significantly higher for CFeZ than for H-ZSM-5, which indicates that some iron species in the CFeZ catalysts favor the formation of such nitrates. Iron species that are missing in the H-ZSM-5.

4.3.2.4 Study of the standard and fast SCR

In situ FTIR spectra of CFeZ measured in oxidative mixtures and during standard and fast SCR conditions are displayed in Figure 4.36. During NO oxidation (NO/O_2) at 150 °C the NO^+ and adsorbed NO_2 could be distinguished by the bands at 2154 and 1629 cm^{-1}, respectively. Additionally, reduced Fe^{2+} was also seen by the complex Fe^{2+}-NO (band at 1874 cm^{-1}). At 250 °C, only the band of the complex Fe^{2+}-NO was observed (Figure 4.36 A, blue dashed spectrum).

In the standard SCR reaction, the band of NH_4^+ at 1447 cm^{-1} arose and the band of Si(OH)Al groups at 3600 cm^{-1} decreased at both temperatures. At 250 °C the bands of Fe^{2+}-NO and NO^+ were not seen anymore (Figure 4.36 A, pink spectra), due to a probable reaction between these surface species and NH_3. Interestingly, when the NO/O_2 mixture was streamed again after standard SCR, the band of NH_4^+ at 150 °C remained. This suggests a strong chemisorption of ammonia on the Brønsted sites at low temperature. As expected, based on observations with individual gases, the band of NH_4^+ completely vanishes after removing NH_3 from the feed at 250 °C (Figure 4.36 A, blue continue spectra).

By exposing the catalyst to the mixture of $NO/NO_2/O_2$, the adsorbed NO_2 band (1630 cm^{-1}), surface nitrate bands (between 1620 - 1578 cm^{-1}) and the band of Fe-OH (3664 cm^{-1}) were additionally seen at both temperatures. When the complete mixture of fast SCR was flushed, the NH_4^+ band increased and surface nitrates partially consumed. Additionally, some water (product of the reaction) was observed with sharp bands in the region 2000 - 1500 cm^{-1} (Figure 4.36 B, red spectra). Removal of ammonia from the gas mixture recovered the initial spectra, which reflects a reversible behavior and no stable chemisorption of the NH_3 on the Brønsted sites (Figure 4.36 B, gray spectra).

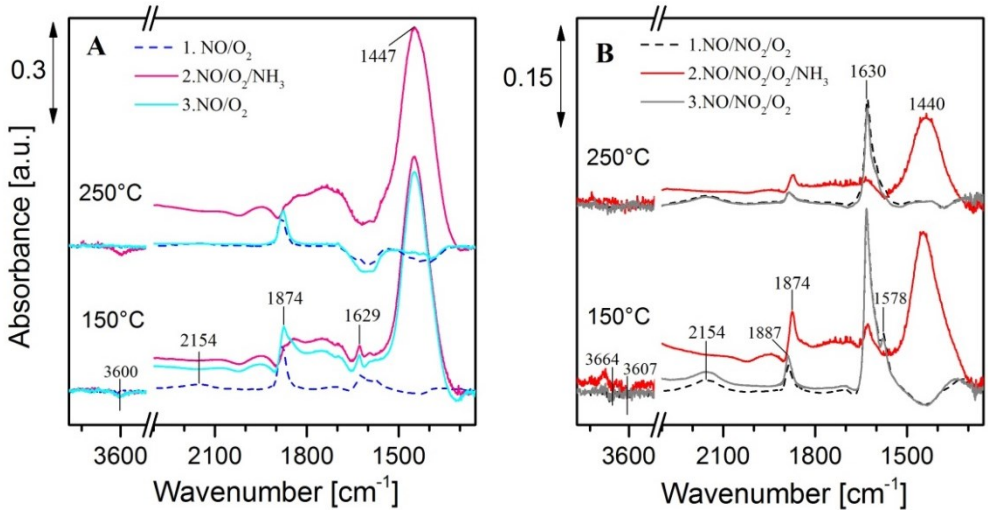

Figure 4.36 *In situ* FTIR spectra of CFeZ during oxidative conditions and standard SCR mixture (A), and oxidative conditions and fast SCR composition (B); at 150 and 250 °C. Feed composition: NO/O_2 and $NO/NO_2/O_2$ (oxidative mixtures), $NO/O_2/NH_3$ (standard SCR) and $NO/NO_2/O_2/NH_3$ (fast SCR).

Indeed, several reactions that were described during exposure to the individual gases occurred simultaneously during the dosing of the complete mixtures of standard and fast SCR. During standard SCR, the oxidation of NO to NO_2 and NO^+ occurs on Fe^{3+}. The formation of NO^+ might also took place in the fast SCR, as detected by FTIR. However, it should not be a main pathway in the reaction mechanism. Nitrate formation is more dominating during fast SCR. The formation of nitrates requires Fe^{3+}, which is reduced to Fe^{2+} (Equations 4.3). Additionally, a reaction in which NO reoxidizes iron by formation of HNO has been proposed (Equation 4.5). HNO might not take part directly in the mechanism of fast SCR, however its formation is expected to involve the reoxidation of isolated iron sites which are needed.

In situ EPR spectra of CFeZ in low magnetic field at 150, 250 and 400 °C during steady-state of standard and fast SCR reactions are shown in Figure 4.37 a) and b), respectively. The corresponding *in situ* EPR spectra in high magnetic field are displayed in Figure 4.37, c) and d). The signal of isolated Fe^{3+} on γ sites was well detected under oxidative conditions for standard and fast SCR, while the signal of isolated Fe^{3+} on β sites in oxidative environments was almost not seen at 150 °C in both reactions. This vanishing of the signal was also noticed at 150 °C in all spectra when only individual NO or NO_2 were dosed (Figure 4.30 A). At higher temperature under oxidative conditions in the absence of NH_3, the signal of isolated iron on β sites was clearly seen (Figure 4.37, a) and b) black lines).

Under standard SCR conditions ($NO/O_2/NH_3$), the signal of Fe^{3+} on β sites completely vanished at 150 and 250 °C, temperatures at which the catalyst did almost not show any NO

conversion. At 400 °C, when the catalyst displayed around 50% NO conversion the signal of iron on β sites remained unchanged. On the other hand, the signal of iron on γ sites just partially diminished at 150 and 250 °C (Figure 4.37, a) colored lines). A similar behavior of these two signals was observed when the catalyst was treated only with NH_3 at 150 and 250 °C (Figure 4.30).

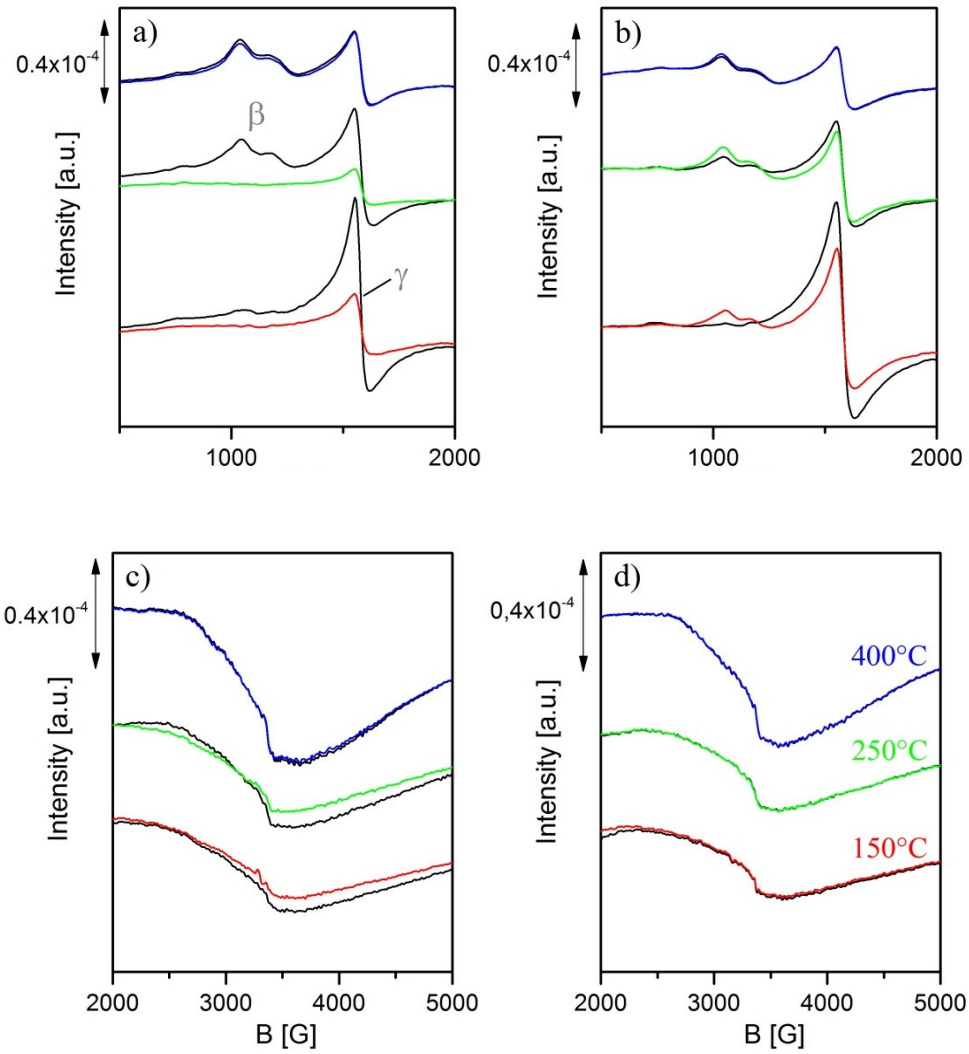

Figure 4.37 *In situ* EPR spectra of CFeZ at 150, 250 and 400 °C under a) standard SCR in low magnetic field, b) fast SCR in low magnetic field, c) standard SCR in a high magnetic field and d) fast SCR in a high magnetic field. Feed: NO/O_2 (black spectra a and c), $NO/O_2/NH_3$ (colored spectra a and c), $NO/NO_2/O_2$ (black spectra b and d) and $NO/NO_2/O_2/NH_3$ (colored spectra b and d).

Upon the fast SCR ($NO/NO_2/O_2/NH_3$), iron on β sites remained oxidized as Fe^{3+} at all temperatures, even at 150 °C; thus, the signal was well distinguished. The signal of isolated iron on γ sites slightly decreased at 150 and 250 °C, while at 400 °C it did not change (Figure 4.37, b) colored lines). In agreement with the findings described in section 4.1 for catalysts

ILIE-0.68, ILIE-0.46, SSIE-I-Na-0.27-rep and LIE-0.15, isolated iron sites on CFeZ remain oxidized, under fast SCR conditions at lower temperature compared to standard SCR, which might be the reason for the higher reaction rate in fast SCR.

EPR spectra in high magnetic field showed a signal of Fe_xO_y clusters as a broad line at $g \approx 2$ superimposed on the signal of highly symmetric iron sites (narrow line at ~ 3370 G). Fe_xO_y clusters were partially reduced during standard SCR conditions at 150 and 250 °C, temperatures in which CFeZ shows almost no conversion (Figure 4.37 c). During fast SCR conditions, these clusters remained in an oxidized state at all temperatures, since the same spectra were recorded for oxidative and fast SCR conditions (Figure 4.37 d, black and colored lines). Partial reduction of the clusters was also observed on CFeZ when NH_3 was dosed as an individual gas, after reaction with NO or NO_2 (Figure 4.34 and Figure 4.35). In the case of other Fe-ZSM-5 catalysts studied in this work (section 4.1.3) no modification of the signals for clusters and single Fe^{3+} on α sites at $g \approx 2$ under standard or fast SCR conditions could be seen. It suggests higher stability against reduction of the clusters in the samples prepared by ILIE, SSIE and LIE than in the commercial CFeZ.

4.3.3 Mechanism of NH_3-SCR of NO_x

Several mechanisms have been proposed for standard and fast SCR, while only few studies have been done regarding the role of the iron species in the formation of reaction intermediates. In particular, Ruggeri et al. [2] recently proposed the formation of nitrites/HONO over monomeric ferric sites in Fe-ZSM-5 during standard SCR. The nitrite species were evidenced by *ex situ* IR analysis of the mechanically separated mixture Fe-ZSM-5 + BaO/Al_2O_3. On the other hand, Chen et al. [49] have found that iron oxide in Fe-ZSM-5 samples enhanced the interaction between adsorbed NH_3 and NO/O_2; therefore, iron oxide was also assumed to favor the standard SCR.

Our results described above can be used to propose a mechanistic scheme for standard and fast SCR (Schema 4.1). Similar to the observations by Ruggeri et al. [2], our findings point to the formation of HNO_2 over Fe^{3+} (Schema 4.1, 1), observed as adsorbed NO_2; especially formed over Fe^{3+} on β sites, as observed by their reduction in the EPR spectra when reacted with NO (Figure 4.30).

It was also previously reported [5] that one pathway in the mechanism of standard SCR in presence of water occurs via formation of NO^+. In this work, we show evidence of the NO^+ species upon reaction with NO by FTIR (Figure 4.34 A) and describe its favored formation over Fe^{3+} on β sites (Schema 4.1, 2).

On the other hand, Chen et al. [49] have discussed the importance of Fe_xO_y in the standard SCR, which agree with our EPR observations (Figure 4.37 c), where the reduction of Fe_xO_y under standard SCR conditions occurred at low temperature, when the catalysts is not active. The reoxidation of Fe^{2+} to active Fe^{3+} species has been described as the rate determining step of the standard SCR [1]. In this chapter we have discussed that NO at high temperature (250 °C) acts also as oxidizing agent over isolated iron on β and γ sites (Figure 4.30 B). Moreover, when gas phase oxygen is added together with NO the oxidation was more remarkable, significantly at 250 °C for iron on β and γ sites (Figure 4.33). These two reactions are summarized in Schema 4.1, 3 and 4.

In a previous work Ruggeri et al. [33] have also investigated the fast SCR at low temperature over Fe-ZSM-5 by *in situ* FTIR, finding that NO_2 is stored as ferric nitrate without reduction of the iron center. Contrary to that and based on our FTIR and EPR investigations, the formation of surface nitrates is enhanced by Fe^{3+} on β sites, reducing Fe^{3+} species to Fe^{2+} (Schema 4.1, 5).

In the fast SCR, iron can be reoxidized by NO_2 which is reduced to NO, and to lower extent by reduction of NO at 250 °C (Schema 4.1, 4 and 6). During the fast SCR, the formation of NH_4NO_3 is favored at low temperature (150 °C), which decomposes into the undesired N_2O. At higher temperature (250 °C) in the fast SCR, NO reacts with surface nitrates to form HNO_2, which further reacts with NH_3 to produce N_2 and H_2O (Schema 4.1, fast SCR). Additionally, a considerable amount of NH_3 was found to be stored as NH_4^+ on Brønsted acid sites of the zeolite.

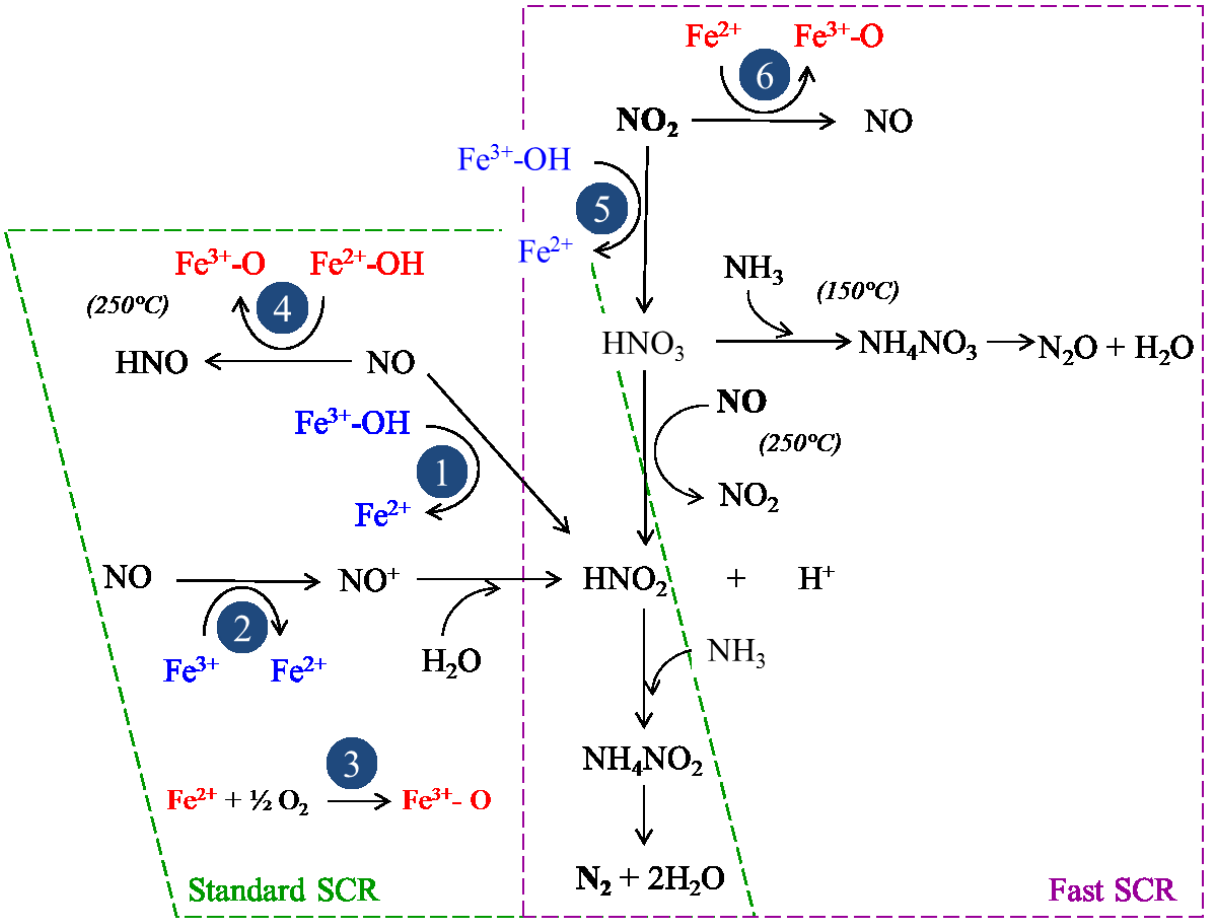

Schema 4.1 Proposed scheme with iron contribution to intermediate reactions in the mechanism of standard and fast SCR over Fe-ZSM-5 catalysts.

5. Conclusions

As a result of the extensively Fe-ZSM-5 characterization, it is valid to conclude that the samples prepared by LIE and ILIE methods contain mainly isolated iron sites, while SSIE synthesis method produces additionally significant amount of the Fe_xO_y clusters. Furthermore, the pre-loading of a co-cation (Na or Ca) in the extraframework cationic positions of the lattice promotes the formation of more Fe_xO_y clusters and nanoparticles as demonstrated for the SSIE-I-Ca/Na samples.

The characteristic EPR signals of isolated Fe^{3+} (in Fe-ZSM-5) could be assigned to extraframework cationic positions for the first time in this work. Hence, the signal of distorted tetrahedral Fe^{3+} ($g \approx 6$) correspond to the β sites, the signal of distorted octahedral Fe^{3+} ($g \approx 4.3$) to the γ sites, and the signal of highly symmetric Fe^{3+} ($g \approx 2$) to the α sites.

In the standard SCR, the catalytic activity correlates roughly with the iron content of the investigated Fe-ZSM-5 catalysts, an exception occurs for the sample SSIE-I-Na-0.27-rep, containing higher amount of clusters which limits the accessibility to all iron species. About 50% NO conversion is achieved in the standard SCR at 400 °C with the samples containing higher amounts of iron (ILIE-0.68, ILIE-0.46).

According to our results obtained by *in situ* UV-Vis and *operando* EPR spectroscopic studies, the activity of the standard SCR is mainly attributed to Fe^{3+} on α sites and Fe_xO_y clusters at temperatures below 400 °C. The participation of iron on β and γ sites can be excluded, since those species remain reduced as the inactive Fe^{2+} at these temperatures in the standard SCR.

For the fast SCR, the catalytic activity does not correlates with the iron content of the investigated samples. The most active sample (ILIE-0.46) reaches > 90% NO conversion at 250 °C. At this temperature, the sample with lower amount of iron (LIE-0.15) achieves more than 70% NO conversion, despite its low iron content. This supports the idea that just small amounts of iron species are responsible for the fast SCR.

Taking into account the results of the comprehensive *in situ* and *operando* EPR, UV-Vis and FTIR spectroscopic investigations, it is possible to establish that the isolated Fe^{3+} in distorted tetrahedral and octahedral positions (β and γ sites) inside of the pore framework are responsible for the activity at low temperatures (250 °C). Since they remain oxidized or reoxidize fast enough, they are able to experience the redoxcycle needed for the fast SCR

reaction at these temperatures. Certainly, the addition of NO_2 in the gas mixture of the fast SCR (in comparison to the standard SCR conditions) facilitates the reoxidation of the isolated iron species on β and γ sites, keeping them catalytically active as Fe^{3+}.

According to investigations of the NO oxidation over Fe-ZSM-5 catalysts, the capability to oxidize NO to NO_2 is greatly boosted by previous contact with standard SCR conditions, which is described as "activated NO oxidation". In a series of the samples loaded with a co-cation (Na or Ca), the performance of the activated NO oxidation decreases while increasing the co-cation occupancy.

Despite the comprehensive *in situ* UV-Vis and *operando* EPR spectroscopic studies of the activated NO oxidation, the reason for this activation effect could not be clarified. It seems that the activation effect might occur on a small minority of iron species which are not detectable by these techniques. By *in situ* FTIR studies it was found that fixation of NO on iron sites is needed to undergo further oxidation to NO_2. As a result of our *in situ* FTIR and EPR spectroscopic investigations, it can be concluded that oxygen from the lattice can be used for the oxidation of NO to NO_2, while gaseous oxygen in the feed aids mainly to oxidize the isolated Fe^{2+} to Fe^{3+} species.

For some of the investigated samples, the activated NO oxidation proceed faster that the whole standard SCR. Therefore, the NO oxidation cannot be proposed as a rate limiting step of the standard SCR.

Regarding the mechanistic studies of the SCR reactions over CFeZ, our results demonstrate that NO_2 oxidizes preferentially Fe^{2+} on γ sites, by its reduction to NO; while NO oxidizes mainly Fe^{2+} on β sites. On the other hand, the oxidation of NO to NO_2^- and/or NO^+, as well as NO_2 to NO_3^- might occur over Fe^{3+} on β sites. The formation of nitrates is definitely promoted by iron sites, since the band intensity of surface nitrates observed by *in situ* FTIR was considerable higher for CFeZ than for H-ZSM-5 sample.

The main mechanism of the fast SCR involves formation of nitrates over isolated Fe^{3+} sites. They are detectable by *in situ* FTIR mainly in terms of NH_4NO_3, which reacts with NO only at 250 °C but not at 150°C. The standard SCR proceeds via formation of NO^+ and NO_2 on Fe-ZSM-5 catalysts. Additionally, a strong chemisorption of NH_3 on the Brønsted sites at 150 °C is observed.

6. References

[1] G. Delahay, D. Valade, A. Guzmán-Vargas, B. Coq, Selective catalytic reduction of nitric oxide with ammonia on Fe-ZSM-5 catalysts prepared by different methods, Applied Catalysis B: Environmental, 55 (2005) 149-155.

[2] M.P. Ruggeri, T. Selleri, M. Colombo, I. Nova, E. Tronconi, Identification of nitrites/HONO as primary products of NO oxidation over Fe-ZSM-5 and their role in the Standard SCR mechanism: A chemical trapping study, Journal of Catalysis, 311 (2014) 266-270.

[3] Y.H. Yeom, B. Wen, W.M.H. Sachtler, E. Weitz, NOx Reduction from Diesel Emissions over a Nontransition Metal Zeolite Catalyst: A Mechanistic Study Using FTIR Spectroscopy, The Journal of Physical Chemistry B, 108 (2004) 5386-5404.

[4] T.C. Brüggemann, F.J. Keil, Theoretical Investigation of the Mechanism of the Selective Catalytic Reduction of Nitrogen Oxide with Ammonia on Fe-Form Zeolites, The Journal of Physical Chemistry C, 115 (2011) 23854-23870.

[5] S. Brandenberger, O. Kröcher, A. Tissler, R. Althoff, The State of the Art in Selective Catalytic Reduction of NO_x by Ammonia Using Metal-Exchanged Zeolite Catalysts, Catalysis Reviews, 50 (2008) 492-531.

[6] A. Grossale, I. Nova, E. Tronconi, D. Chatterjee, M. Weibel, The chemistry of the NO/NO_2–NH_3 "fast" SCR reaction over Fe-ZSM5 investigated by transient reaction analysis, Journal of Catalysis, 256 (2008) 312-322.

[7] M. Schwidder, S. Heikens, A. De Toni, S. Geisler, M. Berndt, A. Brückner, W. Grünert, The role of NO_2 in the selective catalytic reduction of nitrogen oxides over Fe-ZSM-5 catalysts: Active sites for the conversion of NO and of NO/NO_2 mixtures, Journal of Catalysis, 259 (2008) 96-103.

[8] X. Shi, F. Liu, W. Shan, H. He, Hydrothermal Deactivation of Fe-ZSM-5 Prepared by Different Methods for the Selective Catalytic Reduction of NO_x with NH_3, Chinese Journal of Catalysis, 33 (2012) 454-464.

[9] J. Li, S. Li, A DFT Study toward Understanding the High Activity of Fe-Exchanged Zeolites for the "Fast" Selective Catalytic Reduction of Nitrogen Oxides with Ammonia, The Journal of Physical Chemistry C, 112 (2008) 16938-16944.

[10] M. Schwidder, M.S. Kumar, K. Klementiev, M.M. Pohl, A. Brückner, W. Grünert, Selective reduction of NO with Fe-ZSM-5 catalysts of low Fe content: I. Relations between active site structure and catalytic performance, Journal of Catalysis, 231 (2005) 314-330.

[11] S. Brandenberger, O. Kröcher, A. Tissler, R. Althoff, The determination of the activities of different iron species in Fe-ZSM-5 for SCR of NO by NH_3, Applied Catalysis B: Environmental, 95 (2010) 348-357.

[12] S. Brandenberger, O. Kröcher, A. Tissler, R. Althoff, Estimation of the fractions of different nuclear iron species in uniformly metal-exchanged Fe-ZSM-5 samples based on a Poisson distribution, Applied Catalysis A: General, 373 (2010) 168-175.

[13] P. Forzatti, I. Nova, E. Tronconi, Enhanced NH3 Selective Catalytic Reduction for NO_x Abatement, Angewandte Chemie, 121 (2009) 8516-8518.

[14] L.K. Wang, N.C. Pereira, Y.-T. Hung, Advanced Air and Noise Pollution Control, Humana Press, Totowa, New Jersey, 2004.

[15] Past and present in DeNox Catalysis, (2007).

[16] Environmental Protection Agency, http://epa.gov/climatechange/ghgemissions/gases/n2o.html.

[17] L. Sloss, Nitrogen Oxides Control Technology Fact Book, Noyes Data Corporation, United States of America, 1992.

[18] Pollution Prevention and Abatement Handbook United States of America, 1998.

[19] Environmental Protection Agency, http://www.epa.gov/, in.

[20] European Environment Agency, http://www.eea.europa.eu/highlights/nitrogen-oxide-emissions-still-a, in.

[21] P.C.M. Sánchez, J.P. Pariente, Zeolites and Ordered Porous Solids: Fundamentals and Applications, Universitat Politècnica de València, 2011.

[22] EUR-Lex (access European Union law), http://eur-lex.europa.eu/LexUriServ/LexUriServ.do?uri=CELEX:32007R0715:EN:NOT, in.

[23] United States department of Labor, https://www.osha.gov/pls/oshaweb/owadisp.show_document?p_table=standards&p_id=9992, in.

[24] X. Liu, Y.D. Deng, S. Chen, W.S. Wang, Y. Xu, C.Q. Su, A case study on compatibility of automotive exhaust thermoelectric generation system, catalytic converter and muffler, Case Studies in Thermal Engineering, 2 (2014) 62-66.

[25] R. Zukerman, L. Vradman, M. Herskowitz, E. Liverts, M. Liverts, A. Massner, M. Weibel, J.F. Brilhac, P.G. Blakeman, L.J. Peace, Modeling and simulation of a smart catalytic converter combining NOx storage, ammonia production and SCR, Chemical Engineering Journal, 155 (2009) 419-426.

[26] P.S. Metkar, N. Salazar, R. Muncrief, V. Balakotaiah, M.P. Harold, Selective catalytic reduction of NO with NH_3 on iron zeolite monolithic catalysts: Steady-state and transient kinetics, Applied Catalysis B: Environmental, 104 (2011) 110-126.

[27] E. Tronconi, I. Nova, C. Ciardelli, D. Chatterjee, M. Weibel, Redox features in the catalytic mechanism of the "standard" and "fast" NH_3-SCR of NOx over a V-based catalyst investigated by dynamic methods, Journal of Catalysis, 245 (2007) 1-10.

[28] J. Li, H. Chang, L. Ma, J. Hao, R.T. Yang, Low-temperature selective catalytic reduction of NO_x with NH_3 over metal oxide and zeolite catalysts—A review, Catalysis Today, 175 (2011) 147-156.

[29] M. Koebel, M. Elsener, M. Kleemann, Urea-SCR: a promising technique to reduce NO_x emissions from automotive diesel engines, Catalysis Today, 59 (2000) 335-345.

[30] M. Koebel, G. Madia, M. Elsener, Selective catalytic reduction of NO and NO_2 at low temperatures, Catalysis Today, 73 (2002) 239-247.

[31] P. Forzatti, I. Nova, E. Tronconi, New "Enhanced NH3-SCR" Reaction for NOx Emission Control, Industrial & Engineering Chemistry Research, 49 (2010) 10386-10391.

[32] P.S. Metkar, V. Balakotaiah, M.P. Harold, Experimental and kinetic modeling study of NO oxidation: Comparison of Fe and Cu-zeolite catalysts, Catalysis Today, 184 (2012) 115-128.

[33] M.P. Ruggeri, A. Grossale, I. Nova, E. Tronconi, H. Jirglova, Z. Sobalik, FTIR in situ mechanistic study of the NH_3NO/NO_2 "Fast SCR" reaction over a commercial Fe-ZSM-5 catalyst, Catalysis Today, 184 (2012) 107-114.

[34] G.D. Pirngruber, P.K. Roy, R. Prins, On determining the nuclearity of iron sites in Fe-ZSM-5-a critical evaluation, Physical Chemistry Chemical Physics, 8 (2006) 3939-3950.

[35] M. Rivallan, G. Ricchiardi, S. Bordiga, A. Zecchina, Adsorption and reactivity of nitrogen oxides (NO_2, NO, N_2O) on Fe–zeolites, Journal of Catalysis, 264 (2009) 104-116.

[36] E.V. Kondratenko, J. Pérez-Ramírez, Oxidative functionalization of propane over FeMFI zeolites: Effect of reaction variables and catalyst constitution on the mechanism and performance, Applied Catalysis A: General, 267 (2004) 181-189.

[37] T.C. Brüggemann, F.J. Keil, Theoretical Investigation of the Mechanism of the Oxidation of Nitrogen Oxide on Iron-Form Zeolites in the Presence of Water, The Journal of Physical Chemistry C, 115 (2011) 2114-2133.

[38] A.-Z. Ma, W. Grunert, Selective catalytic reduction of NO by ammonia over Fe-ZSM-5 catalysts, Chemical Communications, (1999) 71-72.

[39] Z. Sobalík, Z. Tvarůková, A. Vondrová, M. Schwarze, Targeted preparation of Fe-zeolites with iron prevailing in extraframework cationic positions, in: M.D.D.E.D.V.S.H.P.A.J.J.A.M. E.M. Gaigneaux, P. Ruiz (Eds.) Studies in Surface Science and Catalysis, Elsevier, 2006, pp. 889-896.

[40] M. Santhosh Kumar, On the nature of different Fe sites in Fe-containing micro and mesoporous materials and their catalytic role in the abatement of nitrogen oxides from exhaust gases, in, Humboldt-Universität zu Berlin, 2005.

[41] International Zeolite Association, http://www.iza-online.org/, in.

[42] J. Dědeček, D. Kaucký, B. Wichterlová, Co^{2+} ion siting in pentasil-containing zeolites, part 3.: Co^{2+} ion sites and their occupation in ZSM-5: a VIS diffuse reflectance spectroscopy study, Microporous and Mesoporous Materials, 35–36 (2000) 483-494.

[43] L.J. Lobree, I.-C. Hwang, J.A. Reimer, A.T. Bell, Investigations of the State of Fe in H–ZSM-5, Journal of Catalysis, 186 (1999) 242-253.

[44] M. Iwasaki, K. Yamazaki, K. Banno, H. Shinjoh, Characterization of Fe/ZSM-5 DeNOx catalysts prepared by different methods: Relationships between active Fe sites and NH_3-SCR performance, Journal of Catalysis, 260 (2008) 205-216.

[45] M. Iwasaki, H. Shinjoh, NO evolution reaction with NO_2 adsorption over Fe/ZSM-5: In situ FT-IR observation and relationships with Fe sites, Journal of Catalysis, 273 (2010) 29-38.

[46] M. Li, Y. Yeom, E. Weitz, W.H. Sachtler, An acid catalyzed step in the catalytic reduction of NO_x to N_2, Catal Lett, 112 (2006) 129-132.

[47] M. Schwidder, M. Santhosh Kumar, U. Bentrup, J. Pérez-Ramírez, A. Brückner, W. Grünert, The role of Brønsted acidity in the SCR of NO over Fe-MFI catalysts, Microporous and Mesoporous Materials, 111 (2008) 124-133.

[48] S. Brandenberger, O. Kröcher, A. Wokaun, A. Tissler, R. Althoff, The role of Brønsted acidity in the selective catalytic reduction of NO with ammonia over Fe-ZSM-5, Journal of Catalysis, 268 (2009) 297-306.

[49] X. Chen, W. Li, J.W. Schwank, Reactivity of NH_3 over (Fe)/H-ZSM-5 zeolite: Studies of temperature-programmed and steady-state reactions, Catalysis Today, 175 (2011) 2-11.

[50] M. Santhosh Kumar, M. Schwidder, W. Grünert, U. Bentrup, A. Brückner, Selective reduction of NO with Fe-ZSM-5 catalysts of low Fe content: Part II. Assessing the function of different Fe sites by spectroscopic in situ studies, Journal of Catalysis, 239 (2006) 173-186.

[51] M. Devadas, O. Kröcher, M. Elsener, A. Wokaun, G. Mitrikas, N. Söger, M. Pfeifer, Y. Demel, L. Mussmann, Characterization and catalytic investigation of Fe-ZSM-5 for urea-SCR, Catalysis Today, 119 (2007) 137-144.

[52] I. Ellmers, R.P. Vélez, U. Bentrup, A. Brückner, W. Grünert, Oxidation and selective reduction of NO over Fe-ZSM-5 – How related are these reactions?, Journal of Catalysis, 311 (2014) 199-211.

[53] Y.H. Yeom, J. Henao, M.J. Li, W.M.H. Sachtler, E. Weitz, The role of NO in the mechanism of reduction with ammonia over a BaNa–Y catalyst, Journal of Catalysis, 231 (2005) 181-193.

[54] P. Forzatti, I. Nova, E. Tronconi, A. Kustov, J.R. Thøgersen, Effect of operating variables on the enhanced SCR reaction over a commercial V_2O_5–WO_3/TiO_2 catalyst for stationary applications, Catalysis Today, 184 (2012) 153-159.

[55] A. Grossale, I. Nova, E. Tronconi, Ammonia blocking of the “Fast SCR” reactivity over a commercial Fe-zeolite catalyst for Diesel exhaust aftertreatment, Journal of Catalysis, 265 (2009) 141-147.

[56] J.W. Niemantsverdriet, Spectroscopy in Catalysis, Second ed., 2000.

[57] F. Thibault-Starzyk, F. Maugé, Infrared Spectroscopy, in: Characterization of Solid Materials and Heterogeneous Catalysts, Wiley-VCH Verlag GmbH & Co. KGaA, 2012, pp. 1-48.

[58] A. Davydov, The Nature of Oxide Surface Centers, in: Molecular Spectroscopy of Oxide Catalyst Surfaces, John Wiley & Sons, Ltd, 2003, pp. 27-179.

[59] K.I. Hadjiivanov, Identification of Neutral and Charged N x O y Surface Species by IR Spectroscopy, Catalysis Reviews, 42 (2000) 71-144.

[60] P. Pietrzyk, Z. Sojka, E. Giamello, Electron Paramagnetic Resonance Spectroscopy, in: Characterization of Solid Materials and Heterogeneous Catalysts, Wiley-VCH Verlag GmbH & Co. KGaA, 2012, pp. 343-406.

[61] H.G. Karge, Weitkamp, Jens Characterization I (Molecular Sieves) Science and Technology, in: H.G. Karge, J. Weitkamp (Eds.), Springer Berlin Heidelberg, 2004.

[62] F.C. Jentoft, Electronic Spectroscopy: Ultra Violet-Visible and near IR Spectroscopies, in: Characterization of Solid Materials and Heterogeneous Catalysts, Wiley-VCH Verlag GmbH & Co. KGaA, 2012, pp. 89-147.

[63] B.M. Weckhuysen, Recent advances in the in-situ characterization of heterogeneous catalysts, Chemical Society Reviews, 39 (2010) 4541-5072.

[64] J.C.H.a.P.J.C. José A. Rodriguez, In-situ Characterization of Heterogeneous Catalysts, in: In-situ Characterization of Heterogeneous Catalysts, John Wiley & Sons, Inc., 2013, pp. i-22.

[65] F.C. Meunier, The design and testing of kinetically-appropriate operando spectroscopic cells for investigating heterogeneous catalytic reactions, Chemical Society Reviews, 39 (2010) 4602-4614.

[66] M.A. Bañares, Operando methodology: combination of in situ spectroscopy and simultaneous activity measurements under catalytic reaction conditions, Catalysis Today, 100 (2005) 71-77.

[67] A. Bruckner, In situ electron paramagnetic resonance: a unique tool for analyzing structure-reactivity relationships in heterogeneous catalysis, Chemical Society Reviews, 39 (2010) 4673-4684.

[68] W.M. Heijboer, A.A. Battiston, A. Knop-Gericke, M. Havecker, H. Bluhm, B.M. Weckhuysen, D.C. Koningsberger, F.M.F. de Groot, Redox behaviour of over-exchanged Fe/ZSM5 zeolites studied with in-situ soft X-ray absorption spectroscopy, Physical Chemistry Chemical Physics, 5 (2003) 4484-4491.

[69] Z. Sobalík, K. Jíša, H. Jirglová, B. Bernauer, Simultaneous FTIR/UV-Vis study of reactions over metallo-zeolites: Approach to quantitative in situ studies, Catalysis Today, 126 (2007) 73-80.

[70] S. Brandenberger, O. Kröcher, M. Casapu, A. Tissler, R. Althoff, Hydrothermal deactivation of Fe-ZSM-5 catalysts for the selective catalytic reduction of NO with NH_3, Applied Catalysis B: Environmental, 101 (2011) 649-659.

[71] I. Ellmers, Selektive Katalytische Reduktion von NOx durch NH3 an Fe-Zeolithen: Neue Erkenntnisse zu aktiven Zentren und Reaktionsmechanismen, in, Ruhr-Universität Bochum, 2014.

[72] A. Saito, H.C. Foley, Curvature and parametric sensitivity in models for adsorption in micropores, AIChE Journal, 37 (1991) 429-436.

[73] A.M. Volodin, G.M. Zhidomirov, K.A. Dubkov, E.J.M. Hensen, R.A. van Santen, Spin design of iron complexes on Fe-ZSM-5 zeolites, Catalysis Today, 110 (2005) 247-254.

[74] M. Devadas, O. Kröcher, M. Elsener, A. Wokaun, N. Söger, M. Pfeifer, Y. Demel, L. Mussmann, Influence of NO_2 on the selective catalytic reduction of NO with ammonia over Fe-ZSM5, Applied Catalysis B: Environmental, 67 (2006) 187-196.

[75] G. Mul, J. Pérez-Ramírez, F. Kapteijn, J.A. Moulijn, NO Adsorption on Ex-Framework [Fe,X]MFI Catalysts: Novel IR Bands and Evaluation of Assignments, Catal Lett, 80 (2002) 129-138.

[76] M. Iwasaki, H. Shinjoh, A comparative study of “standard”, “fast” and “NO_2” SCR reactions over Fe/zeolite catalyst, Applied Catalysis A: General, 390 (2010) 71-77.

[77] Chemistry of the Elements, in: N.N. Greenwood, A. Earnshaw (Eds.) Chemistry of the Elements (Second Edition), Butterworth-Heinemann, Oxford, 1997, pp. 406-472.

[78] S.E. Malykhin, A.M. Volodin, G.M. Zhidomirov, Spin States of Iron-Nitrosyl Adsorption Complexes Formed in Fe-ZSM5 Zeolites, Appl Magn Reson, 33 (2008) 153-166.

Liste der Publikationen

1. I. Ellmers, R. Pérez Vélez, U. Bentrup, W. Schwieger, A. Brückner, W. Grünert, *SCR and NO oxidation over Fe-ZSM-5 - the influence of the Fe content*, Catal. Today, submitted (**2014**).

2. R. Pérez Vélez, I. Ellmers, H. Huang, U. Bentrup, V. Schünemann, W. Grünert, A. Brückner, *Identifying active sites for fast NH3-SCR of NO/NO2 mixtures over Fe-ZSM-5 by operando EPR and UV-Vis spectroscopy*, J. Catal. **2014**, 316, 103-111.

3. I. Ellmers, R. Pérez Vélez, U. Bentrup, A. Brückner, W. Grünert, *Oxidation and selective reduction of NO over Fe-ZSM-5 – How related are these reactions?*, J. Catal. **2014**, 311, 199-211.

4. R. Pérez Vélez, M. P. Elizalde Gonzáles, U. Bentrup, *Preparation and in situ spectroscopic characterization of Cu-clinoptilolite catalysts for the oxidative carbonylation of methanol*, Microporous Mesoporous Mater. **2012**, 164, 93-98.

Erklärung

Hiermit erkläre ich, dass diese Arbeit bisher von mir weder an der Mathematisch-Naturwissenschaftlichen Fakultät der Universität Rostock noch einer anderen wissenschaftlichen Einrichtung zum Zwecke der Promotion eingereicht wurde. Ich erkläre auch, dass ich diese Arbeit selbständig angefertigt und ohne fremde Hilfe verfasst habe, keine außer den von mir angegebenen Hilfsmitteln und Quellen dazu verwendet habe und die den benutzten Werken inhaltlich und wörtlich entnommen Stellen als solche kenntlich gemacht habe.

Rostock, den Oktober 2014 Roxana Pérez Vélez